Cape Peninsula University of Technology

OPTIMISATION OF DOPING PROFILES FOR mm-WAVE GaAs AND GaN GUNN DIODES

by

SMITA FRANCIS

Thesis submitted in fulfilment of the requirements for the degree

Doctor of Engineering: Electrical Engineering

in the Faculty of Engineering

at the Cape Peninsula University of Technology

Supervisor: Professor R.R. Van Zyl

Bellville
Date submitted February 2017

DECLARATION

I, Smita Francis, declare that the content of this thesis represents my own presentation and contributions under the guidance of my supervisor, and the thesis has not been submitted for academic examination towards any qualification. Furthermore, it represents my own opinions and not necessarily those of Cape Peninsula University of Technology.

Signed **Date**

ABSTRACT

Gunn diodes play a prominent role in the development of low-cost and reliable solid-state oscillators for diverse applications, such as in the military, security, automotive and consumer electronics industries. The primary focus of the research presented here is the optimisation of GaAs and GaN Gunn diodes for mm-wave operations, through rigorous Monte Carlo particle simulations.

A novel, empirical technique to determine the upper operational frequency limit of devices based on the transferred electron mechanism is presented. This method exploits the hysteresis of the dynamic velocity-field curves of semiconductors to establish the upper frequency limit of the transferred electron mechanism in bulk material that supports this mechanism. The method can be applied to any bulk material exhibiting negative differential resistance. The simulations show that the upper frequency limits of the fundamental mode of operation for GaAs Gunn diodes are between 80 GHz and 100 GHz, and for GaN Gunn diodes between 250 GHz and 300 GHz, depending on the operating conditions. These results, based on the simulated *bulk* material characteristics, are confirmed by the simulated mm-wave performance of the GaAs and GaN Gunn devices. GaAs diodes are shown to exhibit a fundamental frequency limit of 90 GHz, but with harmonic power available up to 186 GHz. Simulated GaN diodes are capable of generating appreciable output power at operational frequencies up to 250 GHz in the fundamental mode, with harmonic output power available up to 525 GHz.

The research furthermore establishes optimised doping profiles for two-domain GaAs Gunn diodes and single- and two-domain GaN Gunn diodes. The relevant design parameters that have been optimised, are the dimensions and doping profile of the transit regions, the width of the doping notches and buffer region (for two-domain devices), and the bias voltage. In the case of GaAs diodes, hot electron injection has also been implemented to improve the efficiency and output power of the devices. Multi-domain operation has been explored for both GaAs and GaN devices and found to be an effective way of increasing the output power. However, it is the opinion of the author that a maximum number of two domains is feasible for both GaAs and GaN diodes due to the significant increase in thermal heating associated with an increase in the number of transit regions. It has also been found that increasing the doping concentration of the transit region exponentially over the last 25% towards the anode by a factor of 1.5 above the nominal doping level enhances the output power of the diodes.

The RF performance of the devices is simulated in terms of output power in fundamental and harmonic modes of operations, admittance and conversion efficiency. The Monte Carlo

simulations incorporate thermal effects consistently with the evolution of the electrons' dynamic behaviour throughout the device, which is essential in the reliable simulation of Gunn diodes. The simulated results are therefore more conservative than those published in the literature, where thermal effects are generally not adequately modelled.

The optimised two-domain GaAs yields an RF output power of 218 mW at the fundamental frequency limit of 62 GHz and RF output powers of 42 mW and 890 μW at the second and third harmonics of 124 GHz and 186 GHz, respectively. Beyond a fundamental frequency of 62 GHz, the efficiency of the two-domain diode degrades significantly to less than 0.1%.

The single-domain GaN Gunn diode yields RF output power of 3.4 W, 259 mW and 42 mW at the fundamental frequency of 175 GHz and at its second and third harmonics, respectively. For the two-domain diode, the corresponding RF output power increases to 5 W, 514 mW and 57 mW. The expected fourfold increase in power has not been realised, which is ascribed to the higher operational temperature of the two-domain device, and non-identical growth of Gunn domains in each of the two domains.

Heating of Gunn diodes, especially for GaN devices, is a major concern and is addressed by proper heat sinking and decreasing the effective bias current and voltage. In this work an integral heat sink is assumed. The bias current and voltage have been reduced by applying a pulsed bias voltage with duty cycles of less than 1.5% to the diode.

PUBLICATIONS EMANATING FROM THIS RESEARCH

Conference presentations

- Van Zyl R.R., **Francis S.,** Perold W.J. and Botha R. 2009, "Optimisation strategies for W Band GaAs Gunn diodes", paper presented at the *South African Conference on Semi-and Superconducting Technology*, Stellenbosch, South Africa.

- Van Zyl R.R., **Francis S.** and Perold W.J. 2011, "State of the art Gunn Diodes: Current and future trends in design and optimisation", paper presented at the *Sensors, MEMS, Electro-Optic Systems Conference*, Berg-en-Dal, South Africa.

Accredited scientific journal publications

- **Francis S.** and Van Zyl R.R. 2013, "Evaluating graded doping profiles of single-domain GaN Gunn diodes for THz applications", *Terahertz Science and Technology*, Vol. 6(3), pp.177-182, USA.
- **Francis S.**, Van Zyl R.R. and Perold W.J. 2015, "An empirical determination of upper operational frequency limits of transferred electron mechanism in bulk GaAs and GaN through ensemble Monte Carlo particle simulations", *Indian Journal of Physics*, Vol. 89(8), pp.825-828, India.

- **Francis S.** and Van Zyl R. R. 2015, "Evaluating the microwave performance of a two-domain GaN Gunn diode for THz applications", *Terahertz Science and Technology,* Vol. 8(1), pp.25-34, USA.

ACKNOWLEDGEMENTS

I wish to thank:

- Prof. R.R. Van Zyl, my supervisor, for his guidance and support during the research. This work would have never materialised without his guidance, critique, and patience.
- The French South African Institute of Technology and the Department of Electrical, Electronic and Computer Engineering at Cape Peninsula University of Technology for their support and assistance.
- The Namibia University of Science and Technology (NUST) for the constant support and encouragement given to me throughout my research endeavours.
- Lastly, I thank my family and friends for their encouragement and support.

The financial assistance of the National Research Foundation towards this research is acknowledged. Opinions expressed in this thesis and the conclusions arrived at, are those of the author, and are not attributed to the National Research Foundation or the Cape Peninsula University of Technology.

DEDICATION

MY PARENTS

TABLE OF CONTENTS

LIST OF FIGURES

LIST OF TABLES

ACRONYMS

BTE	Boltzmann transport equation
CVD	Chemical vapour deposition
CW	Continuous wave
DC	Direct current
EM	Electromagnetic
EMCPST	Ensemble Monte Carlo particle simulation technique
IHS	Integral heatsink
I-V	Current-Voltage
MCPST	Monte Carlo particle simulation technique
NDR	Negative differential resistance
RF	Radio frequency
TED	Transferred electron device
TEM	Transferred electron mechanism
v-E	Velocity-field

1 INTRODUCTION

1.1 Background

The “Gunn effect” was discovered on 19 February 1962 by J.B. Gunn. He observed random “noise”-like oscillations when an n-type GaAs sample was biased above a threshold voltage level (Gunn, 1963:88-91). Gunn explained the observed oscillations as a “transit time” mode of oscillation. Group III-IV materials exhibit this Gunn effect. Today, Gunn diodes are widely used in commercial and military applications, for example in house alarm systems, security screening, surveillance, medical imaging, astronomy, spectroscopy, and radar systems.

GaAs and GaN Gunn diodes are found to be less noisy, producing signals with lower frequency drift and with more stable and reliable operation as compared to IMPATT diodes, or Gunn diodes based on InP (Dunn and Kearney, 2003:794-802; Hughes, Castro and Johnston, 2005:595-600). However, due to their low power conversion efficiencies, Gunn diodes operate at very high temperatures. This poses significant challenges in terms of fabrication and the mitigation thereof (Buniatyan and Arountionian, 2007:6355-6385; Hao, Yang and Zhang, 2008:51-64).

GaN, with its wider energy band gap, high breakdown field and high electron drift velocities, has drawn wide interest for use as a potential microwave source (Alekseev and Pavlidis, 2000:245-252; Wu, Tsai, Chen and Chang, 2007:1276-1280; Benbakhti, Rousseau, Soltani and De Jaeger, 2009:1-5). Furthermore, nitride-based Gunn diodes are suitable for integration in upcoming nitride technologies (Aloise, Vitanov and Palankovski, 2011).

The major disadvantages of GaAs Gunn diodes, compared to their GaN counterparts, are lower power capability and much lower operational frequencies.

The research presented here on GaAs Gunn diodes builds on the work by Van Zyl (2006) regarding the optimisation of two-domain diodes with appropriate doping profile engineering and hot electron injection. The simulated output power of the optimised diode at 94 GHz was 160 mW with an efficiency of 2%. More recent experimental results for single-domain GaAs Gunn diodes indicate that the operational frequency of GaAs Gunn diodes extends to 122 GHz, where second harmonic output power of 40 mW has been reported (Priestly and Farrington, 2010:1-10).

The performance of GaN Gunn diodes, as reported in the literature, is mostly based on simulation. Output power at frequencies as high as 675 GHz has been simulated (Garcia, Íñiguez-de-la-Torre, Pérez, Mateos and González, 2013:1-24), although these predictions unrealistically assume that the effects of self-heating do not degrade the efficiency of the diode significantly. The investigation of multi-domain GaN diodes has been reported, for example a 4-domain diode yielding simulated output power of 1.9 W at 340 GHz (Joshi, Viswanadha, Shah and del Rosario, 2003:4836-4842). This, again, is an unrealistic expectation. It will be shown in this research that thermal heating for GaN Gunn diodes, specifically, is inhibitive and that multi-domain diodes can only be operated in extremely low duty-cycle modes.

1.2 Research objectives

The principal objective of the research is to optimise GaAs and GaN Gunn diodes for operation at mm-wave frequencies through doping profile engineering and the incorporation of multi-domain structures.

The research further investigates the expected practical operational frequency limit of these devices. This is assessed by determining the upper frequency limit of the transferred electron mechanism in bulk GaAs and GaN empirically though Monte Carlo simulations. This novel approach exploits the degradation of the effective negative slope of the dynamic velocity-field characteristics of bulk GaAs and GaN at frequencies approaching the limit of the transferred electron mechanism.

The aforementioned broad research objectives can be subdivided into two groups; the first dealing with the bulk material, and the second with the actual devices based on these materials. The specific objectives are summarised below.

Group 1: Bulk semiconductor material

- Estimate the upper operational frequency limit of the transferred electron mechanism supported in bulk GaAs and GaN.
- Determine the effect of doping concentration and temperature on the upper frequency limit of the transferred electron mechanism in bulk GaAs and GaN.

Group 2: Device level

GaAs Gunn diode

- Optimise the performance of a two-domain diode in the mm-wave range (benchmarked against the work by Van Zyl (2006)).
- Determine the maximum fundamental and harmonic frequencies of operation of a two-domain diode operating within its physical and thermal limits.

GaN Gunn diode

- Establish a benchmark single- and two-domain diode.
- Optimise the performance of the single- and two-domain diodes in the upper mm-wave and terahertz regions.
- Determine the maximum fundamental and harmonic frequencies of operation of the single- and two-domain diodes operating within their physical and thermal limits.

1.3 Research questions

The research objectives translate into the following research questions.

Group 1: Bulk semiconductor material

- How can the dynamic velocity-field curves of GaAs and GaN bulk material be interpreted to determine the upper operational frequency limit of the transferred electron mechanism in these materials?
- What is the maximum operational frequency limit of the transferred electron mechanism supported in bulk GaAs and GaN material?
- What is the effect of doping concentration and temperature on this maximum operational frequency limit?

Group 2: Device level

- Which device parameters influence the microwave performance of Gunn diodes?
- What are the effects of these parameters on the microwave performance of single- and two-domain GaAs and GaN Gunn diodes?

- Which set of parameters yields optimum output power and efficiency for these diodes at the fundamental and harmonic frequencies of operation, whilst ensuring practical device impedances?
- How does thermal heating impact the performance of the optimised diodes, and how can its effect be mitigated?

1.4 Research methodology

Due to the absence of local infrastructure to develop the specialised GaAs and GaN diodes, an ensemble Monte Carlo particle simulation technique (EMCPST) is employed to simulate these diodes realistically. The EMCPST developed for this purpose is based on the work done by Van Zyl (2006). The simulation results are verified by comparing its performance with experimental data as far as is feasible. Notably, the EMCPST incorporates a thermal model that is dynamically consistent with the evolution of the electrons through the device; thus, rendering a realistic model of the Gunn diodes.

Figure 1.1 gives an outline of the workflow of the research, indicating the three major areas of investigation, namely the:

- empirical estimation of the upper frequency limit of the transferred electron mechanism in bulk GaAs and GaN;
- optimisation of a two-domain GaAs Gunn diode and determining its operational frequency limit; and
- optimisation of a single- and two-domain GaN Gunn diode and determining its operational frequency limits.

Following the research design plan in Figure 1.1, a step-by-step overview of the research is summarised as follows:

- The operational frequency limits of the transferred electron mechanism in bulk GaAs and GaN are established.
- The effects of doping concentration and operating temperature on this operational frequency limit are determined to assist in baseline device design.
- A 94 GHz benchmark two-domain GaAs Gunn diode with multiple hot electron launchers is established, based on the work of Van Zyl (2006).
- The benchmark two-domain GaAs Gunn diode is further optimised for output power and efficiency.

- The upper operational frequency limit of two-domain GaAs Gunn diodes is determined.
- A benchmark single-domain GaN Gunn diode is established.
- The benchmark single-domain GaN Gunn diode is further optimised for output power and efficiency.
- The upper operational frequency limit of single-domain GaN Gunn diodes is determined.
- A two-domain GaN Gunn diode, based on the single-domain diode design, is further optimised for output power and its upper frequency limit determined.

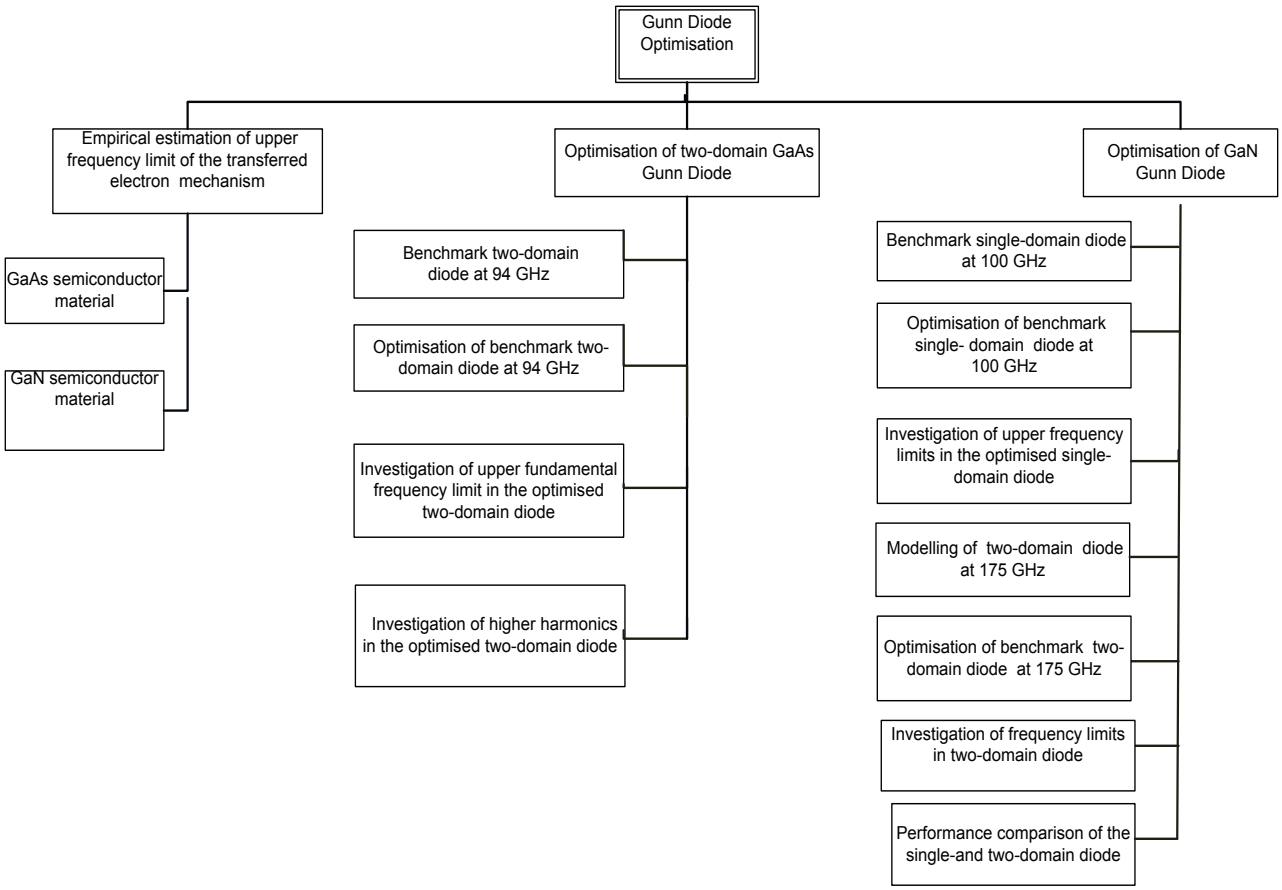

Figure 1.1 Research design plan

1.5 Delineation of the research

The scope of the research is delineated as follows:

- Only Gunn diodes based on GaAs and GaN are investigated.

- Only the first, second and third harmonics of the terminal currents and voltages are considered to determine the maximum operational frequencies of the diodes.
- The RF performance parameters of the diodes are limited to output power at the fundamental and harmonics, device admittance, and conversion efficiency.
- The noise performance of the diodes is not investigated.
- The number of domains for both GaAs and GaN diodes is limited to two, due to the expected excessive thermal heating of diodes when more domains are incorporated.
- Only meso-style diodes are simulated. Planar diodes are not considered.
- Simulations are limited to one dimension, as this is acceptable where the diameter of the diode is much larger than the active region of the device.

1.6 Significance of the research

As mentioned earlier, Gunn diodes have found wide industrial application. Although alternative technologies, such as SiGe, GaAs and GaN MMICs have become available, Gunn diodes are still preferred due to their relative simplicity, cost and output power (Priestley and Farrington, 2010). Increasing the operational frequencies of these devices and improving their output power and efficiencies will extend their usefulness well into the future.

This research puts forward optimised models of GaAs and GaN Gunn diodes at mm-wave frequencies. The simulated operational frequency limits for these devices are deemed more realistic than most simulation-based results reported in the literature. This is chiefly due to the modelling of thermal heating throughout the devices, linked with the 'realism' that is implicit to Monte Carlo simulations.

The investigation of GaN Gunn diodes presented here is especially significant. This technology is comparatively new and therefore not as well-published as GaAs diodes.

Furthermore, the proliferation of space applications through the emergence of nano-satellites (Müncheberg, Krischke and Lemke, 1996:799-808) gives impetus to this work. Nano-satellite platforms require low-cost solutions that are reliable, relatively simplistic and power efficient. These solutions are also required at increasingly higher mm-wave frequencies. CPUT has embarked on a nano-satellite programme in 2009 and has witnessed tremendous growth and development of this technology. Communications and

radar applications are now being developed on these platforms. Hence, the development of GaN Gunn diodes that can integrate with nitride technologies is very relevant, due to the robustness of these materials in the harsh space environment.

1.7 Dissertation layout

The research is presented in six chapters.

Chapter 2 gives a technical literature review of GaAs and GaN Gunn diodes. The underlying Gunn effect and how it is exploited in Gunn devices are described. An overview of the ensemble Monte Carlo particle simulation technique is also presented.

Chapter 3 introduces an innovative empirical technique to determine the maximum frequency at which the transferred electron mechanism can be sustained in bulk GaAs and GaN semiconductors and, by implication, the upper fundamental frequency limit of Gunn devices based on these materials.

Chapter 4 presents the optimisation of the mm-wave performance of a two-domain GaAs Gunn diode. The optimised diode is further investigated for its upper fundamental and harmonic frequency limits.

Chapter 5 investigates the operational feasibility of single- and two-domain GaN Gunn diodes. A benchmark single-domain diode is established and its performance optimised. The optimised diode is further investigated for its upper fundamental and harmonic frequency limits. This approach is repeated for a two-domain diode, based on the single-domain design. The chapter concludes with a comparison of the mm-wave performance of single- and two-domain diodes.

Chapter 6 concludes the thesis with a discussion of the findings and briefly summarises future research work.

For purposes of continuity, the simulation results and findings of the Monte Carlo ‘experiments’ are graphically represented, analysed and discussed in each section.

2 TECHNICAL LITERATURE REVIEW

2.1 Introduction

This chapter describes the Gunn effect and its manifestation as negative differential resistance exhibited by Gunn devices. An overview of optimisation techniques to enhance the mm-wave performance of Gunn diodes is presented. This is followed by a summary of the technological evolution of GaAs and GaN Gunn diodes. The chapter concludes with a discussion of the Monte Carlo particle simulation technique.

2.2 The Gunn effect

Gunn ascribed the "noise"-like oscillations that he observed when an n-type GaAs sample was biased above a certain threshold voltage level to a "transit time" mode of oscillation and further postulated that (Gunn, 1963:88-91)

- the device exhibits a *negative differential resistance* (NDR);
- the oscillating frequency of the device is a function of bias voltage and temperature; and
- the terminal current waveform consists of narrow spikes indicating high harmonic content and low efficiency at the fundamental frequency.

These macroscopic characteristics of Gunn devices are attributed to the *transferred electron mechanism* whereby electrons in the conduction band of Group III-IV materials are accelerated and achieve sufficient energy to transfer from the central to the satellite valleys of the conduction band. The satellite valleys are associated with higher effective electron mass than for the central valley; hence, the electrons literally slow down and "pile up". These "Gunn domains" then traverse the device and give rise to current spikes at the terminals, effectively presenting a negative differential resistance to the external circuit (Gunn, 1963:88-91; Sze *et al.*, 2007:511-540). A negative differential resistance can also be achieved through the dispersion of electrons, as in the case of GaN.

The underlying transferred electron mechanism and Gunn effect are extensively documented in the literature, for example Gunn (1963), Bullman *et al.* (Bullman, Hobson, Taylor, 1972), Bosch *et al.* (Bosch and Engelman, 1975) and Shur (1990), and will only be discussed briefly in subsequent sections.

2.2.1 Gunn domain formation

Consider a sample of uniformly doped n-type GaAs (or GaN) of length L, biased with a constant voltage source V_0 as shown in Figure 2.1(a) (Van Zyl, Francis, Perold and Botha, 2009).

The initial electrical field (E_0) is assumed to be constant, with a magnitude of $E_0 = V_0/L$. Due to the application of the electric field, the electrons flow from cathode to anode with a constant velocity υ_3 as shown in Figure 2.1(d). The flow of electrons causes a small local perturbation (at a random location) in the net charge at $t = t_0$, which gives rise to the resulting electric field distribution as indicated by the solid curve in Figure 2.1(c). The electrons at point A experience an electric field E_{L1} and drift towards the anode with velocity υ_4, whereas the electrons at point B that are subjected to an electric field E_{H1}, drift towards the anode with velocity υ_2. The velocity υ_2 is smaller than υ_4. Consequently, a 'pile-up' of electrons occurs between points A and B, effectively further increasing the net negative charge in that region. Furthermore, the electron drift velocity at B is lower than that of the electrons immediately to the right of B (towards the anode); hence, this region becomes more depleted of electrons. The progressive piling up and depletion of electrons cause the initial charge perturbation to grow into dipole 'Gunn' domains. The domains grow while propagating towards the anode until a stable Gunn domain has formed, as indicated by the dashed curve in Figure 2.1(c). At this instant, the electrons at points C and D drift at the same velocity υ_1.

The formation of the Gunn domain decreases the electric field in the rest of the sample, inhibiting the formation of a second Gunn domain. As soon as the Gunn domain is absorbed at the anode contact region, the average electric field in the sample rises and Gunn domain formation starts again. This successive formation and drift of Gunn domains through the sample lead to alternating current oscillations observed at the contacts.

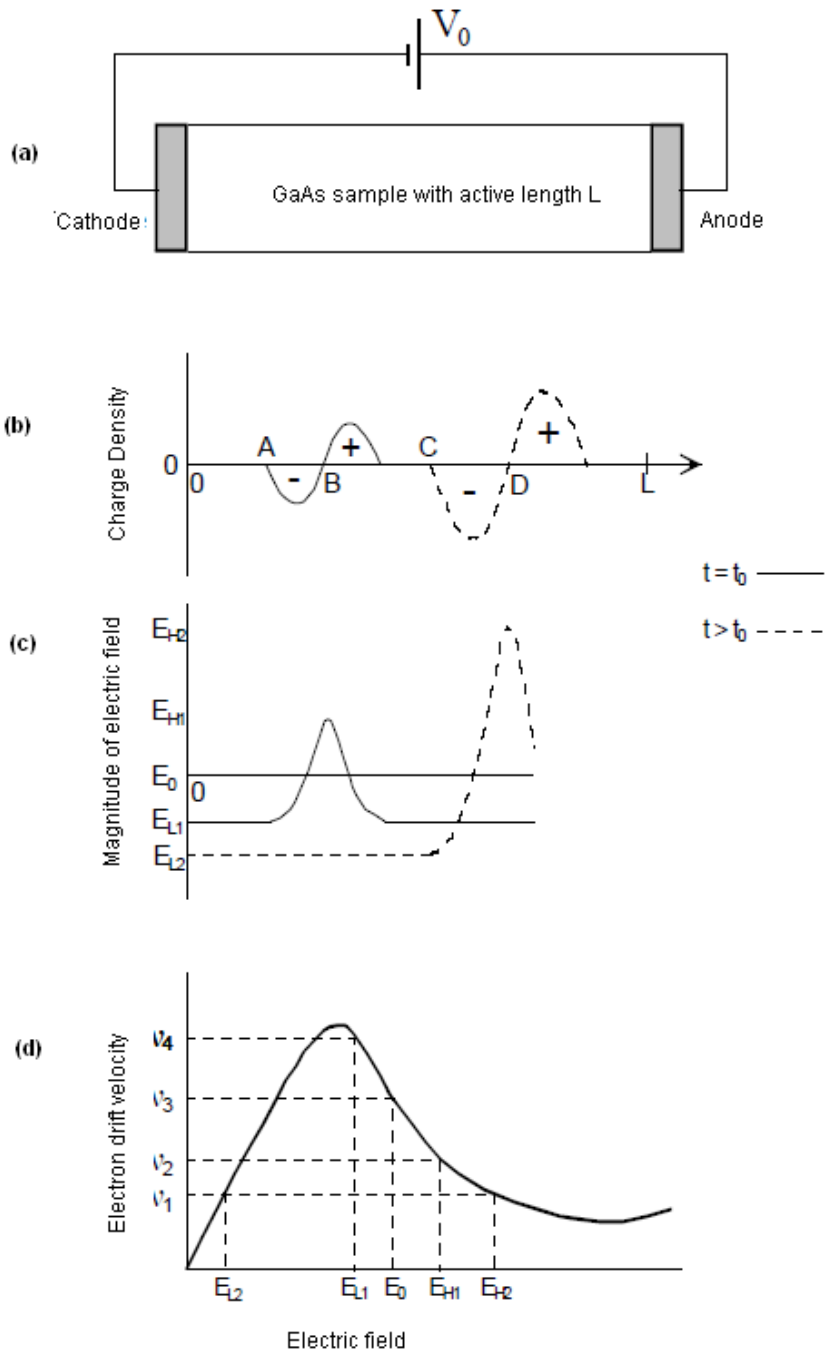

Figure 2.1 Gunn domain formation in a uniformly doped GaAs or GaN sample

(From Van Zyl *et al.*, 2009)

The fundamental frequency of these current pulses is inversely proportional to the time it takes for the domains to traverse the transit region of the diode. This relationship between transit region length and the fundamental operational frequency for GaAs diodes is illustrated in Figure 2.2 (Teoh *et al*., 2002:1090-1095).

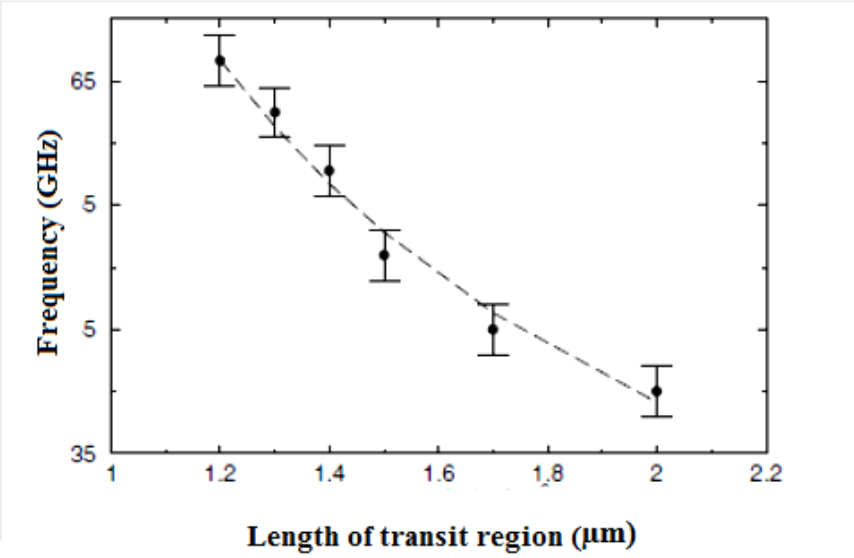

Figure 2.2 Illustration of GaAs Gunn diode frequency and transit region length

(From Teoh *et al*., 2002:1090-1095)

Gunn domains are well formed only if the product of the nominal doping concentration (n_0) and length of the transit region (L) of the Gunn diode satisfy the condition (Bosch *et al.,* 1975*;* Sze *et al.,* 2007; Zhao *et al.*, 2000:334-342; Joshi *et al.,* 2003:4836-4842; Caroll, 1970)

$$n_0 L > k \times 10^{16}\ m^{-2} \qquad \textbf{Equation 2.1}$$

with k = 1 for GaAs and k = 5 for GaN.

The various modes of operation of Gunn diode oscillation have been investigated by Bosch *et al.* (1975:83-145), who classified these as *delayed dipole domain oscillation*, *quenched dipole domain oscillation*, *limited space charge accumulation oscillation*, and *travelling accumulation layer oscillation*. Dipole domain oscillation is only possible at lower frequencies. Van Zyl (2006) confirms that the primary mode of Gunn diode oscillation at mm-wave frequencies is the travelling accumulation layer.

It is important to note that domains will only form if the sample is biased such that the internal electrical field is in the negative slope region of the velocity-field characteristic curve, also referred to as the region of *negative differential resistance*.

2.2.2 Negative differential resistance

As mentioned above, the transferred electron mechanism in GaAs and GaN gives rise to the negative differential resistance presented by Gunn diodes. Figure 2.3 (Sze and Kwog, 2007) illustrates the typical current-voltage (I-V) characteristic curve of a Gunn diode, which shows an expected resemblance to the velocity-field curve of the bulk material. The diode exhibits Ohm's law in the linear region of the I-V characteristic curve, until it reaches a threshold voltage (V_{th}). Increasing the bias voltage beyond this threshold value, the electrons in the central conduction band valley accelerate and obtain sufficient energy to transfer to the satellite valleys. The higher energy satellite valleys are associated with heavier electrons and a decrease in their mobility. This causes a decrease in the electron current, which manifests as a negative differential resistance region.

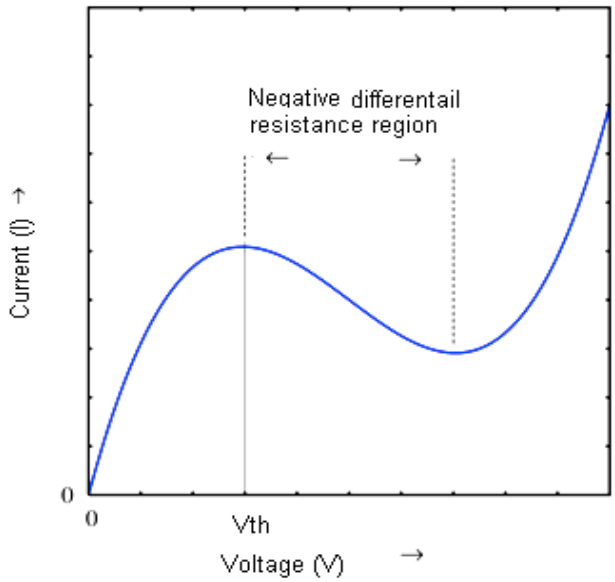

Figure 2.3 GaAs Gunn diode I-V characteristic curve

(From Sze *et al.,* 2007)

GaAs Gunn diodes exhibit NDR through the transferred electron mechanism only, whereas GaN Gunn diodes can exhibit NDR through two mechanisms, namely:

- inter-valley electron transfer exhibited by GaN (Wz), similar to GaAs; and
- dispersion of electrons in the central valley exhibited by GaN (Zb) (Gelmont *et al.*, 1993; Krishnamurthy *et al.*, 1997:1999-2001; Alekseev *et al.,* 2000:941-947; Chitara *et al*., 2009:205-209).

The dispersion mechanism will be described briefly below, although it was not investigated due to the absence of a realistic energy band model for GaN (Zb) to simulate this mechanism.

Dispersion of electrons and NDR

Dispersion of the group velocity of electrons in the central Γ-valley leads to negative differential resistance without electrons being transferred to the satellite valleys as in the case of inter-valley electron transfer. Dispersion of electrons in the Γ-valley occurs if the following two conditions are satisfied (Foutz *et al.,* 1997:2849-2852; Krishnamurthy *et al.*, 1997:1999-2001; Alkeseev *et al.,* 2000:941-947):

- the energy gap between the central Γ-valley and the satellite L-valleys is small; and
- the inflection point of the Γ-valley is located below the lowest satellite energy level.

Figure 2.4 (Krishnamurthy *et al.,* 1997:1999-2001) is an illustration of the conduction energy band and group velocity of electrons in GaN (Zb). The upper curve illustrates the conduction energy band and the lower curve represents the group velocity of electrons. Point '*A*' denotes the peak group velocity of electrons, while 'E_i' (dotted curve) denotes the inflection point.

In the absence of any scattering mechanisms and under the influence of an applied electric field, the electrons slow down when their energies exceed the inflection point energy. This is due to the semi-classical effective mass of the electrons acquiring a negative value (Chen and Hao, 1995:5451-5456; Krishnamurthy *et al.,* 1997:1999-2001).

Of the two negative differential resistance mechanisms exhibited by GaN, the mechanism that predominates depends on the relative ordering of the inflection point and the energy of the satellite valley at the inflection point (Krishnamurthy *et al.,* 1997:1999-2001).

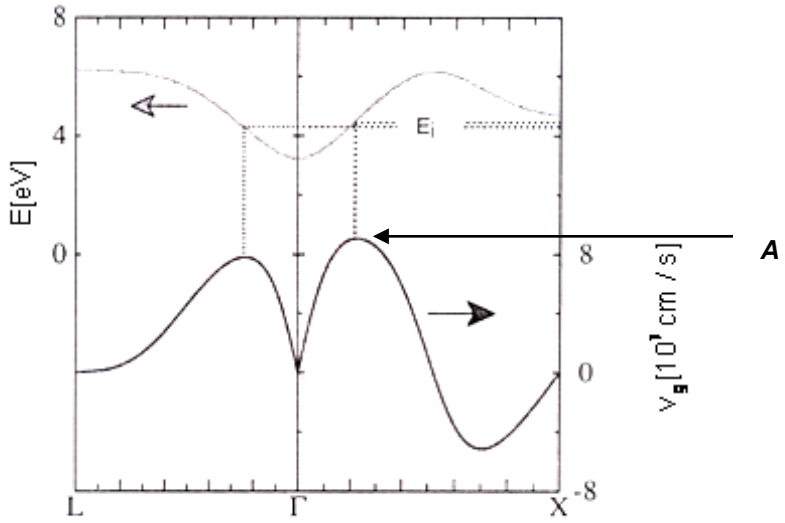

Figure 2.4 Conduction energy band and group velocity of electrons in GaN (Zb)

(From Krishnamurthy *et al.,* 1997:1999-2001)

2.2.3 Operational frequency limit of NDR

From Section 2.2.1, it is evident that Gunn domain formation is not instantaneous. For domains to form, electrons must first accelerate to gain sufficient energy to transfer to the satellite valleys. The transfer mechanism itself is also associated with a finite duration. Mathematically, the time τ_{tot} required to exhibit negative differential resistance through the transfer electron mechanism can be stated as (Sze *et al.,* 2007)

$$\tau_{tot} = \tau_{ER} + \tau_{ET} \qquad \textbf{Equation 2.2}$$

where τ_{ER} is the energy relaxation time and τ_{ET} the inter-valley relaxation time. The energy relaxation time is approximated as the time an electron with effective mass m_{eff} takes to accelerate to the threshold energy ΔE under an applied threshold electric field E_{TH}, and is given by (Sze et al., 2007)

$$\tau_{ER} = \frac{\sqrt{2m_{eff}\Delta E}}{qE_{TH}} \quad . \qquad \textbf{Equation 2.3}$$

The intervalley-transfer relaxation time is evaluated from the results of Monte Carlo studies of the electron ballistic transport in GaAs and GaN (Alekseev and Pavlidis, 2000; Eisele and Haddad, 1998; Foutz *et al*., 1993).

An *NDR relaxation frequency* (f_{NDR}) can now be defined as (Alekseev *et al.,* 2000:245-252)

$$f_{NDR} = \frac{1}{\tau_{ER} + \tau_{ET}} \qquad \textbf{Equation 2.4}$$

which is the highest frequency at which the Gunn effect can still effectively yield NDR. At operational frequencies above f_{NDR}, Gunn domains will not have sufficient time to form and, hence, the NDR characteristic of the device will deteriorate. This is further investigated in Chapter 3.

Where NDR is based on the dispersion of electrons, as is the case with GaN (Zb), there is no inter-valley scattering. This means that τ_{ET} = 0, which results in a much higher frequency limit of inflection point Gunn operation than for operation based on the transferred electron mechanism.

From Equation 2.4 the operational frequency limits intrinsic to GaAs and GaN Gunn devices are estimated as (Foutz *et al*., 1997:2849-2852; Alekseev *et al*., 2000:941-947; Pavlidis, 2004:551-554):

- 105 GHz for GaAs;
- 740 GHz for GaN if NDR is based on the transferred-electron mechanism; and
- 4 THz for GaN if NDR is based on the dispersion of electrons.

2.2.4 Comparison of bulk GaAs and GaN for Gunn operation

The microwave performance of GaAs and GaN Gunn devices can be compared at the hand of three *figures of merit*, namely the Keyes and Johnson's figures of merit, and a quality factor as defined below (Buniatyan *et al.,* 2007:6355-6385).

Keyes figure of merit

The Keyes figure of merit (KM) relates to the switching speed of a device and its thermal limitation due to heat generation.

Johnson's figure of merit

The Johnson's figure of merit (JM) is defined with reference to the high frequency and high power capability of the Gunn device and places a limit on the device's performance.

The *Quality factor* (QF) is the thermal figure of merit for the heat sink material and the active device area in the power device.

Table 2.1 tabulates a comparison of the figures of merit for GaAs and GaN devices and their limitations (Pearton *et al.*, 2000:55-212; Alekseev *et al.,* 2000:941- 947; Buniatyan *et al.,* 2007:6355-6385).

Table 2.1 Figures of merit for GaAs and GaN devices

Material	JM	KM	QF	Processing maturity	Key technical issues and limitations
GaAs	7.1	0.45	5.2	High	Contact stability at high temperature
GaN	756	1.6	560	Very low	Material quality and ohmic contacts

From Table 2.1 it is observed that overall the frequency and thermal figures of merit for GaN are significantly higher than for GaAs. The superior Gunn performance of GaN, as compared to GaAs, is a result of the following material properties and characteristics (Foutz *et al.*, 1997:2849-2852; Alekseev *et al.,* 2000:941-947):

- Energy band gap: GaN 3.4 eV, GaAs 1.3 eV.
- Thermal conductivity: GaN 130 W/m-K, GaAs 50 W/m-K.
- Critical electrical field: GaN 200 MV/m, GaAs 50 MV/m.
- Saturation velocity: GaN 2 x 10^5 m/s, GaAs 1 x 10^5 m/s.
- Inter-valley transfer relaxation time: GaN 1.2 ps, GaAs 7.7 ps.
- Operational thermal limit: GaN is expected to have an operational limit higher than GaAs due to the higher energy band gap.

This section concludes with a further comparison of GaN (Wz) and GaN (Zb) relevant to Gunn operation. These are listed below:

- GaN (Wz) exhibits a higher threshold electric field of 180 x 10^8 V/m as compared to 110 x 10^8 V/m for GaN (Zb) (Krishnamurthy *et al.,* 1997:1999-2001; Kolnik *et al.,* 1995:1933-1038).
- GaN (Wz) exhibits a higher electron drift velocity, supporting higher operational frequencies (Joshi *et al.,* 2003:4836-4842).
- Analytical expressions for the GaN (Wz) energy band structure are available (Joshi *et al.,* 2003:4836-4842).

- At ambient conditions GaN (Wz) exhibits a more thermodynamically stable structure (Alvi *et al.*, 2010: 2431-2435).
- The commonly form of crystallisation in GaN semiconductor material is the Wz crystal form (Alvi *et al.,* 2010: 2431-2435).

The relevant material parameters for GaAs and GaN are listed in Annexure A.

2.3 Concepts in Gunn diode optimisation

2.3.1 Harmonic mode operation

Studies have shown that GaAs Gunn diode oscillators are inefficient at fundamental frequencies above 40 GHz (E2V Technologies, 2002). This inefficiency is mainly due to the transit time of the Gunn domains through the active region of the device that is shorter than the period of oscillation at these frequencies. The Gunn diode also exhibits the presence of a *dead zone* near the cathode (see next section), which further limits the effective length of the transit region over which Gunn domains can form and develop.

GaAs Gunn diodes operating above 40 GHz therefore generally rely on harmonic power generation (Haydl, 1983: 879-889). As will be reported in Chapter 3, the upper frequency limit of the fundamental mode of NDR-based power generation for bulk GaAs is between 80 GHz and 100 GHz depending on the operational temperature and doping densities of the transit regions (Francis *et al.,* 2015: 825-828); likewise, for GaN diodes this limit is expected to be between 250 GHz and 300 GHz.

In this work, harmonic output power at the fundamental, second and third harmonics are investigated.

2.3.2 Dead zone

Due to the finite distance that electrons require to transfer to the higher energy satellite valleys, a so-called *dead zone* exists adjacent to the cathode contact where Gunn domains do not form. The dead zone does not contribute to the active operation of the Gunn diode and effectively adds positive parasitic resistance to the device. Hence, to increase the efficiency of the device, it is imperative to reduce the width of this dead zone. Neylon *et al.* (1989:519-522) proposed that a reduction of the dead zone could be

achieved by using combinations of a doping notch at the cathode, grading the transit region doping profile, and hot electron injection.

These techniques are briefly described in the following sections.

2.3.3 Doping notch

The notch is a nominally under-doped section preceding the transit region on the cathode side. It promotes the formation of Gunn domains closer to the cathode; hence, reducing the dead zone. The *width* and *doping level* of the notch determine its effectiveness in initiating domain formation, whilst not adding unnecessary series resistance to the diode, and are therefore parameters that will be optimised. As an example, Figure 2.5 illustrates the diode efficiency as a function of doping notch width of a GaN Gunn diode (Sevik *et al.,* 2004:188-190). The incorporation of a doping notch has been reported widely in the literature; see as examples the references listed in Tables 2.2 and 2.3.

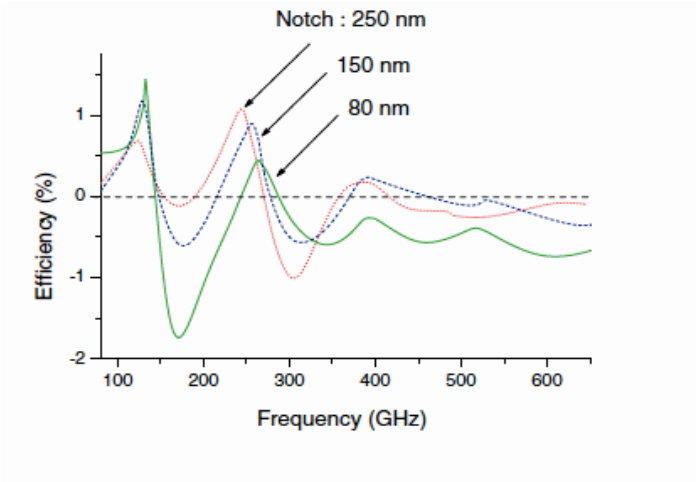

Figure 2.5 GaN diode efficiency as a function of frequency and width of doping notch

(From Sevik *et al.,* 2004:188-190)

2.3.4 Graded transit region doping profile

Batchelor (1992:735-741) reported that a uniform resistivity profile across the active (transit) region yields an optimum device efficiency, which has led to the implementation of a graded doping profile across this region. Additionally, appropriate grading of the doping profile reduces the heating effect associated with hot electron injection and therefore further enhances the microwave performance of the device. Increasing the

doping density from cathode to anode enhances both diode efficiency and output power (Vaidyanathan *et al.,* 1991:1555-1557).

In the work presented here, the doping concentration is increased exponentially towards the anode over the last 25% of an otherwise uniformly doped transit region. Notably, to reliably simulate the effect of the graded doping profile on the internal heating of the diode, the temperature profile is determined throughout the device and not assumed constant.

2.3.5 Hot electron injection

The electrons are injected from the cathode contact into the transit region with an elevated energy, typically of the order of the energy gap between the central and satellite valleys (Greenwald *et al.*, 1988:1211-1214; Beton *et al.*, 1988:434-435; Neylon *et al.,* 1989:519-522; Couch and Spooner, 1989:34-35). This enhances the probability of immediate electron scatter and transfer to the satellite valleys; hence, reducing the dead zone.

Figure 2.6 illustrates the general energy diagram of a hot electron launcher for zero bias and forward bias. The electrons essentially traverse a potential energy 'cliff', gaining additional energy as they move across the injector into the active region.

The $Al_xGa_{1-x}As$ heterostructure launcher implemented in GaAs diodes, typically, is undoped and has a linearly increasing Al mole fraction over a distance l_1, followed by a decreasing Al mole fraction over a much shorter distance l_2. This is followed by a very narrow n^+ doping spike, which acts as a non-equilibrium connector that prevents a depletion region to extend into the transit region.

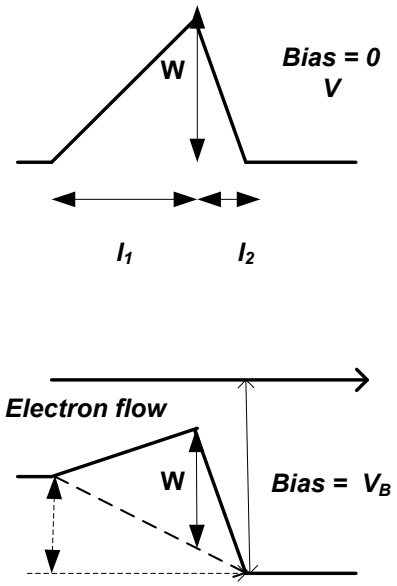

Figure 2.6 Typical hot electron launcher energy diagram

(From Greenwald *et al.,* 1988:1211-1214)

Figure 2.7 illustrates the typical doping profile of a single-domain Gunn diode incorporating a hot electron launcher and doping notch:

- Regions 1 and 6 are highly doped ohmic contact regions.
- Region 2 is an un-doped $Al_xGa_{1-x}As$ layer with linearly increasing Al concentration.
- Region 3 is a narrow n^+ doping spike.
- Region 4 is an under-doped notch.
- Region 5 is the transit region (nominally flat doping profile shown here).

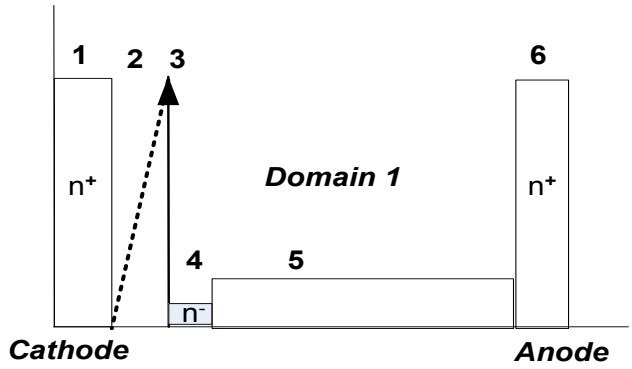

Figure 2.7 Doping profile of a single-domain Gunn diode using hot injectors

(Adapted from Van Zyl, 2006)

The energy gained by the electrons is mainly dependent on the graded Al composition profile 'x' and less on the bias voltage. Furthermore, the electron temperature associated with the launcher far exceeds the crystal temperature of the diode. The hot electron injector therefore reduces the dependence of the diode's operating frequency on bias voltage as well as ambient temperature, in addition to reducing the dead zone. Further advantages include improved oscillator turn-on characteristics at low temperatures and a decrease in the turn-on voltage of the Gunn diode.

Hot electron injection, however, causes high electric fields at the anode side of the transit region and leads to excessive heating in this area. This offsets the expected increase in output power and efficiency of diodes with hot electron launchers (Neylon *et al.,* 1989:519-522). As stated above, grading of the transit region doping profile can reduce this heating effect (Batchelor, 1992:735-741) and should be incorporated.

2.3.6 Multi-domain Gunn diode operation

A multi-domain Gunn diode essentially consists of multiple series-connected transit regions, separated by highly doped buffer regions that quench the electric field. Kroemer (1964:1980-1981) first stated that increasing the number of domains 'N' in a Gunn device could enhance its output power. When comparing the performance of a single-domain diode with an N-domain diode, it should be assumed that the bias conditions in each transit region, as well as the overall device impedance, are similar. Hence, an N-domain diode requires a bias voltage and a cross-section that are N-times larger than that for the single-domain diode. This results, theoretically, in an N^2 increase in both output power and power dissipation (Tsay *et al.,* 1990:54-60; Lau *et al.,* 2007:245-248; Teoh *et al.,* 2002:1090-1095). However, the N^2 increase in output power is never achieved due to excessive thermal losses associated with multi-domain Gunn diodes.

Multi-domain GaAs diodes

Multi-domain diodes were first proposed in the 1960's when Thim (1968) stacked several wafers on top of the other, forming a multi-domain GaAs Gunn diode. In subsequent research, a horizontal diode was implemented with multi-domain nucleation centers forced by literally scratching the surface of the active layer (Slater and Harrison, 1976: 560-567). Talwar (1979) reported a two-domain GaAs Gunn diode oscillator operating at

a frequency of 73 GHz, predicting twice the output power as compared to a single-domain Gunn diode.

Teoh *et al.* (2002:1090-1095) investigated the performance of multi-domain GaAs Gunn diodes using the MCPS technique. Figure 2.8(a) illustrates the output power as a function of the number of regions, indicating that the output power is approximately proportional to the number of transit regions. The power conversion efficiency of the diode is, however, much less sensitive to the number of domains. It was further shown that multi-domain Gunn diodes having unequal transit regions display a broader frequency response, as compared with a device with identical transit region lengths. Diodes with unequal transit lengths (1L, 2L, 3L, …) exhibit multiple resonating frequencies, implying that these diodes can be used in oscillating circuits to widen the electronic tuning range (Teoh e*t al.*, 2005:418-422).

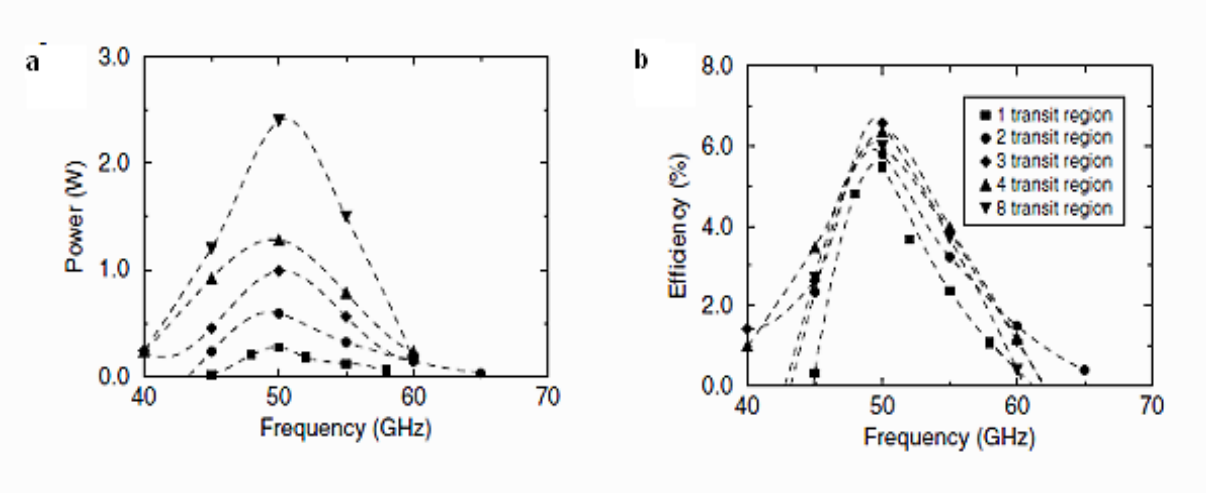

Figure 2.8 (a) Output power and (b) efficiency of multi-domain GaAs Gunn diodes as a function of frequency

(From Teoh *et al.* 2005: 418-422)

Multi-domain GaN Gunn diodes

Joshi *et al.* (2003: 4836-4842) investigated the multi-domain operation of a notched GaN (Wz) Gunn diode as presented in Figure 2.9 (3-domain diode shown). The output power of these diodes is shown in Figure 2.10.

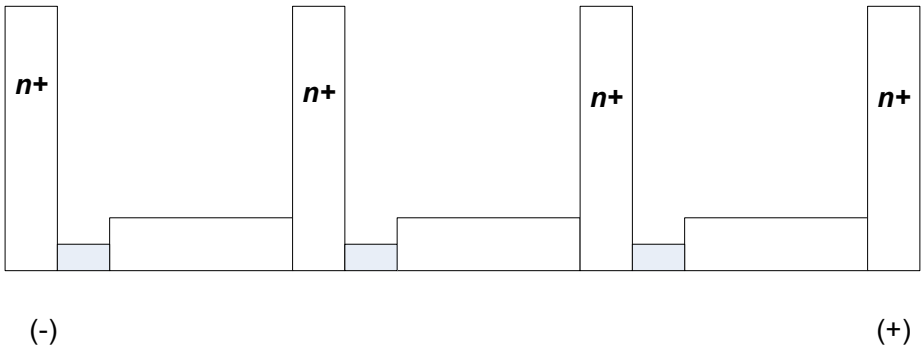

Figure 2.9 Three-domain GaN Gunn diode with doping notch

(Adapted from Joshi *et al*., 2003: 4836-4842)

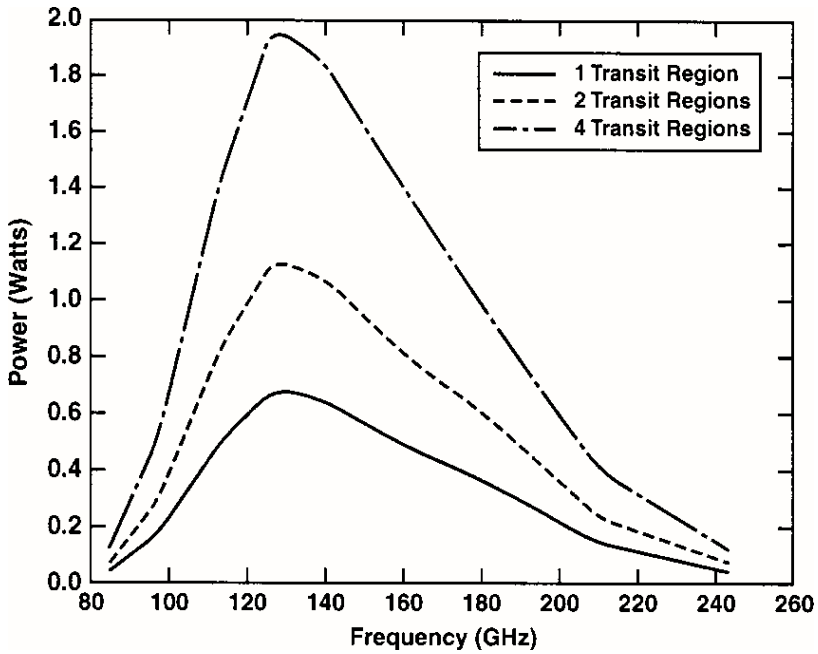

Figure 2.10 Simulated output power of a multi-domain GaN Gunn diode

(From Joshi *et al*., 2003: 4836-4842)

Joshi *et al.* (2003: 4836-4842) further reasoned that the noise performance of a single-domain diode is superior to that of multi-domain diodes. This is attributed to the charge carriers in a single-domain diode being thermalised, with similar energies. The thermalisation of the charge carriers leads to a "closely bunched" charge distribution. The overall effect of the closely bunched charge distribution is reduced noise. On the other hand, in a multi-domain GaN Gunn diode the charge distribution at the start of each successive transit region is not periodic. This leads to a thermal gradient between the two terminals of the diode, exhibiting a larger inconsistency in the inter-valley transfer

of electrons. This translates into increased thermal noise in multi-domain diodes as compared to single-domain diodes.

Note: The simulations above for both GaAs and GaN diodes are deemed unrealistic, as they do not take into consideration the increase in power dissipation due to increased heating with an increasing number of domains. As is evident from the simulations presented in Chapters 4 and 5, where thermal heating is incorporated into the simulations, the maximum number of domains appears to be two for both GaAs and GaN diodes.

Multi-domain operation with multiple hot-electron launchers

Van Zyl (2006) proposed a diode structure incorporating multiple domains, each incorporating a hot electron injector, graded doping profile and doping notch. This structure is illustrated in Figure 2.11.

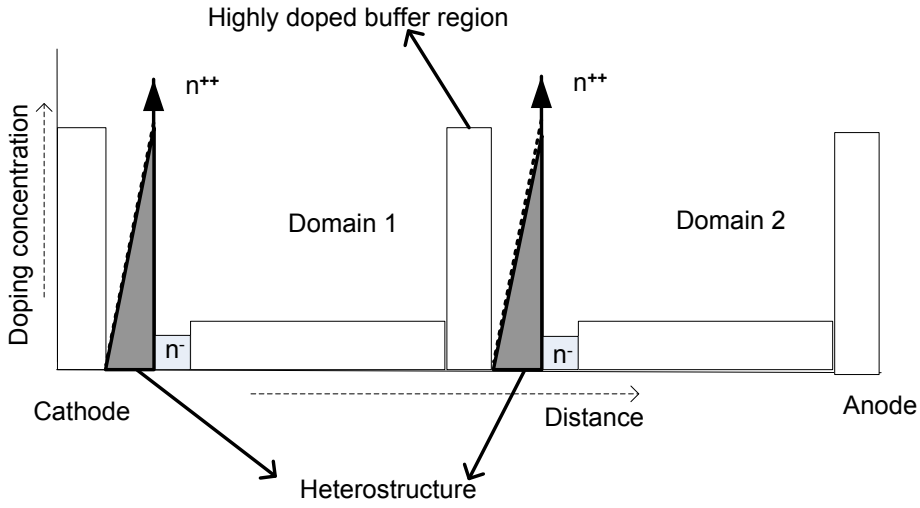

Figure 2.11 Typical doping profile of a two-domain Gunn diode with hot electron injection and doping profile engineering

(Adapted from Van Zyl 2006)

2.4 Development trends in GaAs and GaN Gunn diode technology

With the above brief background of the various concepts in Gunn diode optimisation, this section deals with notable technological developments of GaAs and GaN diodes.

2.4.1 GaAs Gunn diodes

Recent technological developments are listed chronologically in Table 2.2.

Table 2.2 Technological developments of GaAs Gunn diodes from 1989 to 2015

Year	Reference	Number of domains	Structure	Simulation/ Experimental	Output characteristics: Frequency 'f' Output power 'P_o' Efficiency 'η'
1989	Spooner and Couch, 1989:34-35	1	Heterostructure, doping notch	Simulation	f = 75 to 110 GHz P_o = 80 mW (90 GHz) P_o = 58 mW (94 GHz) η = 2.4 %
2000	Alekseev *et al.,* 2000:941- 947	1	Doping notch	Simulation at fundamental frequency	f = 40 GHz P_0 = 6 mW
2002	Teoh *et al.,* 2002:830-831	1 2 3 4 8	Doping notch	Simulation at fundamental frequency	f ~ 50 GHz P_o = 0.25 W η = 5.4 % f ~ 50 GHz, P_o = 0.5 W η = 5.5 % f ~ 50 GHz, P_o = 1 W η = 6.7 % f ~ 50 GHz, P_o = 1.4 W η = 6.2 % f ~50 GHz, P_o = 2.5W η = 6 %
2005	Teoh *et al.,* 2005:418-422	2 (I_1~I_2) 2 ($I_2 = 2I_1$) 3 ($I_3 = 3I_1$ $I_2 = 2I_1$)	Doping notch	Simulation at fundamental frequency	f = 57 & 62 GHz (two resonating peaks) P_o = 0.6 W η = 6 % f = 25 & 50 GHz (two resonating peaks) P_o = 0.4 W η = 6 % f = 15, 30 & 50 GHz (three resonating peaks) P_o = 0.1 W η = 3%
2006	Van Zyl, 2006	2	Heterostructure, doping notch	Simulation at second harmonic	f = 94 GHz P_o = 160 mW η = 1.9%

2006	Förster *et al.,* 2006:350-360	1	Heterostructure	Experimental at second harmonic	f = 77 GHz P_0 = 50 mW to 90 mW
2007	Lau *et al.,* 2007:245-248	1 2	Doping notch	Experimental Experimental	f = 77 GHz P_0 = 54 mW f = 77 GHz P_0 = 64 mW
2009	Mohamed *et al.,* 2009	1	Heterostructure	Simulation second harmonic Experimental at second harmonic	f = 98 GHz P_o = 21 mW f = 98 GHz P_o = 21 mW
2010	Farrington *et al.*, 2010:281-284	1	Heterostructure	Experimental at second harmonic	f = 122 GHz P_o = 40 mW
2013	Khalid *et al.*, 2013:686-688	Multi-channel	Planar structure	Simulation at Fundamental frequency	f = 109 GHz P_o = -4 dBm
2014	Maricar *et al.,* 2014:2449-2451	1	Planar structure	Simulation at Fundamental frequency	f = 120 GHz P_o = -9.14dBm
2015	Sharma *et al.,* 2015:619-624	1	Heterostructure	Simulation at Second harmonic	f = 94 GHz peak current = 0.86 A

The current state of the art

Priestley and Farrington (2010), at the time, reported record RF output power of 40 mW at 122 GHz with a single-domain diode. The average RF output power from a batch of ten diodes was 32 mW. The diode structure incorporates a thin (<50 μm) n^+ doping spike and a graded $Al_xGa_{1-x}As$ launcher. The major fabrication challenge was heat sinking. A gold Integral Heat Sink was used, supported by alumina as its packaging material.

Figure 2.12 summarises a compilation of published state-of-the-art performance results up to 400 GHz for GaAs and InP Gunn diodes under CW operation (Farrington *et.al*., 2008).

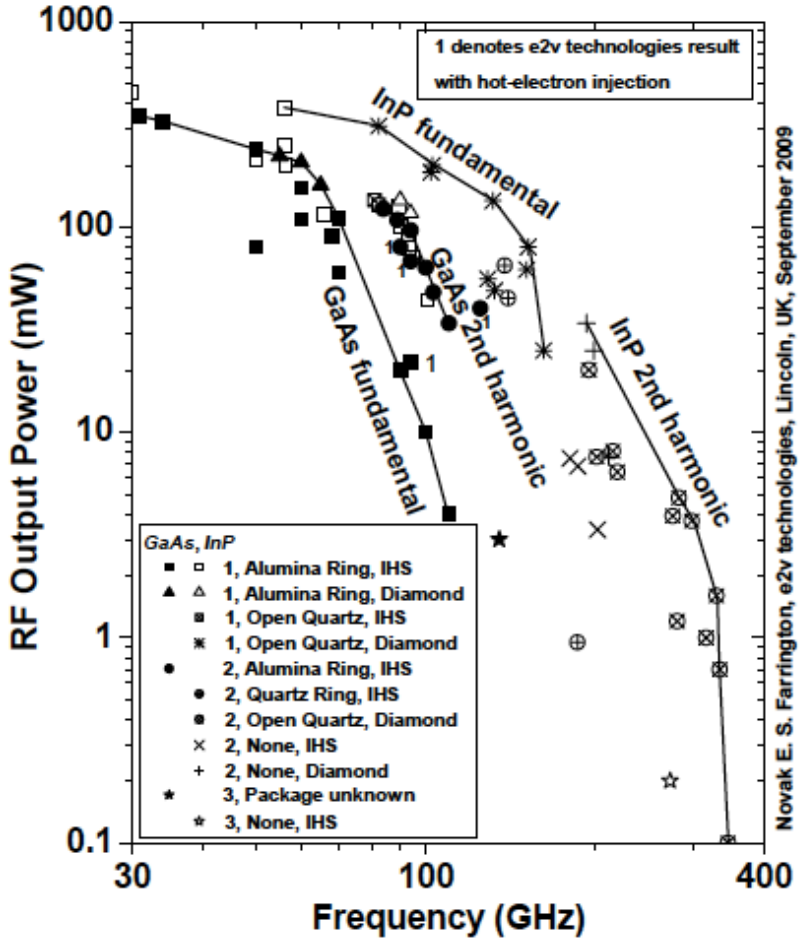

Figure 2.12 State-of-the-art GaAs and InP Gunn diode RF performance

(From Farrington *et.al.,* 2008)

The first epitaxially grown two-domain GaAs Gunn diode was reported in 2007 (Lau *et al*., 2007:245-248). The output power of the two-domain diode was 64 mW at 77 GHz, compared to 54 mW for the single-domain diode.

2.4.2 GaN Gunn diodes

Littlejohn, Hauser and Glisson (1975) first reported the phenomenon of negative differential resistance in GaN semiconductor material and postulated that GaN semiconductor devices can be used as a source of microwave energy. The development of GaN Gunn diodes has been hampered due to the poor mechanical properties and crystal imperfections of the semiconductor material, which hinder the fabrication of these devices consistently and reliably (Kelly, 1993:723-729).

Major challenges in fabricating GaN devices are (Hao *et al.,* 2008:51-64):

- control of threading location in the GaN crystal;
- ionised impurity scattering in semiconductor material growth; and
- formation of excellent ohmic contacts on the device.

GaN crystallises in Wurtzite (Wz) and Zincblende (Zb) crystal forms with slightly different material properties (Min, Chan and Ho, 1992:1159) that lead to varying energy band diagrams, and different mechanisms of negative differential resistance (Kolnick *et al.,* 1995:1933-1038; Krishnamurthy *et al.,* 1997:1999-2001). A comparison of the GaN (Wz) and GaN (Zb) material properties is listed in Annexure A.

Recent technological developments are summarised chronologically in Table 2.3.

Table 2.3 Technological developments of GaN Gunn diodes from 2000 to 2015

Year	**Reference**	**Number of domains**	**Structure**	**Simulation/ Experimental**	**Output characteristics Frequency 'f' (GHz) Output power 'P_o' Power density 'P_D' Efficiency 'η'**
2000	Alekseev *et al.,* 2000:941-947	1	Homogenous doping	Simulation at fundamental frequency	f = 87 GHz P_0 = 6.3 W
2001	Alekseev *et al.,* 2001:1462-1469	1	Homogenous doping	Simulation at harmonic frequency	f = 774 GHz P_0 = 1 W η = 0.7%
2003	Joshi *et al.,* 2003:4836-4842	1	Doping notch	Simulation at harmonic frequency	f = 135 GHz P_o = 0.67 W
		2			f = 135 GHz P_o = 1.1 W
		4			f = 340 GHz P_o = 1.9 W
2004	Sevik *et al.,* 2004:369-377	1	Doping notch	Simulation at fundamental frequency	f = 150 GHz η = 0.9 ~ 1%

2004	Pavlidis, 2004:551-554	1	Doping notch	Simulation	f = 750 GHz η = 1%
2007	Yilmazoglu *et al.,* 2007:1-3	1	Doping notch	Experimental at fundamental frequency	f = 38 GHz P_o = 2.7 W η = 1%
2008	Macpherson *et al.,* 2008:005-012 2008:103-105	1 1 1	Homogenous doping Doping notch Doping spike	Simulation	f = 300 GHz f = 280 GHz f = 230 GHz
2009	Panda, 2009:4-6	1	Doping notch	Simulation	f = 94 GHz P_D = 1.4 x 10^6 W/cm^2
2011	Aloise *et al.,* 2011:599-602	1	Doping notch	Simulation	f = 200 GHz P_D = 6 x 10^4 W/cm^2
2013	Francis *et al.,* 2013:177-182	1	Doping notch	Simulation at 3rd harmonic	f = 525 GHz P_o = 42 mW
2013	Garcia *et al.,* 2013:001-024	1	Doping notch	Simulation at 6th harmonic, constant temperature	f = 675 GHz η = 0.1 %
2015	Francis *et al.,* 2015:177-182	2	Doping notch	Simulation at 3rd harmonic	f = 525 GHz P_o = 87 mW

2.4.3 Gunn oscillator characteristics

Gunn oscillator performance is dependent on frequency, bias conditions and temperature.

Output power versus frequency

Gunn diodes can operate in a wide range of frequencies if used in a properly designed resonant circuit. Maximum output power is obtained at an optimum frequency, with roll off either side of the centre frequency. The diode also has an inherent cut-off frequency, as described in previous sections, above which no output power is predicted (Haydl, 1983: 879-889).

Output power versus temperature

The frequency of oscillation of the Gunn diode is a function of its operating temperature as it impacts the electron dynamics underlying the transit mode of operation (E2V Technologies, 2002). Output power is also sensitive to temperature, as an increase in temperature decreases the efficiency of the diode. This is a major challenge in Gunn diode design.

Output power versus bias voltage

The frequency of oscillation of the Gunn diode is dependent on the bias voltage (Batchelor, 1990). A minimum bias voltage (V_{ON}) is required for power generation in a Gunn diode. This minimum bias voltage provides the energy required to scatter the electrons into the higher energy satellite valleys. An increase in the bias voltage beyond the peak power voltage decreases the output power. This is mainly due to an increase in power dissipation in the Gunn diode.

2.5 Ensemble Monte Carlo particle simulation of devices

2.5.1 Overview of the algorithm

This section provides but a brief overview of the ensemble Monte Carlo particle simulation technique (EMCPST) that is deployed in this work. The reader is referred to a number of sources for more comprehensive discussions of this technique; see, for example, Jacoboni and Lugli (1989), Tomizawa (1993) and Moglestue (1993). The algorithm used in this work is implemented in parallel on a cluster of personal computers (Van Zyl *et al.,* 2000).

Applied to electron transport in semiconductors, the technique is capable of providing a statistically accurate solution of the Boltzmann Transport Equation (BTE) through simulating the probabilistic transport behaviour of electrons in real and momentum space (Moglestue, 1993). The algorithm follows the sequence of physical events as experienced by charge carriers within the confines of the device, and in fact closely resembles a *physical experiment*.

Typically, large sample spaces are required to reduce the statistical noise inherent to Monte Carlo simulations; hence, these algorithms are costly in terms of computational resource requirements. However, this powerful technique renders reliable simulations of

stead-state and *non-stationary* particle transport in semiconductors. Both of these mechanisms are relevant to the dynamic behaviour of electrons in the mm-wave Gunn devices simulated in this work. Classic simulations are based on drift-diffusion models (Sze, 2007) under the unrealistic assumption that charge carriers assume steady-state immediately after a field variation. Steady-state is in fact only reached after a finite time and associated distance. Drift-diffusion models can therefore not be used in simulations where the physical size of the device or the frequency of operation prohibits steady-state.

Figure 2.13 illustrates the typical flow diagram of an EMCPST algorithm for the simulation of devices (Van Zyl *et al.*, 2000:369-380).

An ensemble of charge carriers (in this case electrons) is accelerated under the influence of the electric field experienced by each individual carrier. This classical acceleration of the electrons is characterised by free flights with duration t_r, interrupted by scattering events. These events change the momentum state of the electron instantaneously. Each electron is then accelerated again until the next scattering event. The simulation of successive free flights and scattering events of the electrons in the ensemble continues until the electric field is updated throughout the device through solving Poisson's equation (Sze, 2007). This is done at intervals of T_{step}. To ensure consistency between the time-evolution of the electrons and the electric field distribution inside the device, T_{step} is usually of the order 5.10^{-15} s. Electrons that cross the contacts are removed from the simulation. Charge neutrality at the contact is maintained, which may require the reintroduction of electrons to those regions. The total number of electrons simulated is not kept constant artificially, but tends to fluctuate around the initial ensemble size.

The modelling of the electrons' dynamics is intrinsically dependent on the energy band of the bulk material, and the scattering mechanisms implemented. In this work, a 3-valley energy band with non-parabolicity has been implemented for GaAs and GaN. The following scattering mechanisms have been implemented (Van Zyl, 2006): acoustic phonon (intra-valley scatter), polar optical phonon (intra-valley), inter-valley (both acoustic and optical phonon), and ionised-impurity (intra-valley).

Lastly, it should be noted that the simulation of the two-terminal Gunn devices are treated as 1-dimensional problems.

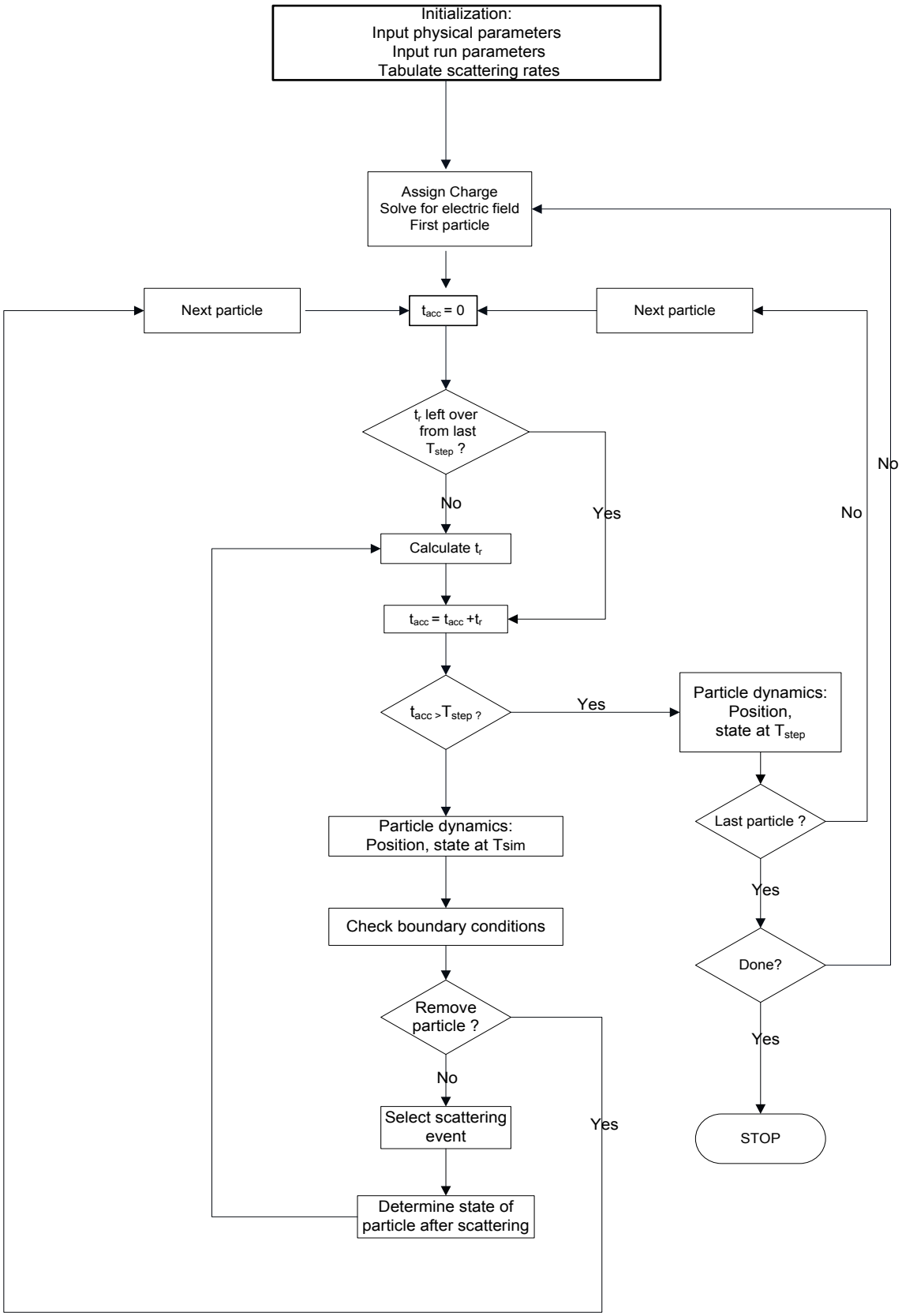

Figure 2.13 EMCPST algorithm for Gunn device simulation

(Adapted from Van Zyl *et al.*, 2000)

2.5.2 Output charaterisation of device

The simulation of the device within a resonant cavity is achieved through applying a terminal voltage $v_d(t)$ across the Gunn diode of the form

$$v_d(t)=V_{DC} + V_1 \sin(\omega_0 t) + V_2 \sin(2\omega_0 t + \phi_2) + V_3 \sin(3\omega_0 t + \phi_3) \quad \textbf{Equation 2.5}$$

where V_{DC} is the DC bias voltage, ω_0 is the fundamental frequency, and V_1, V_2 and V_3 denote the harmonic voltage amplitudes of the fundamental, second and third harmonics, respectively. The i^{th} harmonic is, generally, phase delayed by Φ_i. The foregoing parameters are varied to maximise the output power, which is akin to tuning the diode in the cavity.

The microwave conversion efficiency of the diode at its i^{th} harmonic is given by

$$\eta_i = \frac{P_i}{P_{DC}} = \frac{P_i}{I_{DC}V_{DC}} \quad \textbf{Equation 2.6}$$

where P_i represents the output power at the i^{th} harmonic and $P_{DC} = I_{DC}V_{DC}$ is the DC input power.

At any instant of time the total device terminal current is the sum of its displacement and particle current components. The particle current can be determined by counting the number of electrons crossing the contacts during each time step. However, this method of determining the particle current leads to a 'noisy current' and potentially corrupts the output power calculation. The method adopted here is the one proposed by Van Zyl (2006), where the particle current is determined by

$$i_p = \frac{q_s A}{k_2 - k_1} \sum_{m=k_1}^{k_2} n_m v_m \quad \textbf{Equation 2.7}$$

where: q_s is the "super particle" charge;

A is the cross-sectional area of the active region;

n_m is the number of super particles at mesh point m;

v_m is the electron velocity at mesh point m; and

k_1, k_2 denote the mesh points corresponding to the respective boundaries of the ohmic region.

The displacement current in the contact regions is insignificant due to the small temporal variation in the electric field in these regions. The device current is therefore accurately

determined through Equation 2.7. The concept of a "super particle" is required because of the relative small number of electrons simulated, compared to the actual number of electrons in the real device. The charge of the super particle is weighted to compensate for the shortage of actual electrons in the simulation.

The bias current I_{DC} is of course not known at the start of the simulation, but is built up through the accumulated time-average of the total terminal current.

Fourier analyses of the device terminal current and applied voltage are used to determine the harmonic output power P_i as well as the device admittance Y_{Di} at each harmonic. The device admittance is usually of the form $Y_{Di} = -G_{Di} + jB_{Di}$ [S] due to the negative differential resistance and capacitive nature of the Gunn device under normal operating condition.

Electrical losses due to the bonding wires and packaging of the diode are simply modelled with a resistor R_{loss} in series with the admittance of the device. Typical values for R_{loss} are of the order 0.1 Ω at around 50 GHz to 0.2 Ω at 100 GHz.

2.5.3 Thermal modeling of the device

The internal temperature profile of the diode is calculated through solving the steady-state heat flow equation (Carslaw and Jaeger, 1950)

$$\nabla(K \nabla T) + Q = 0 \qquad \textbf{Equation 2.8}$$

where K is the thermal conductivity of the material, Q is the steady-state heat dissipation density within the device and T the temperature distribution. For one-dimensional simulations, the steady-state heat dissipation density $Q(y)$ is simply the product of the bias current density and electric field at any position y.

To solve Equation 2.8 discretely, Zybura *et al.* (1995: 873-880) divided the device into layers, with the assumption that the thermal conductivity and heat generation throughout each layer is constant. They treated the transit region of the diode as a single layer, which is a crude assumption. In fact, grading the doping profile throughout the active region can reduce heating of the diode (Batchelor, 1992). In the simulations presented here, the active region is also divided into layers and the temperature distribution updated at regular intervals. Thus, the determination of the temperature profile of the

transit region is improved and *consistent with the steady-state distribution of the electrons in the active region*.

2.6 Thermal management in Gunn diodes

The thermal management of Gunn diodes is very important, as they suffer from significant heating due to their low efficiencies. As pointed out earlier, both the output power and operating frequency are sensitive to the temperature of the diode.

GaN Gunn diodes are especially vulnerable to thermal dissipation due to their higher bias voltage than for GaAs diodes. The heating of GaN diodes also leads to an increased leakage current (Kohn *et al.*, 1998:105-112), which results in a reduction of the channel mobility (Seelman *et al.*, 2001:744-749).

A reduction of the operating temperature of the diode is achieved by spreading the heat from the localised Gunn diode source over a larger part of the device through proper heat sinking. Heat dissipation takes place primarily in the transit region close to the anode (Van Zyl, 2006). The heat sink should therefore be placed as close as possible to the active region of the device, and on the anode side. An effective technique is that of incorporating an *integral heat sink* (IHS). This heat sink structure is suitable for high frequency, high output power microwave devices, due to the efficiency of heat sinking and thermal impedance profile shaping.

The fabrication process of the IHS is illustrated in Figure 2.14. The IHS is bonded to a heat stud. Gold is generally used for the IHS and copper for the heat stud due to their high thermal conductivities (K_{Au} = 311 $Wm^{-1}K^{-1}$, K_{Cu} = 393 $Wm^{-1}K^{-1}$ at 400 K).

Materials with a higher thermal conductivity can be used for more effective heat sinking. Diamond exhibits a high thermal conductivity exceeding 2000 $Wm^{-1}K^{-1}$ at room temperature and a high electrical resistance in the range of 10^{12} to 10^{16} Ω. Indeed, at temperatures of above 50 K, diamond exhibits the highest thermal conductivity of any known material (Graebner and Jin, 1998:52-55; Gurbuz *et al.,* 2005:1055-1070).

Another form of diamond generally used, is Chemical Vapour Deposited (CVD) diamond (Coeu and Sussmann, 2000:1726-1729). CVD diamond is artificially produced and exhibits material properties similar to that of diamond. The thermal conductivity of CVD

diamond varies between 2000 $Wm^{-1}K^{-1}$ and 3000 $Wm^{-1}K^{-1}$ depending on its quality, which makes this material highly suitable for effective heat sinking (Graebner *et al.,* 1998:52-55; Coeu *et al.,* 2000:1726-1729).

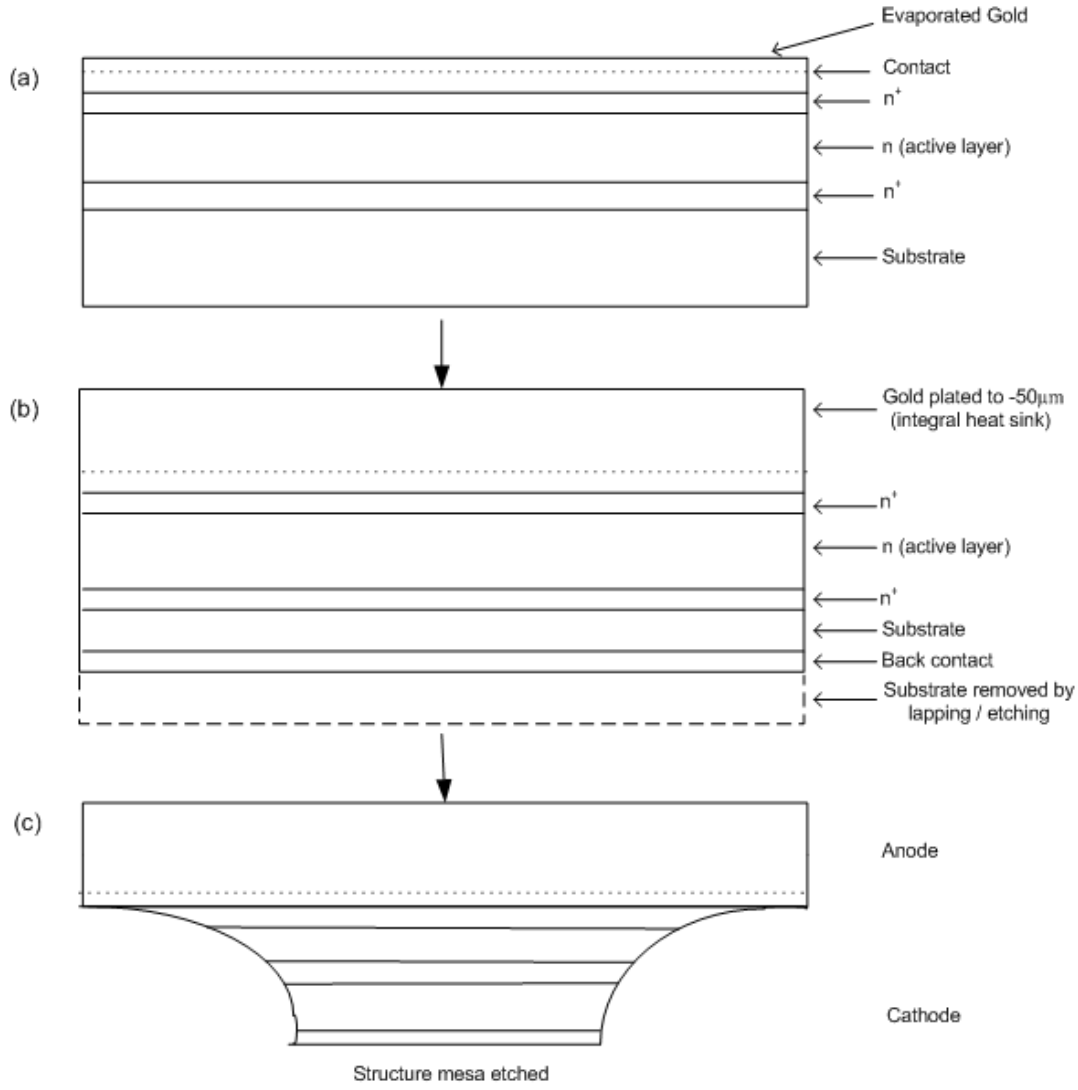

Figure 2.14 Fabrication process of an integral heat sink

(From Van Zyl, 2006)

2.7 Conclusion

Chapter 2 gives an overview of the historical and contemporary developments in GaAs and GaN Gunn diodes. This is contextualised with a discussion on the theory of the

Gunn effect. The various design parameters to enhance the performance of Gunn diodes at mm-wave frequencies are discussed.

The Monte Carlo particle simulation technique and how it is applied to the simulation of Gunn diodes is briefly described. The reader is referred to a number of sources in the literature for a deeper discussion of this method.

Chapter 3 investigates the operational frequency limits of GaAs and GaN Gunn diodes *empirically* through the simulation of the velocity-field characteristic of electrons in those bulk materials. The frequency limit of the transferred electron effect that gives rise to negative differential resistance and the Gunn effect is useful in predicting the highest fundamental frequency of operation of transferred electron devices, such as Gunn diodes.

3 SIMULATED EMPIRICAL DETERMINATION OF UPPER OPERATIONAL FREQUENCY LIMITS OF TRANSFERRED ELECTRON MECHANISM IN BULK GAAS AND GAN

3.1 Introduction

This chapter describes a novel, empirical technique to determine the upper operational frequency limit of the transferred electron mechanism in bulk GaAs and GaN (Francis and Van Zyl, 2015). The dynamic electron velocity versus electric field characteristic curve, or simply "*v-E* curve", is analysed to predict the highest operational frequency at which these materials still exhibit negative differential resistance (NDR) characteristics.

In Chapter 2 this limit was defined as the *NDR relaxation frequency* (f_{NDR}) in terms of the energy and inter-valley relaxation time constants (see Equation 2.4). However, linking the operational frequency limit of the NDR mechanism in a bulk material to f_{NDR} (in terms of the time constants) is overly simplistic. This estimation for f_{NDR} neglects the effects of temperature, electron scattering and doping on the non-stationary electron dynamics underlying the NDR mechanism at the operational limits of this mechanism. The empirical approach described in this chapter, whereby the dynamic *v-E* curves of GaAs and GaN are simulated and analysed, incorporates these effects implicitly and consistently in a time-dependent bulk ensemble Monte Carlo simulation of the material.

It is postulated that the upper operational frequency limit of the transferred electron and NDR mechanisms also constitutes the highest fundamental frequency of operation of transferred electron *devices*, which will be explored further in Chapters 4 and 5.

It should be noted that the predicted operational frequency limit of the NDR mechanism does not depend on the structure of the devices that exploit this mechanism, but is an intrinsic characteristic of the material. The actual operational frequency limit of transferred electron devices will be further reduced by structural constraints of the device, as well as the dynamics of Gunn domain formation within the device.

3.2 Method

As described in Chapter 2, the *v-E* curves of semiconductors that exhibit NDR have a characteristic negative slope above the threshold bias voltage (electric field). Furthermore, the dynamic *v-E* curves of transferred electron materials exhibit *hysteresis* (Bullman *et al.*, 1972). Towards the operational frequency limit of the transferred electron mechanism, this hysteresis behaviour progressively degrades the average slope of the *v-E* curve over an RF cycle to such an extent that the effective negative

differential resistance described by the curve disappears. Figure 3.1 illustrates the typical static and dynamic *v-E* curves for bulk material that exhibits NDR.

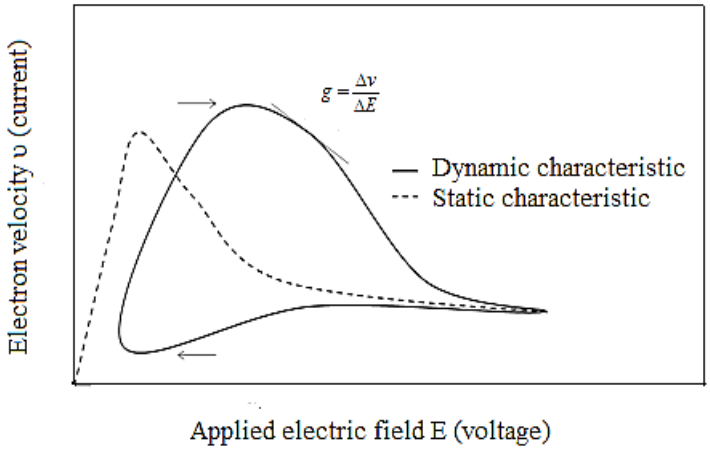

Figure 3.1 Typical static and dynamic velocity-field characteristic curves for bulk semiconductor that exhibits NDR

(From Bullman *et al.,* 1972)

Simulating the dynamic *v-E* curves of GaAs and GaN at increasing frequencies and analysing the average gradient over a complete cycle of the applied alternating electric field provide an empirical tool to determine the NDR relaxation frequency f_{NDR} and the operational frequency limit of the transferred electron mechanism. As stated earlier, this approach implicitly considers the *non-stationary* dynamics of electrons at frequencies approaching f_{NDR}, and at different temperatures and doping conditions. This estimation of f_{NDR} is considered to be more accurate than the time-constant approach described in Chapter 2.

For the purposes of this investigation, a variable g_{ave} is defined as

$$g_{ave} = \frac{1}{N}\sum_{i=1}^{N}\frac{\Delta v_i}{\Delta E_i} \qquad \textbf{Equation 3.1}$$

which is the average slope of the *v-E* characteristic curve over a complete cycle of an applied alternating electric field. The average is determined in a discrete manner over *N* samples.

The *v-E* curve of the bulk material corresponds to the *I-V* curve of the device that is based on that material (Sze *et al.,* 2007; Dinesh and Shirvastava, 2009). The g_{ave} parameter is therefore proportional to the average large signal conductance of the Gunn diode based on that particular material, at a certain frequency and bias voltage. A

negative value of g_{ave} indicates the existence of NDR in the bulk material. This gives a quantitative assessment of the strength of the NDR mechanism in the Gunn diode at the same frequency, and under similar bias, temperature and doping conditions.

The electric field applied to the bulk material is biased above the threshold to ensure that the conditions for the transferred electron mechanism are maintained.

3.3 Simulation

The method described above is applied to bulk GaAs and GaN at various operating conditions of temperature, doping concentration and frequency. The values of these parameters are chosen to correspond to the operating conditions of typical GaAs and GaN Gunn diodes to ensure a realistic estimation of the frequency limits of these devices. The doping concentration reflects typical values of the *transit regions* of Gunn diodes.

3.3.1 Simulated *v-E* curves and analyses of g_{ave} for bulk GaAs

Table 3.1 lists the simulation sets performed for bulk GaAs.

Table 3.1 Simulation sets for generating *v-E* curves of bulk GaAs

Simulation set	Doping concentration (m^{-3})	Frequency (GHz)	Temperature (K)	
1	$1x10^{22}$	40	300	450
2	$1x10^{22}$	50	300	450
3	$1x10^{22}$	60	300	450
4	$1x10^{22}$	80	300	450
5	$1x10^{22}$	100	300	450
6	$2x10^{22}$	40	300	450
7	$2x10^{22}$	50	300	450
8	$2x10^{22}$	60	300	450
9	$2x10^{22}$	80	300	450
10	$2x10^{22}$	100	300	450

Figures 3.2 and 3.3, respectively, illustrate the applied electric field and the average electron drift velocity of the ensemble of electrons in response to the applied electric field. Each graph is subdivided into eight equal intervals to determine g_{ave} by applying Equation 3.1.

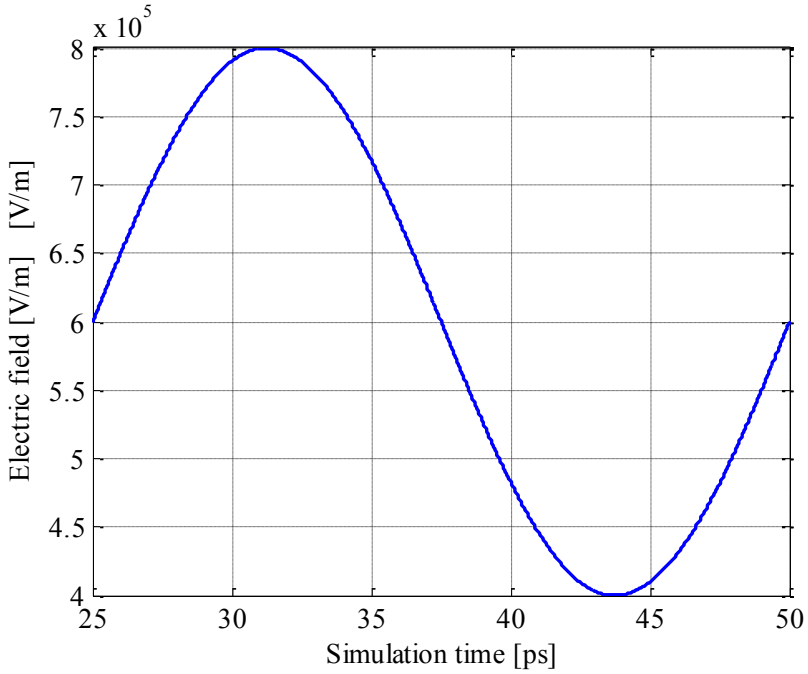

Figure 3.2 Applied electric field for generating *v-E* curves of bulk GaAs

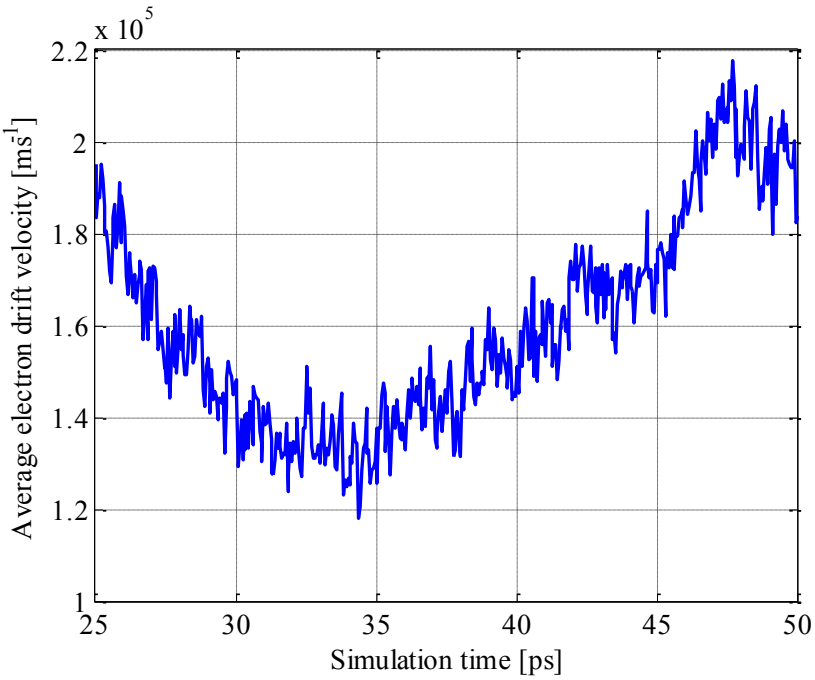

Figure 3.3 Average electron drift velocity of an ensemble of electrons in response to the applied electric field in Figure 3.2 for bulk GaAs

From the above, the dynamic *v-E* curves are generated. Figure 3.4, for example, shows the *v-E* curve for a relatively low operating frequency of 40 GHz, a temperature of 300 K, and a typical doping concentration of $1x10^{22}$ m^{-3}. As expected, the curve exhibits

hysteresis with a clear negative average gradient (g_{ave} = -0.075 (arbitrary unit)) over one complete RF cycle. The negative value of g_{ave} indicates the existence of negative differential resistance in bulk GaAs at 40 GHz and a temperature of 300 K. In contrast, Figure 3.5 presents the dynamic *v-E* curve at a higher operational frequency of 100 GHz and a temperature of 450 K. The value of g_{ave} over one RF cycle is now positive (+0.025 (arbitrary unit)) indicating the *absence* of NDR.

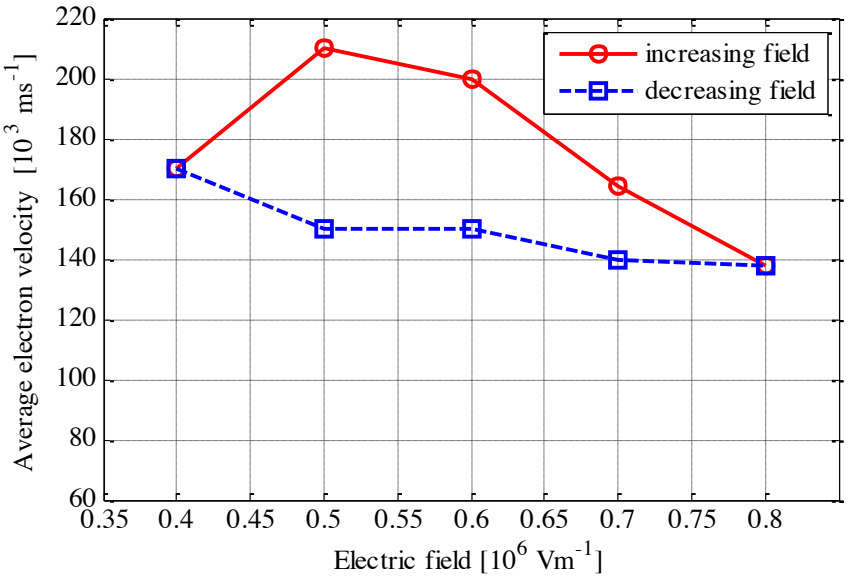

Figure 3.4 Simulated *v-E* curve of bulk GaAs at 40 GHz, 300 K, and doped at 1x10^{22} m^{-3}

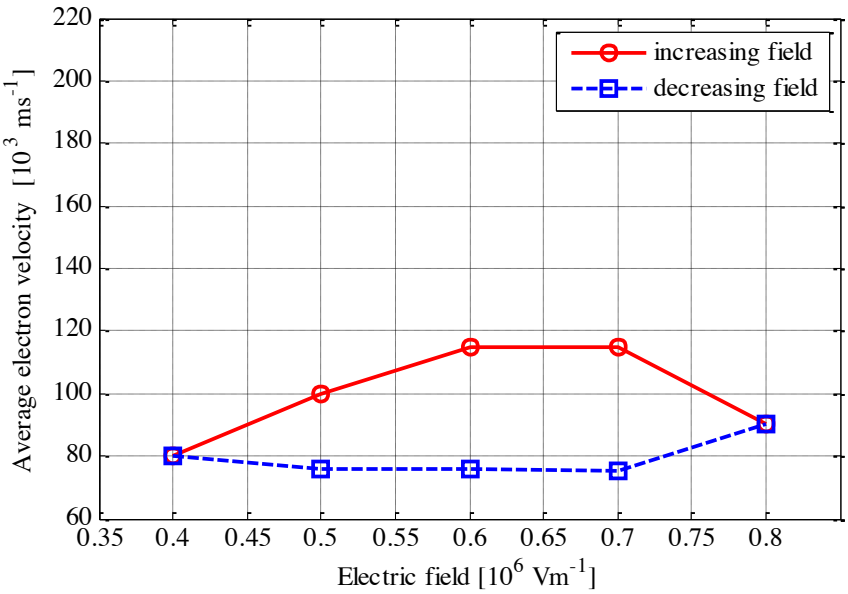

Figure 3.5 Simulated *v-E* curve of bulk GaAs at 100 GHz, 450 K, and doped at 1x10^{22} m^{-3}

From the simulated dynamic *v-E* curves for all simulation sets, the average gradient g_{ave} can be determined as a function of frequency at the various operating temperatures (T) and doping concentration levels (n_c). This is presented in Figure 3.6.

The zero-crossings are interpreted as the frequency limit of the transferred electron mechanism and NDR, and therefore, also the limit of operation in the fundamental mode of GaAs Gunn devices.

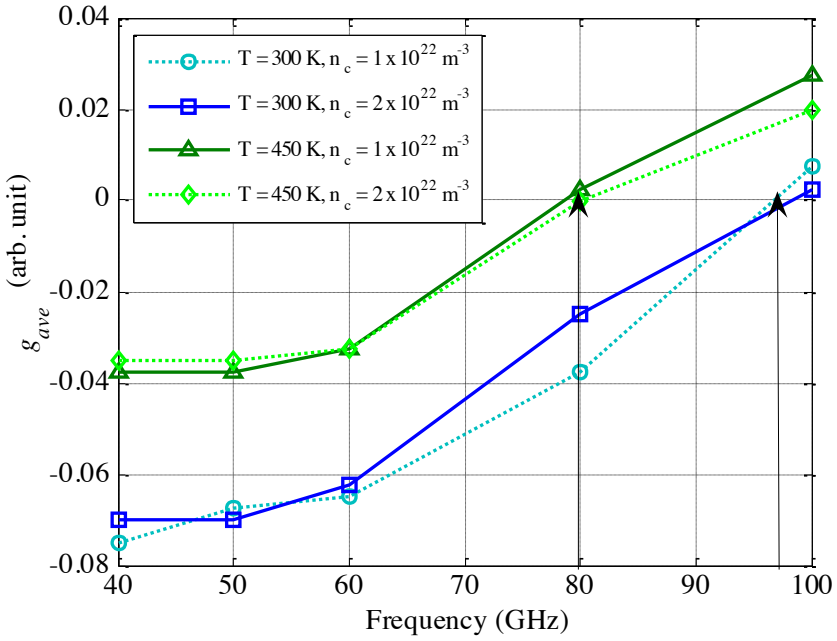

Figure 3.6 Simulated g_{ave} as a function of frequency for bulk GaAs

The following observations can be made from Figure 3.6:

- the value of g_{ave} increases monotonically from negative values at low frequencies to positive values at higher frequencies, indicating a progressive deterioration of the NDR with increased frequency;
- higher ambient temperatures degrade NDR significantly;
- the nominal doping concentration of the bulk material has a negligible effect on the frequency dependence of NDR; and
- the upper frequency limit for bulk GaAs to support NDR is between 80 GHz at 450 K and 100 GHz at 300 K.

3.3.2 Simulated *v-E* curves and analyses of g_{ave} for bulk GaN

A similar approach is followed as described in Section 3.3.1 for bulk GaAs. Table 3.2 lists the simulation sets performed.

Table 3.2 Simulation sets for generating *v-E* curves of bulk GaN

Simulation set	Doping concentration (m^{-3})	Frequency (GHz)	Temperature (K)	
1	$1x10^{22}$	60	300	400
2	$1x10^{22}$	80	300	400
3	$1x10^{22}$	150	300	400
4	$1x10^{22}$	200	300	400
5	$1x10^{22}$	300	300	400
6	$1x10^{22}$	400	300	400
7	$1x10^{23}$	60	300	400
8	$1x10^{23}$	80	300	400
9	$1x10^{23}$	150	300	400
10	$1x10^{23}$	200	300	400
11	$1x10^{23}$	300	300	400
12	$1x10^{23}$	400	300	400

Figures 3.7 and 3.8 illustrate the applied electric field and the average electron drift velocity, respectively, in response to the applied electric field in bulk GaN (Wz). The value of g_{ave} is calculated for each simulation, as explained in Section 3.1.

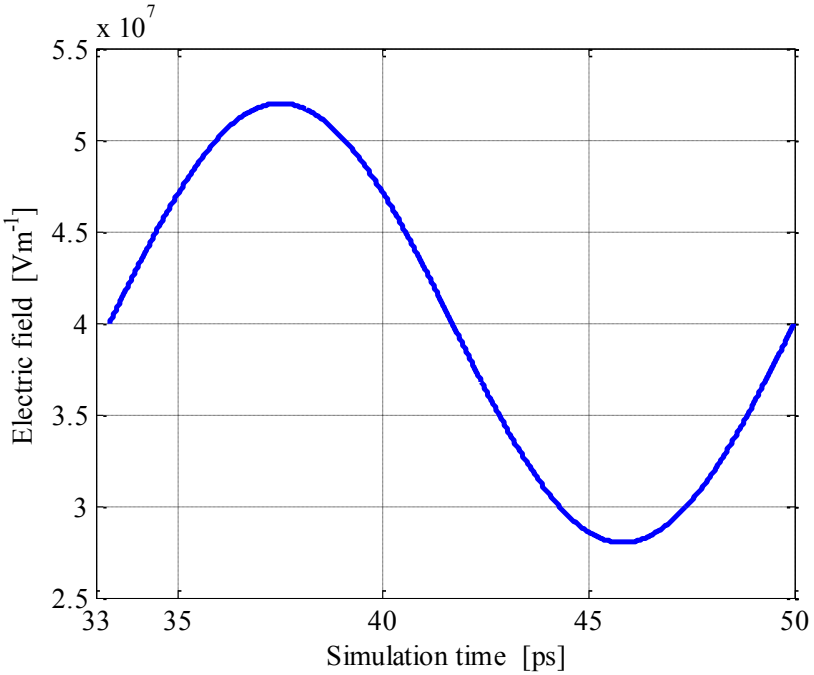

Figure 3.7 Applied electric field for generating *v-E* curves of bulk GaN

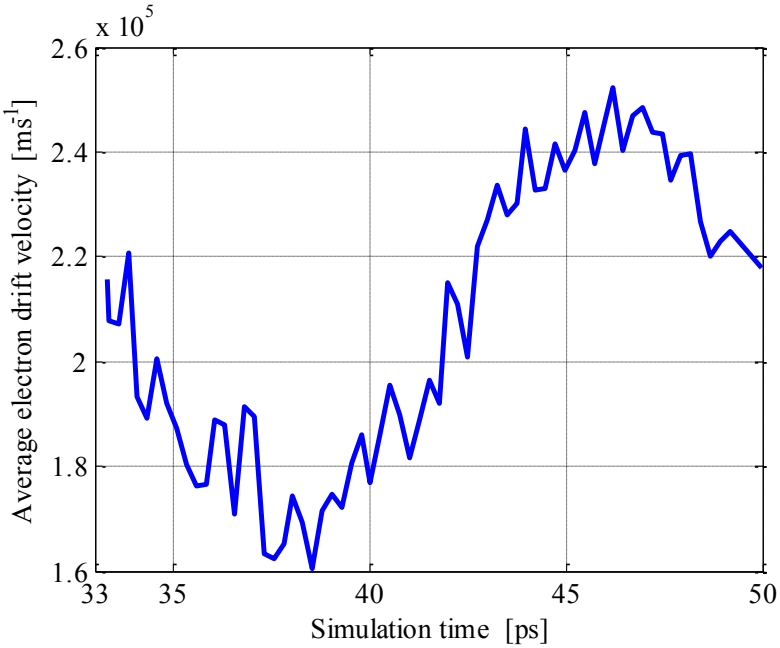

Figure 3.8 Average electron drift velocity of an ensemble of electrons in response to the applied electric field in Figure 3.7 for bulk GaN.

As a representative example, Figure 3.9 presents the simulated dynamic *v-E* curves for a relatively low operating frequency and temperature (60 GHz, 300 K).

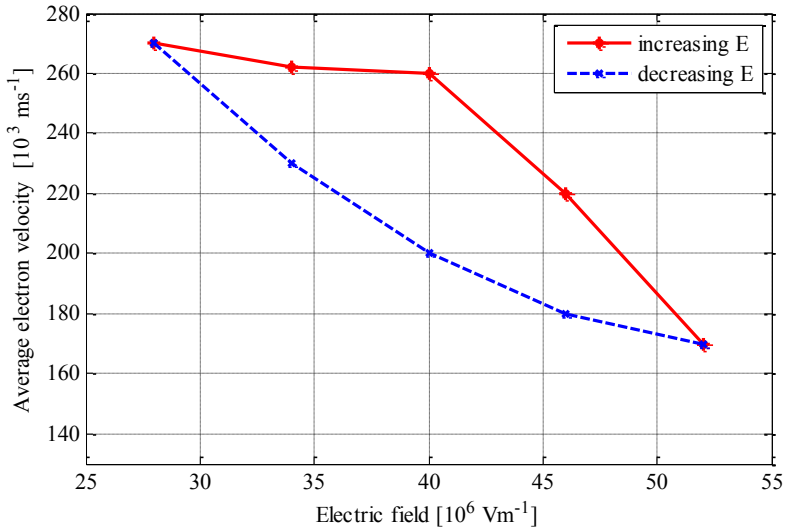

Figure 3.9 Simulated *v-E* curve of bulk GaN at 60 GHz, 300K and doped at $1x10^{22}$ m^{-3}

The frequency dependence of g_{ave} for each simulation set is illustrated in Figure 3.10.

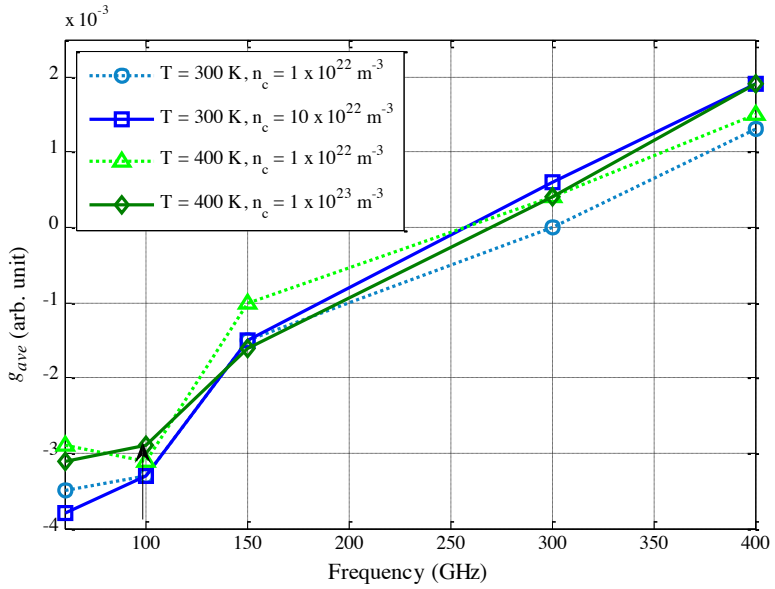

Figure 3.10 Simulated g_{ave} as a function of frequency for bulk GaN

The following observations can be made from Figure 3.10:

- the value of g_{ave} increases monotonically from negative values at low frequencies to positive values at higher frequencies, indicating a progressive deterioration of the NDR with increased frequency;
- higher ambient temperatures degrade NDR significantly;
- the nominal doping concentration of the bulk material has more influence on the on the frequency dependence of NDR than was the case for GaAs; and
- the upper frequency limit for bulk GaN to support NDR is between 250 GHz and 300 GHz, depending on the operating conditions.

3.4 Conclusion

This chapter presents a novel, empirical approach to determine the upper frequency limit at which GaAs and GaN still exhibit NDR. This approach exploits the hysteresis in the dynamic, high frequency velocity-field characteristics of these materials, and inherently considers the non-stationary dynamics of electrons at frequencies approaching the NDR relaxation frequency f_{NDR} for typical operating temperatures and doping conditions.

The prediction of the upper frequency limit of the NDR mechanism using this approach is expected to be more reliable than the theoretical, time-constant based calculation given

in Equation 2.4, and furthermore, does not depend on the structure of the devices that exploit this mechanism.

The upper frequency limit of NDR for bulk GaAs is simulated here to be between 80 GHz and 100 GHz, and between 250 GHz and 300 GHz for GaN, depending on the operating temperature and transit region doping levels. These estimations are indeed lower than those calculated theoretically as ~105 GHz and ~700 GHz, respectively, for GaAs and GaN. The discrepancy for GaN is especially prominent.

As stated earlier, it can be assumed that the actual operational frequency limit of transferred electron devices will be further reduced by the structural constraints of the device, as well as the dynamics of Gunn domain formation within the device, and the elevated temperatures that these devices operate at. The Monte Carlo particle simulations of actual Gunn diodes in the following chapters support this assumption. The upper frequency limits of these devices in the fundamental mode of operation are found to be of the order 90 GHz (see Figure 4.11) and 250 GHz (see Table 5.6) for GaAs and GaN Gunn devices, respectively. It should be noted that the highest fundamental frequency where harmonic output power was still measurable, was 62 GHz for GaAs (see Figure 4.12) and 175 GHz for GaN (see Table 5.6).

Experimental data provides further validation of the empirical method presented here.

State-of-the-art GaAs Gunn diodes can generate second harmonic power at 122 GHz (Priestley *et al.,* 2010), corresponding to a fundamental frequency of 61 GHz. From Figure 4.11 it is also evident that the fundamental mode of operation can extend to 100 GHz (but with negligible harmonic output power).

Measured performance data of GaN diodes are not readily available. However, based on authoritative simulations done by MacPherson, Dunn and Pilgrim (2008), which incorporate internal thermal heating of the diode, fundamental output power is predicted at 240 GHz for a diode operating at 500 K.

It is informative to also note that in the frequency range below 70 GHz, the strength of the NDR mechanism in GaAs exceeds that of GaN, as is evident from comparing g_{ave} for these materials. Simulations show that, for comparable operating temperatures, the (negative) value of g_{ave} for GaAs exceeds that of GaN by a factor of more than 10. This does not imply, however, that GaAs Gunn diode oscillators have improved output power

compared to their GaN counterparts at these frequencies. The output power is also dependent on the square of the magnitude of the harmonic voltage, which is typically much higher for GaN than for GaAs oscillators.

As a final remark, it is evident from Figures 3.6 and 3.10 that the doping levels do not generally have a significant impact on the upper frequency limit of GaAs and GaN devices (although a greater impact for GaN devices). In Gunn diode design, this affords the freedom to select the nominal doping level of the active region to ensure domain formation, and to adjust the nominal admittance levels of the diodes for optimal matching to the external circuitry, without considering the impact of doping levels on the upper frequency limit of Gunn devices.

The upper operational frequency limits of multi-domain GaAs and GaN Gunn devices are investigated in the following chapters.

4 GaAs Gunn diode optimisation

4.1 Introduction

This chapter investigates the optimisation of multi-domain GaAs Gunn diodes and the determination of the operational frequency limits of these devices. The broad outline of the optimisation process was summarised in Chapter 1.

The optimisation of the GaAs diode is approached in two steps, namely:

- establishing a benchmark two-domain diode with hot electron injection, based on the work done by Van Zyl (2006); and
- optimising the benchmark diode for output power.

The optimised two-domain diode is further investigated to determine its operational frequency limit in fundamental and harmonic modes.

The Monte Carlo particle simulation technique described in Chapter 2 is used throughout. The simulation model incorporates an ensemble of 80 000 super particles. The simulated time is 260 ps, ensuring a number of full RF cycles at mm-wave frequencies.

4.2 Simulation and optimisation of benchmark GaAs Gunn diode at 94 GHz

The design and structure of the diode have been described in Chapter 2 (see Figure 2.11). The reference two-domain device of Van Zyl (2006), with a doping notch, hot electron injection and a graded active region doping profile, has an output power of 160 mW and efficiency of 1.9% at 94 GHz (the second harmonic). The objective here is to enhance the output performance of the referenced diode by further optimising the relevant design parameters, namely, the dimensions and doping profile of the transit regions, and the width of the doping notches and buffer region.

4.2.1 Benchmark two-domain Gunn device

Table 4.1 lists the design and simulation parameters and predicted microwave performance of the two-domain reference diode (Van Zyl, 2006).

Table 4.1 Design and simulation parameters and RF performance of reference GaAs Gunn diode

Design parameters		
Region	**Length (10^{-6}m)**	**Doping concentration (m^{-3})**
Cathode contact	0.5	$1.5x10^{23}$
$Al_xGa_{1-x}As$ layer	0.05	undoped x = 0.3
Doping spike 'n^{+}'	0.01	$1x10^{24}$
Doping notches	0.2	undoped
Transit regions	1.4	$1.2x10^{22}$ *G_f* G_F = 0.25 (1) g_f = 1.67 (2)
Buffer region	0.5	$2x10^{23}$
Anode contact	1	$1.5x10^{23}$
Diameter	100	-
Simulation parameters		
Bias voltage (V_{DC})		6 V
Fundamental voltage (V_1)		4.75 V
Second harmonic voltage (V_2)		1.3 V
Simulated RF performance		
Frequency		94 GHz
Output power		160 mW
RF efficiency		1.9 %
Diode admittance		-0.21 + j0.27 S
Cathode contact temperature		465 K

Note 1: G_F is defined as the portion of the active region length adjacent to the anode contact over which the doping profile is exponentially increased.

Note 2: g_f is defined as the factor by which the nominal doping in the active region is increased towards the anode.

The reference diode design has been adopted for the benchmark two-domain design, with the exception of a marginally higher nominal doping concentration of the transit regions ($1.5x10^{22}$ m^{-3} for the benchmark diode, as opposed to $1.2x10^{22}$ m^{-3} for the

reference diode). This had the effect of a marginal increase in the RF conversion efficiency of the diode, but not the output power.

The transit region length and its nominal doping concentration are determined through the application of Equation 2.1 and the graph in Figure 2.2. It should be noted that decreasing the nominal doping concentration leads to a degradation of the diode efficiency. On the other hand, increasing the doping level will increase the bias current, which enhances heating of the diode and leads to a subsequent reduction in the efficiency of the diode.

4.2.2 Optimisation of benchmark two-domain device

The RF performance of the benchmark diode of the previous section is now further optimised at the second harmonic of 94 GHz through tuning of the following design parameters:

- width of the buffer region;
- width of the doping notches;
- Al 'x' moll fraction of the hot electron injector; and
- bias voltage.

Buffer region width

As stated previously, the width of the buffer region between successive transit regions should be wide enough to quench the Gunn domains, but should also be as narrow as possible to prevent the introduction of unnecessary ohmic losses (Tsay *et al.,* 1990:54-60). Initially, a buffer width of 0.5 μm is implemented, based on the reference diode (Van Zyl, 2006). The width of the buffer region is then decreased to 0.2 μm and 0.15 μm, respectively, and the output power determined.

Figure 4.1 shows the simulated output power at 94 GHz as a function of buffer region width. The Gunn diode with a buffer width of 0.2 μm yields the optimum output power of 168 mW, as compared to 160 mW of the reference diode with a buffer width of 0.5 μm.

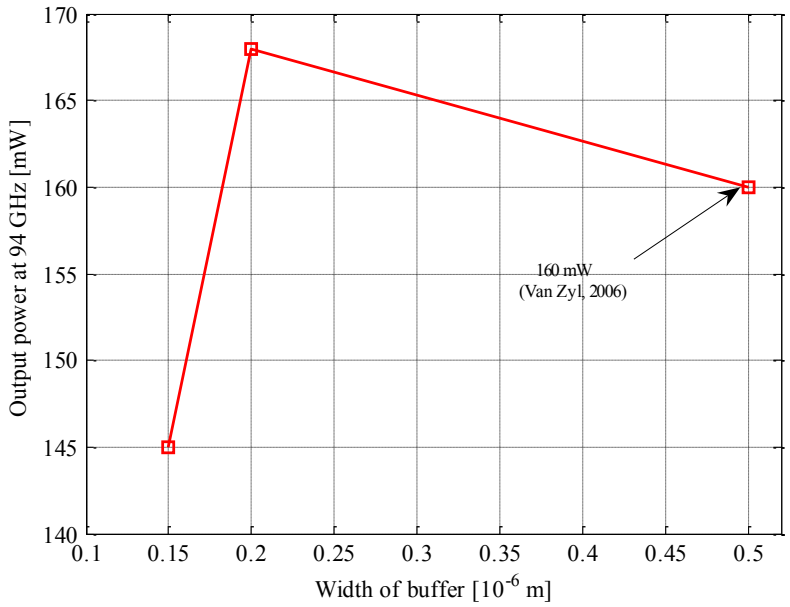

Figure 4.1 Simulated output power at 94 GHz as a function of buffer width for two-domain Gunn diode

It is informative to study the Gunn domain formation in the diode with varying the width of the buffer region. Figures 4.2, 4.3 and 4.4 illustrate the simulated time-averaged electric field distributions in the diode for the cases presented in Figure 4.1.

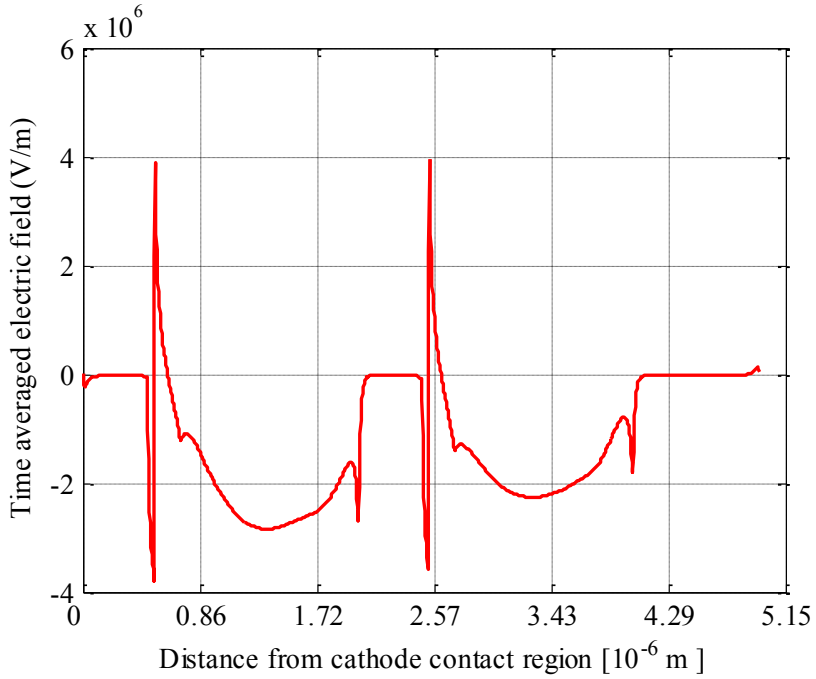

Figure 4.2 Time-averaged electric field distribution in Gunn diode with a 0.5 µm buffer

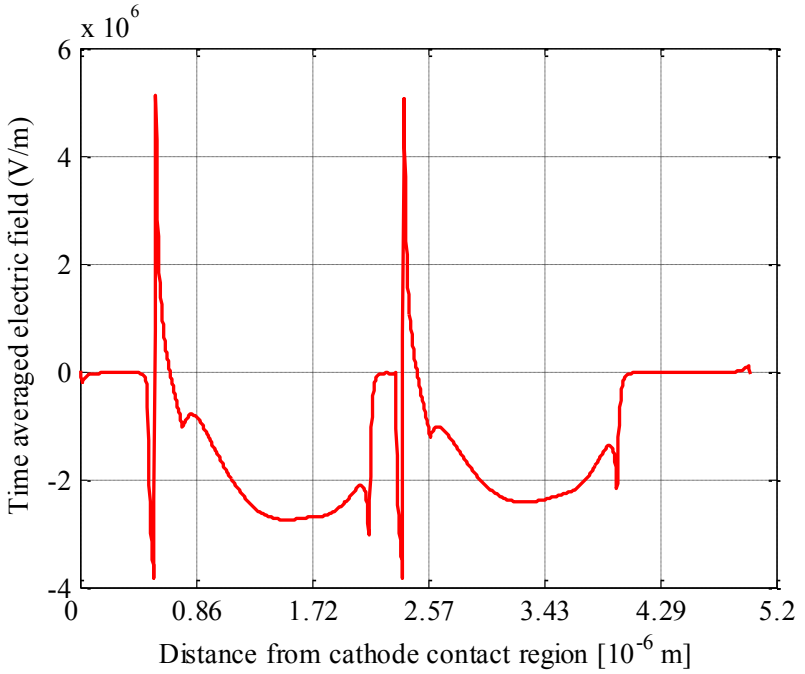

Figure 4.3 Time-averaged electric field distribution in Gunn diode with a 0.2 μm buffer

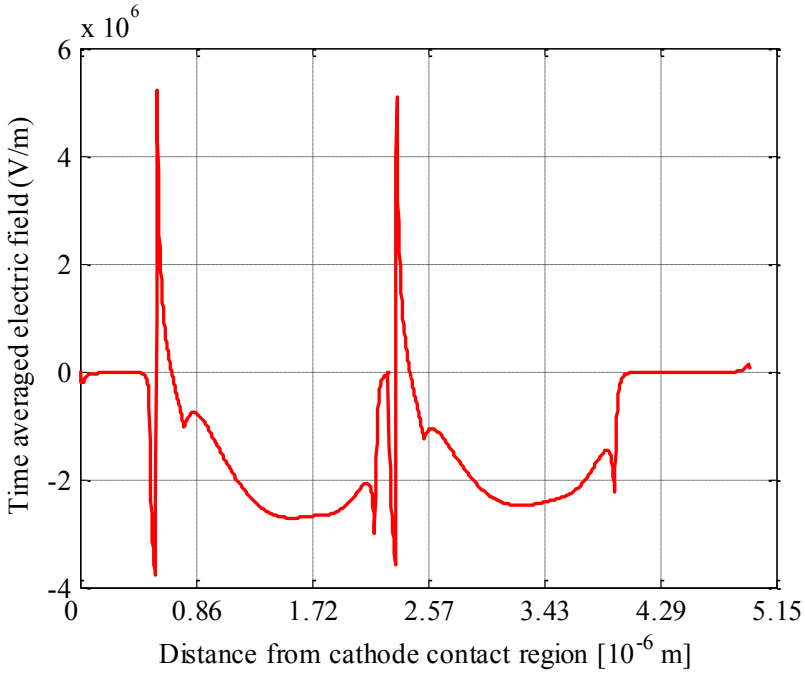

Figure 4.4 Time-averaged electric field distribution in Gunn diode with a 0.15 μm buffer

From these figures it is noted that

- quenching of the Gunn domains deteriorates with the narrower buffer region of 0.15 μm;
- a 0.2 μm buffer quenches the Gunn domains satisfactorily, and yield well-formed Gunn domains in the two regions;

- a 0.5 μm buffer does not improve the quenching of the Gunn domains, as compared to the shorter 0.2 μm buffer, but is expected to add additional parasitic resistance; and
- a buffer width of 0.5 μm results in more dissimilar domain formation in the two domains, which can be attributed to the marginally higher cathode temperature of 465 K for a wider buffer, compared to 458 K for a narrow buffer.

Further to the last bullet above, the marginally lower average operating temperature of the diode with a 0.2 μm buffer enhances the output power as shown in Figure 4.1.

Doping notch width

As described in Chapter 2, doping notches reduce the dead zone. An optimum doping notch width is investigated here by simulating three case; an initial width of 0.2 μm as for the reference diode, and shorter widths of 0.15 μm and 0.1 μm, respectively.

The simulated output power at 94 GHz as a function of varying doping notch width is presented in Figure 4.5.

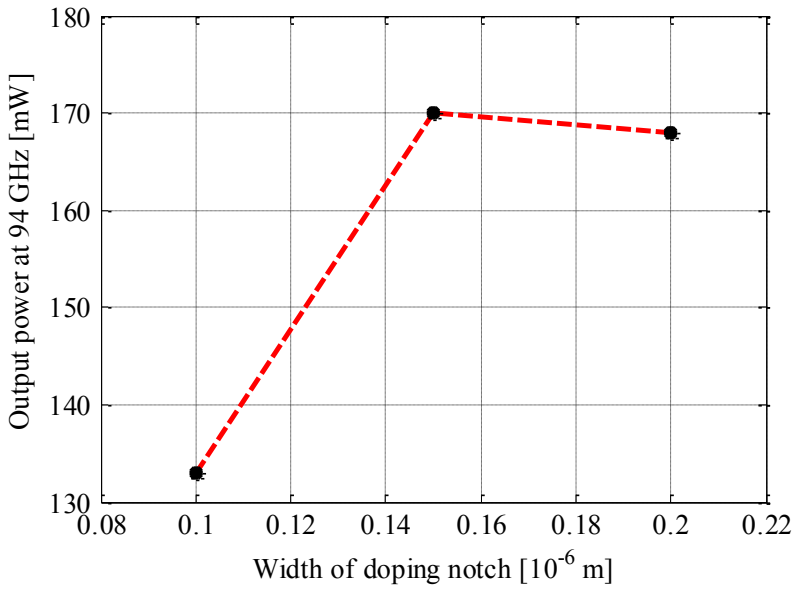

Figure 4.5 Simulated output power as a function of doping notch width for two-domain Gunn diode

The simulations yield an optimum output power of 172 mW with a doping notch of 0.15 μm. It is also evident that the simulated output power drops sharply when reducing the width of the doping notch further. However, the output power drops only marginally for a doping notch width of more than 0.15 μm.

The cathode temperature of the 0.15 μm notch diode was found to be 402 K, compared to 394 K of the 0.2 μm notch diode. Considering the marginal increase in output power of the diode with a 0.15 μm doping notch width, but to limit any further heating of the diode, it was decided to retain the doping notch width at 0.2 μm.

The corresponding time-averaged electric field distributions for the three instances of doping notch width are presented in Figures 4.6, 4.7 and 4.8.

From these figures it is noted that

- Gunn domains are well-formed and more similar in the two domains of the diode with a 0.15 μm doping notch width than in the other two cases; and
- the dead zone increases with the narrower 0.1 μm doping notches, which is also associated with excessive electric fields towards the anode and will lead to increased heating and a degradation of the efficiency of the diode.

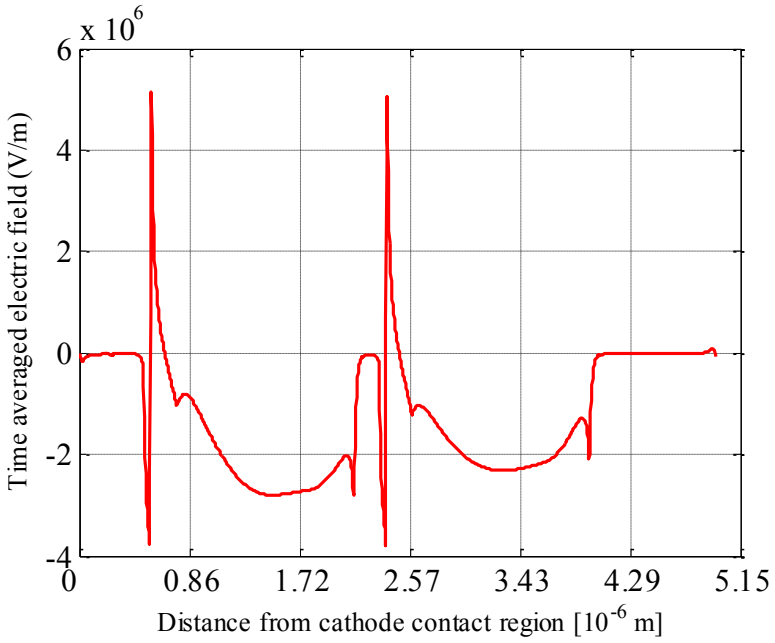

Figure 4.6 Time-averaged electric field distribution in Gunn diode with a 0.2 μm doping notch

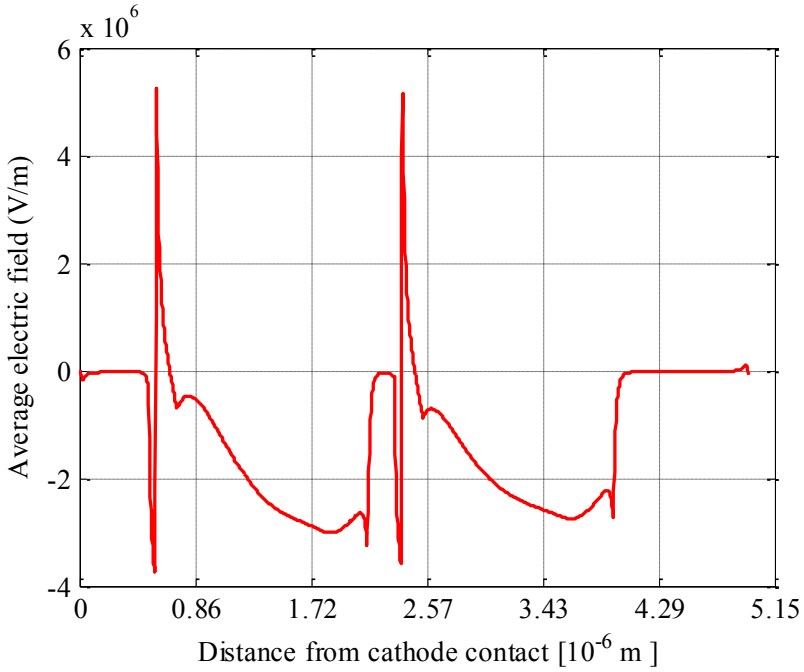

Figure 4.7 Time-averaged electric field distribution in Gunn diode with a 0.15 μm doping notch

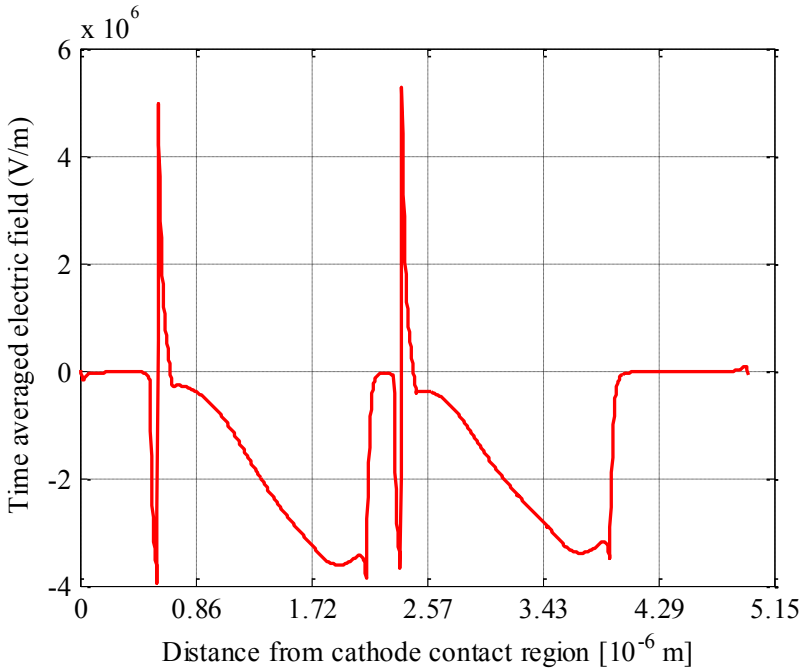

Figure 4.8 Time-averaged electric field distribution in Gunn diode with a 0.1 μm doping notch

Heterostructure hot electron injector

The Al mole fraction 'x' of the $Al_xGa_{1-x}As$ heterostructure determines the gain in potential energy of the electrons being injected. Hence, the optimisation of its value will impact the RF performance of the diode.

The hot electron launcher has a linearly graded Al composition over the width of the launcher from zero to a maximum value. Initially, a maximum value of x = 0.3 is assumed as with the reference diode (see Table 4.1).

Figure 4.9 illustrates the simulated output power at the 47 GHz fundamental and 94 GHz second harmonic for x = 0.2, 0.25, 0.3, and 0.35. It is evident that x = 0.25 is the optimum value for both fundamental and second harmonic output power. Output power of 399 mW at 47 GHz and 182 mW at 94 GHz is achieved.

It is further noted that with x > 0.3 the performance of the diode degrades. This is in agreement with Greenwald *et al.* (1986) that a high value of 'x' reduces the device current and lowers the harmonic efficiency of the device.

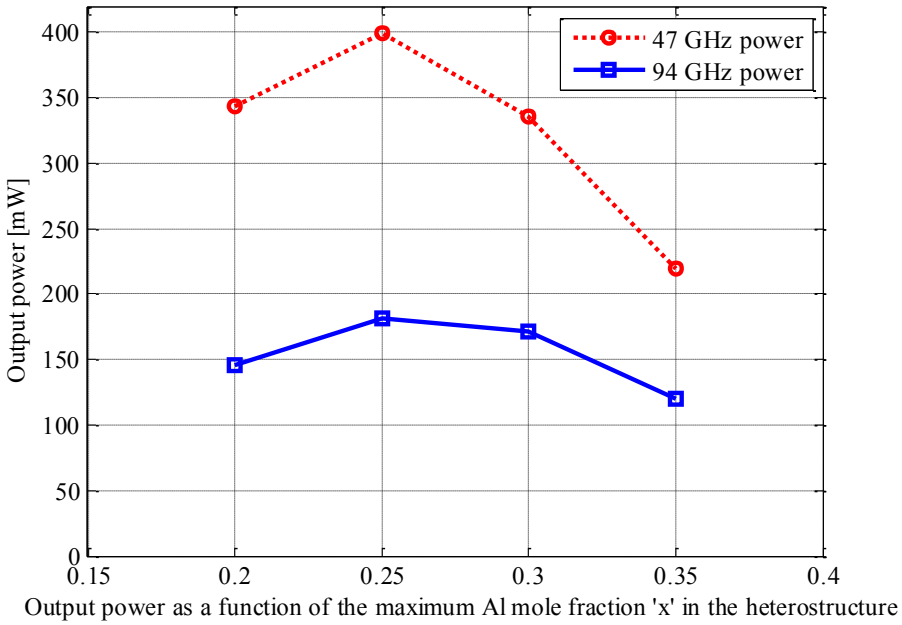

Figure 4.9 Simulated output power as a function of Al mole fraction 'x' of $Al_xGa_{1-x}As$ heterostructure for two-domain Gunn diode

Bias voltage

In conclusion, the effect of bias voltage on the output power of the optimised benchmark diode is simulated. Figure 4.10 illustrates the simulated output power at 94 GHz for bias voltages of 5 V, 6 V and 7 V, respectively.

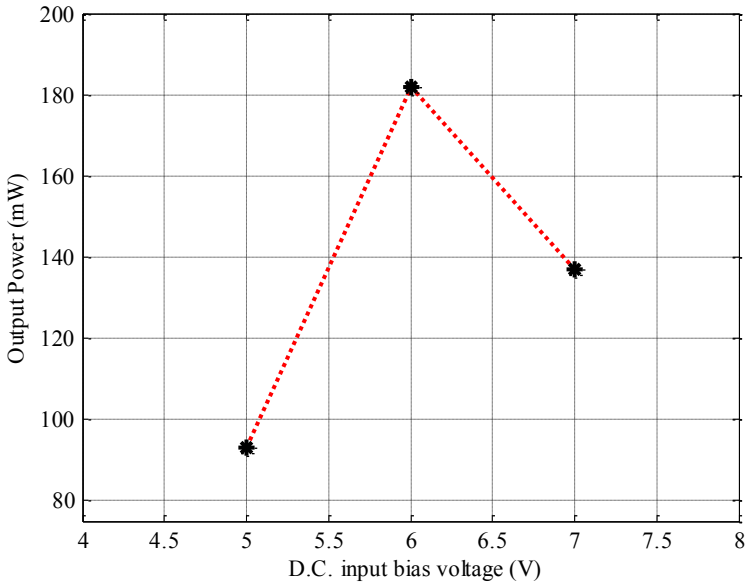

Figure 4.10 Simulated output power at 94 GHz as a function of bias voltage for two-domain Gunn diode

It is evident that the output power is sensitive to bias voltage (as reported in Chapter 2) and that 6 V yields the maximum output power of 182 mW.

4.2.3 RF performance comparison of the benchmark and optimised Gunn diode

Table 4.2 summarises and compares the RF performance of the optimised and benchmark diodes, indicating the relevant design and simulation parameters that have been optimised.

The simulated output power of the optimised diode is 182 mW at the second harmonic of 94 GHz. This is an improvement of 14% over the performance of the benchmark diode. The admittance and RF conversion efficiency of the optimised diode are similar to that of the benchmark diode.

Table 4.2 RF performance comparison of benchmark and optimised two-domain diode

Parameter	Benchmark diode	Optimised diode
Buffer region width	0.5 μm	0.2 μm
Doping notch width	0.2 μm	0.2 μm
Al mole fraction of $Al_xGa_{1-x}As$ layer	x = 0.3	x = 0.25
Bias voltage	6 V	6 V
Bias current	1.37 A	1.5 A
Output power at 94 GHz	160 mW	182 mW
Admittance at 94 GHz	-0.21 + j0.27 S	-0.2 + j0.2 S
RF conversion efficiency	1.9 %	2.1 %

4.3 Investigation of the operational frequency limit of two-domain diodes

In this section, the operational frequency limit of a two-domain diode is investigated.

Note: For simulations at fundamental frequencies exceeding 47 GHz as for the optimised diode, the length and nominal doping concentration of the transit regions of the optimised diode are adjusted to still satisfy the conditions of Equation 2.1.

The output power of the two-domain diode is simulated at fundamental operating frequencies between 47 GHz and 150 GHz. The results are shown in Figure 4.11. The associated output power at the second and third harmonics is presented in Figure 4.12. For these simulations, the lengths of the transit regions have been decreased to 1.2 μm and 0.8 μm for 100 GHz and 150 GHz, respectively, and the doping concentration increased to 1.75×10^{22} m^{-3} and 2.2×10^{22} m^{-3} for these two cases.

As expected, the output power decreases with an increase in frequency, with an apparent limit approaching 100 GHz as the highest fundamental frequency that the diode still operates at. No appreciable power was simulated at fundamental operating frequencies above 100 GHz.

The actual fundamental frequency limit can be expected to be lower than 100 GHz for practical devices, as the simulations here do not model the effects of the external circuitry.

From Figure 4.12 it is apparent that the highest harmonic frequencies that the diode operates at are 124 GHz and 186 GHz for the second and third harmonics, respectively, corresponding to a fundamental frequency of 62 GHz.

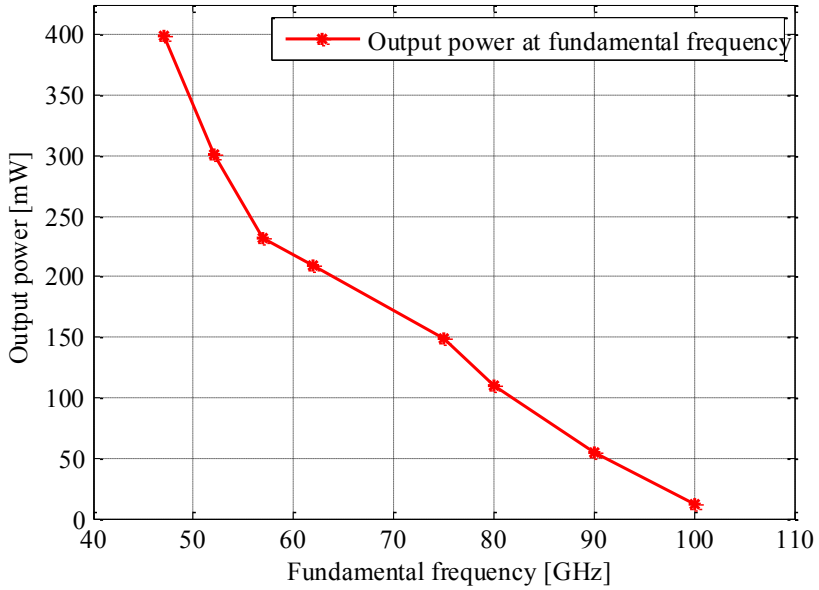

Figure 4.11 Simulated output power at fundamental frequencies between 47 GHz and 100 GHz for two-domain Gunn diode

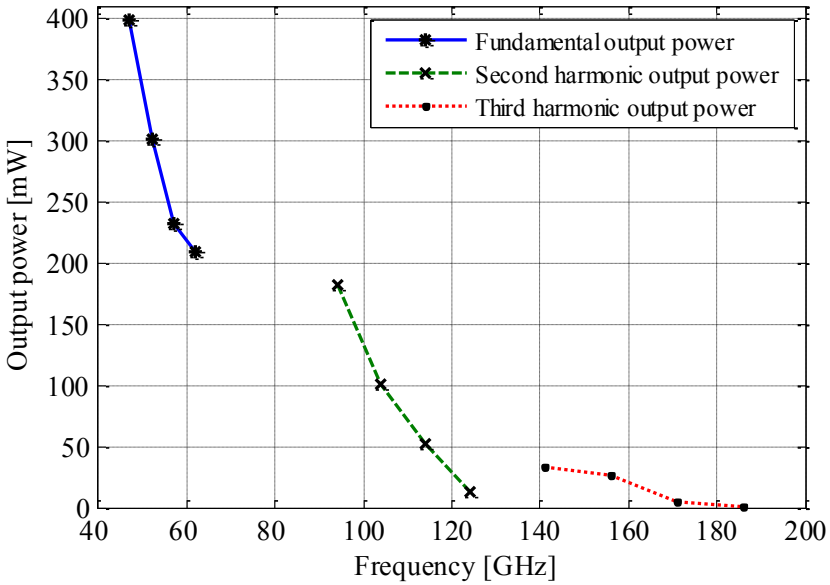

Figure 4.12 Simulated output power at the fundamental, second and third harmonic frequencies for two-domain Gunn diode

Table 4.3 tabulates the simulation results presented in Figure 4.12. The decrease in output power at the higher frequencies is accompanied by an increase in the cathode contact temperature due to the lower efficiency of the diode at higher frequencies. The increased temperature in itself further degrades the RF conversion efficiency of the diode (Levinstein, Rumyantsev and Shur, 2001).

Table 4.3 Simulated RF performance of two-domain GaAs Gunn diode

Parameter	**Unit**	**#1**	**#2**	**#3**	**#4**
Fundamental frequency	GHz	47	52	57	62
Second harmonic frequency	GHz	94	104	114	124
Third harmonic frequency	GHz	141	156	171	186
DC current	A	1.5	1.5	1.7	2.0
DC input power	W	9.1	9.0	10.2	12.1
RF efficiency	%	2.1	1.4	0.5	0.1
Fundamental output power	mW	399	301	232	218
Second harmonic output power	mW	182	101	52	42
Third harmonic output power	mW	33	26	5	0.9
Cathode temperature	K	458	484	498	515

4.4 Performance comparison of single- and two-domain diodes

The optimised two-domain diode is further evaluated by comparing its RF performance with state-of-the-art single-domain diodes.

From Figure 2.12 and Table 2.2 the *measured* output power of state-of-the-art devices ranges from around 50 mW to 120 mW at 77 GHz, to 100 mW at 94 GHz and 40 mW at 122 GHz.

Comparing this trend in measured output power to the simulated output power of the optimised two-domain diode presented in Figure 4.12, it is evident that the two-domain diode is capable of significantly higher output power at frequencies below 94 GHz than single-domain diodes. At 94 GHz, for instance, the output power of the two-domain diode is 1.8 times more than that of the single-domain diode. However, the two-

domain diode exhibits the same apparent second harmonic frequency limit of around 130 GHz.

These observations are consistent with the findings presented in Chapter 3. The broad comparison in output power of the single- and two-domain diodes is illustrated in Figure 4.13.

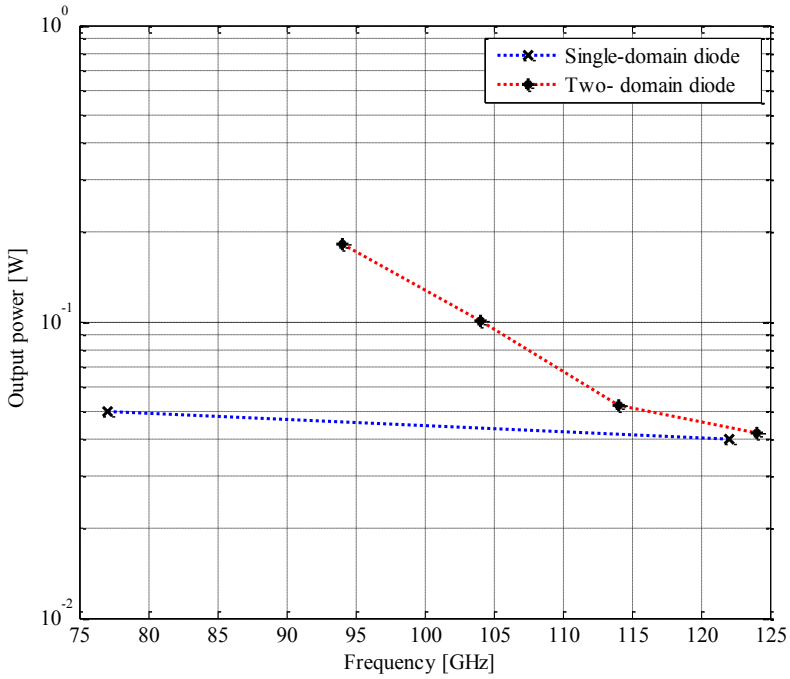

Figure 4.13 Performance comparison of single- and two-domain GaAs Gunn diodes

4.5 Conclusion

An optimised two-domain GaAs Gunn diode is presented. The optimised diode outperforms the reference benchmark diode of Van Zyl (2006) in terms of RF output power, with an increase of 14 % from 160 mW to 182 mW at 94 GHz.

The simulated output power of the optimised diode reaches 218 mW at a fundamental frequency of 62 GHz, and 42 mW and 890 µW at the second and third harmonics of 124 GHz and 186 GHz, respectively. Beyond this fundamental frequency, the performance of the two-domain diode degrades significantly in terms of efficiency and with no appreciable power at the associated harmonics. Output power at fundamental frequencies as high as 90 GHz is observed, but these are not accompanied by measurable second and third harmonic output power.

The simulation results presented in this chapter are in agreement with the measured performance of actual state-of-the-art single-domain diodes reported in the literature (Priestley *et al.,* 2010) and presented in Figure 2.12, except for an increase in the output power levels of the two-domain diode. It was shown that for frequencies below 100 GHz the two-domain diode generates around twice the output power of the single-domain diodes. However, it suffers from the same operational frequency limit as for the single-domain diodes, which is to be expected.

The simulated performance of the two-domain diode furthermore agrees with the findings of the empirical investigation presented in Chapter 3, where a fundamental frequency limit of between 80 GHz and 100 GHz was simulated.

It is the author's opinion that excessive thermal heating will render diodes with more than two domains impractical. Simulations of such devices (Teoh *et al.,* 2002:830-831) are deemed unrealistic, unless proper thermal management is applied through, for example, operating the diodes in a pulsed mode.

Chapter 5 deals with the optimisation of single- and two-domain GaN Gunn diodes.

5 GaN Gunn diode optimisation

5.1 Introduction

From the literature review in Chapter 2 it is evident that GaN supports Gunn operation at much higher frequencies than GaAs. The objective of this chapter is to investigate the operational feasibility and RF performance at mm-wave frequencies of single- and two-domain GaN (Wz) Gunn devices.

First, a single-domain diode with a doping notch, based on the *reference* model presented by Joshi *et al*. (2003:4836-4842), is simulated as a *benchmark* diode at a fundamental frequency of 100 GHz. This benchmark single-domain diode is then further optimised and investigated for its RF performance at fundamental frequencies of up to 200 GHz and the associated second and third harmonics.

The optimised single-domain diode is subsequently used as a basis for a two-domain diode, which is simulated to determine its RF performance at a fundamental frequency of 175 GHz and the second and third harmonics.

The chapter concludes with a comparison of the RF performance of the single- and two-domain diodes (with appropriately scaled design and simulation parameters).

5.2 Simulation and optimisation of single-domain diode

Figure 5.1 presents the doping profile of the *reference* diode by Joshi *et al. (*2003). The reference diode has a transit region length of 1 μm with nominal doping in the range of $5x10^{22}$ m^{-3} to $2x10^{23}$ m^{-3} in order to satisfy Equation 2.1 for the required n_oL product. The cross-sectional area of the reference diode is 10^{-9} m^2. The doping notch is placed at the cathode side of the active region (Sevik *et al.,* 2004:188-190). Its nominal doping concentration is 20% of that for the transit region.

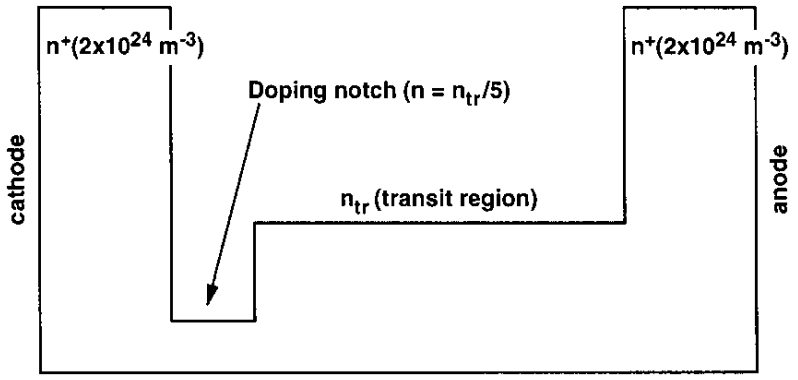

Figure 5.1 Doping profile of reference single-domain GaN Gunn diode

(From Joshi *et al.,* 2003:4836-4842)

The *benchmark* diode is based on the reference diode above. Figure 5.2 illustrates the doping profile of the benchmark diode (Francis and Van Zyl, 2013: 177-182):

- Regions 1 and 4 are the highly doped contact regions;
- Region 2 is the doping notch with a doping concentration of 0.5×10^{23} m^{-3} and width of 0.25 μm; and
- Region 3 is the transit region of length 1.0 μm and with a nominal doping concentration of 1.0×10^{23} m^{-3}.

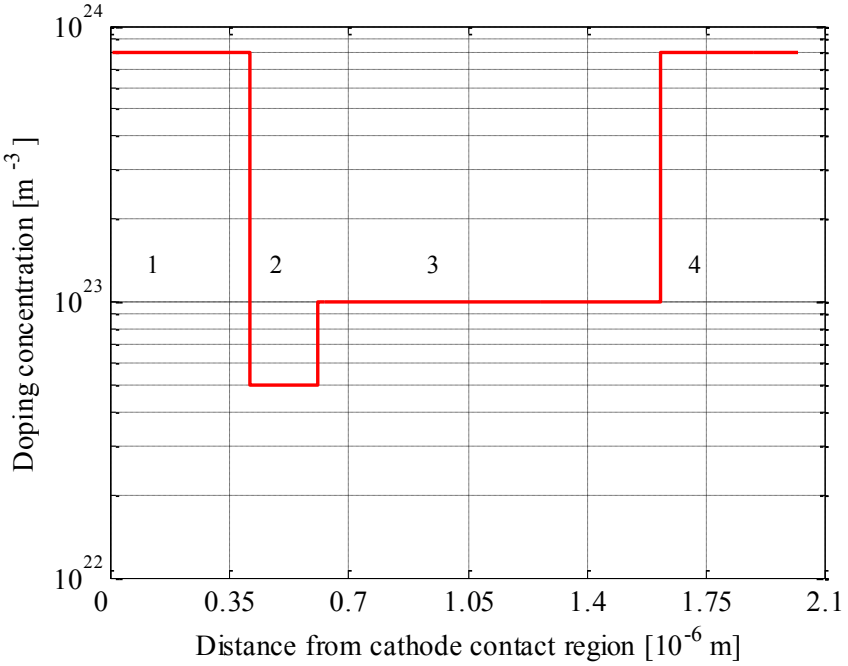

Figure 5.2 Doping profile of the benchmark single-domain GaN Gunn diode

(From Francis *et al.,* 2013:177-182)

The much higher nominal doping concentration of the transit region compared to that of GaAs diodes is noticeable. This is due to the much higher effective mass of electrons in the central valley of GaN than for similar electrons in GaAs. The heavier effective mass translates into lower electron mobility, leading to slower Gunn domain formation. This reduced mobility is countered by increasing the nominal doping concentration of the transit region (Lee and Ravaioli, 1990:425-427; Joshi *et al.,* 2003:4836-4842). However, increasing the doping concentration increases thermal losses, thereby reducing the efficiency of the diode. (This is further exacerbated by the higher biasing conditions than for GaAs diodes.) Hence, optimising the transit region doping concentration is imperative.

Thermal dissipation and reduced efficiency are of primary concern in the optimisation of GaN Gunn devices (Hao *et al.,* 2008:51-68; Sevik *et al.,* 2004:S188-S190). The simulations incorporate a diamond integral heat sink at the anode contact, similar to which was implemented for the GaAs diodes.

Table 5.1 summarises the benchmark design and simulation parameters of the single-domain diode.

Table 5.1 Design and simulation parameters of benchmark single-domain GaN diode

Design parameters		
Region	**Length (10^{-6}m)**	**Doping concentration (m^{-3})**
Cathode contact	0.5	$8x10^{23}$
Doping notch	0.25	$0.5x10^{23}$
Transit region	1.0	$1x10^{23}$
Anode contact	0.5	$8x10^{23}$
Diameter	55	-
Simulation parameters		
Bias voltage (V_{DC})		35 V - 85 V
Fundamental voltage (V_1)		9 V
Fundamental frequency range		100 GHz – 240 GHz
Number of electrons simulated		80 000
Total simulation time		230 ps

5.2.1 Optimisation of the benchmark diode

The benchmark diode presented in the previous section is optimised here at a fundamental frequency of 100 GHz. The device and simulation parameters that are optimised, are the

- bias voltage;
- length and nominal doping concentration of the transit region; and
- width of the doping notch.

Bias voltage

The detrimental effect of heat dissipation on the output power of GaN Gunn diodes is pronounced because of the higher biasing conditions compared to, for example, GaAs diodes (Alekseev *et al.,* 2000:941-947; Joshi *et al.,* 2003:4836-4842; Macpherson *et al.,* 2008:55005-55012; Sevik *et al.,* 2004:369-377; Lau *et al.,* 2007:245-248; Levinstein *et al.,* 2001). Consequently, thermal management of GaN diodes is critical. An effective way of countering the increased thermal losses is to apply a *pulsed* bias voltage with very low duty cycles (Francis *et al.,* 2013:177-182). The effect of a lower duty cycle is to decrease the DC input power. The effective (reduced) DC power is used to determine the temperature distribution within the device (refer to Equation 2.8). A bias voltage with an on-time of less than 2 ns is assumed (Macpherson *et al.,* 2008).

Note: The bias voltage and the harmonic output power listed in the simulations in this chapter are the values during the on-time of the device, and not the effective values. The simulated harmonic power is therefore the peak output level of the pulsed output power.

Both the magnitude and duty cycle of the pulsed bias voltage are optimised. The duty cycle should be as high as possible from a practical and operational perspective, whilst still limiting the device temperature within acceptable levels (chosen here to be 500 K).

The benchmark diode is simulated with bias voltage duty cycles of 1%, 1.5% and 2%. The simulations show that a duty cycle of 1.5% lowers the cathode contact temperature from 508 K for a 2% duty cycle to 500 K. This will also yield an increase in the

conversion efficiency of the device. Hence, a 1.5% duty cycle is selected for all subsequent simulations.

Next, the effect of the bias voltage *magnitude* on the output power of the device is investigated at a fundamental frequency of 100 GHz and its second harmonic. The bias voltage is varied in steps of 5 V, from an initial value of 35 V to 85 V.

Figure 5.3 illustrates the simulated output power of the benchmark single-domain diode as a function of the applied bias voltage. As expected, the output power initially increases with an increase in bias voltage and reaches a maximum at the optimum bias voltage before decreasing with a further increase in bias voltage. This is typical of Gunn oscillators, as described in Section 2.4.3. For the benchmark device and 1.5% bias voltage duty cycle, the optimum bias voltage is between 40 V and 50 V, with only a marginal relative increase in output power at 50 V. However, the cathode contact temperature is reduced to 503 K at 40 V from 515 K at 50 V. Therefore, a 40 V pulsed bias voltage with a 1.5% duty cycle is applied to the device in subsequent simulations to optimise the device parameters mentioned earlier.

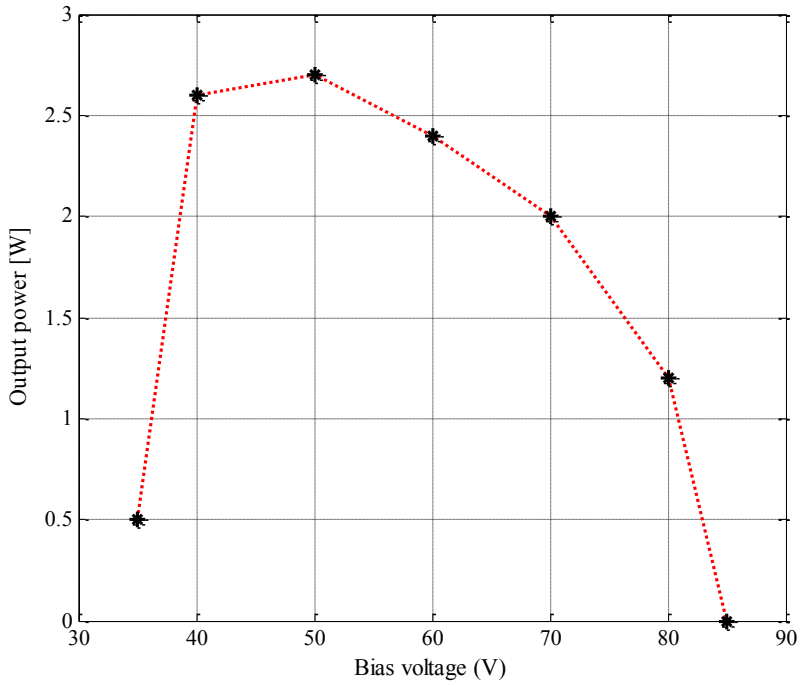

Figure 5.3 Simulated output power of the single-domain benchmark GaN diode as a function of bias voltage at a fundamental frequency 100 GHz

Length and nominal doping concentration of the transit region

The effect of the transit region length on the RF performance of the diode is simulated at a fundamental frequency of 100 GHz and its second harmonic. The transit region length is varied between 0.8 μm and 1.2 μm in 0.2 μm steps.

Figure 5.4 presents the simulated output power for each transit region length. A similar trend is observed in the output power at the fundamental frequency of 100 GHz and second harmonic of 200 GHz. For the given nominal transit region doping concentration, it is evident that the optimum length of the transit region is 1 μm and will be implemented in subsequent simulations.

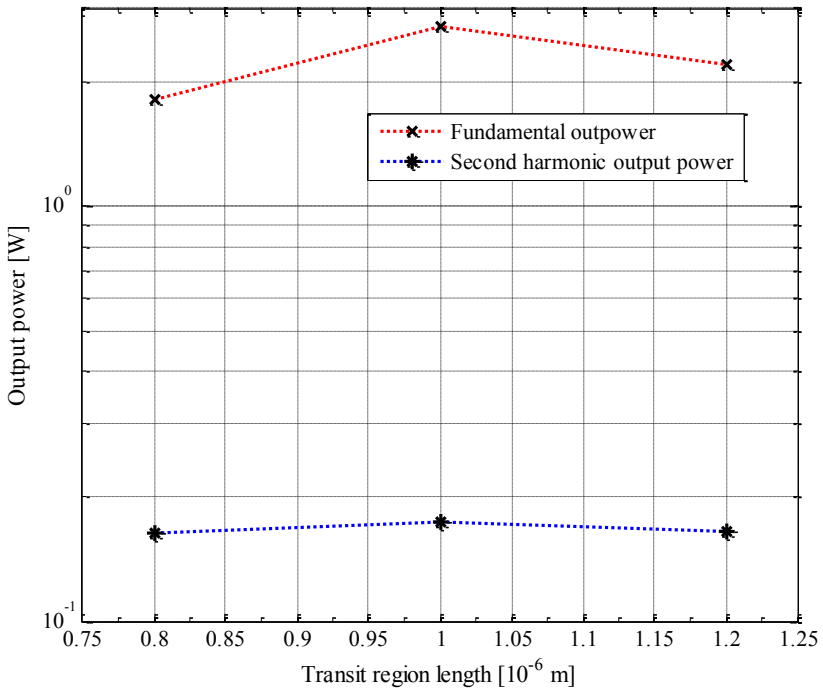

Figure 5.4 Simulated output power of the single-domain benchmark GaN diode as a function of transit region length

Next, the doping concentration of the transit region is varied by a factor of 10 from the nominal value of $1x10^{23}$ m^{-3}. Figure 5.5 presents the simulated RF output power for each doping level. The simulations confirm that the transit region doping concentration of the benchmark diode is an optimum and will be retained henceforth.

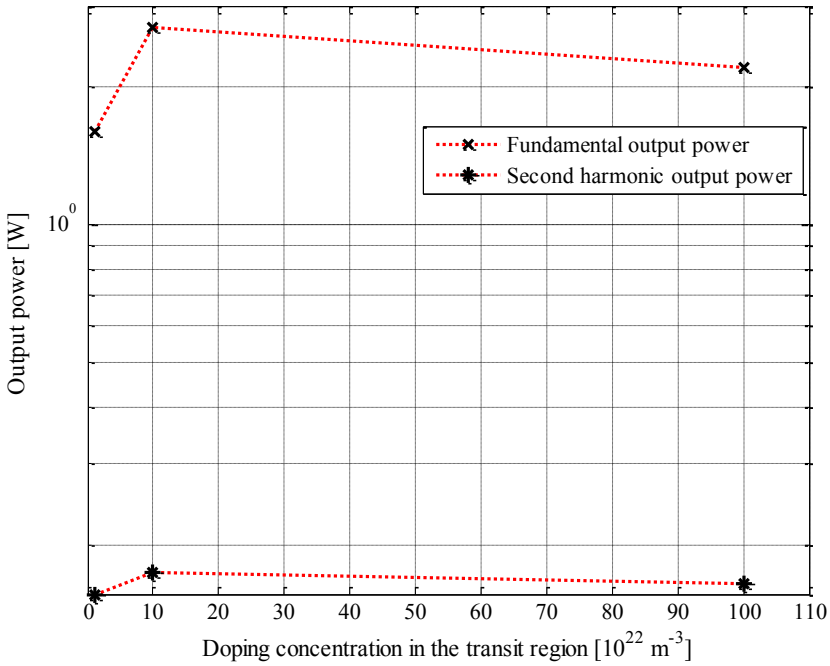

Figure 5.5 Simulated RF output power of the single-domain benchmark GaN diode as a function of nominal transit region doping concentration

Doping notch width

The doping notch width is reduced from the initial 0.25 μm to 0.2 μm and 0.15 μm. Figure 5.6 presents the simulated RF output power at the fundamental and second harmonic frequencies of 100 GHz and 200 GHz, respectively, with varying notch width.

From Figure 5.6 it is apparent that the optimum width of the doping notch is 0.2 μm.

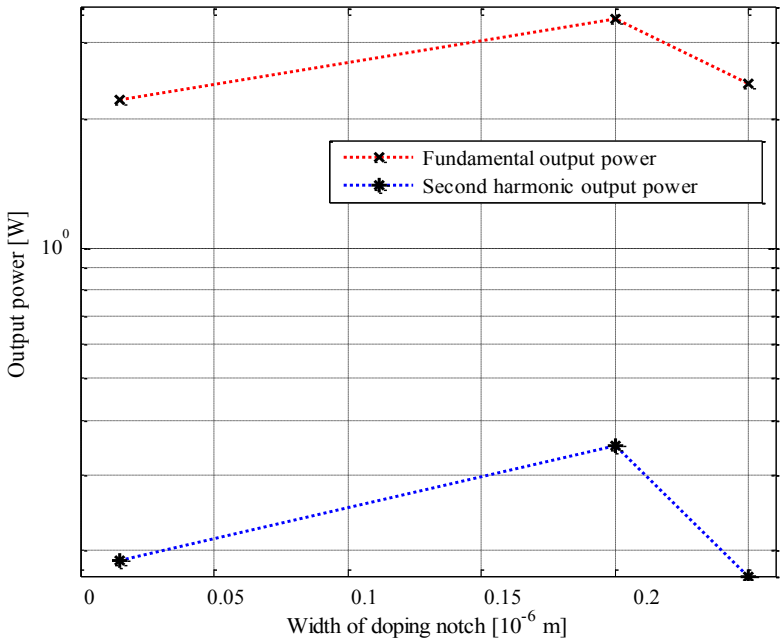

Figure 5.6 Simulated RF output power of the single-domain benchmark GaN diode as a function of doping notch width

The design parameters and microwave performance of the optimised benchmark single-domain diode are summarised in Table 5.2.

The simulated RF admittance of the Gunn diode at 100 GHz and 200 GHz is of the order Y = -0.2 + j0.6 S, which can be modelled as a parallel combination of a capacitor and a negative resistance. This presents a favourable impedance value of ~5 Ω to the external matching network of the Gunn diode oscillator.

Table 5.2 Design parameters and RF performance of optimised single-domain GaN diode

Design parameters		
Region	**Length (10^{-6}m)**	**Doping concentration (m^{-3})**
Cathode contact	0.5	$8x10^{23}$
Doping notch	0.2	$0.5x10^{23}$
Transit region	1.0	$1x10^{23}$
Anode contact	0.5	$8x10^{23}$
Diameter	55	-
Simulated RF performance		
Bias voltage (V_{DC})		40 V
Bias voltage duty cycle		1.5%
Fundamental frequency		100 GHz
Fundamental output power		3.43 W
Second harmonic output power		350 mW
Third harmonic output power		223 mW
RF efficiency at fundamental		7%
Admittance at fundamental		-0.2 + j0.6 S
Admittance at second harmonic		-0.2 + j0.6 S
Admittance at third harmonic		-0.3 + j0.8 S
Cathode contact temperature		500 K

5.2.2 Simulated RF performance of the optimised single-domain diode at higher mm-wave frequencies

In this section, the RF performance of the optimised single-domain diode is further investigated at higher mm-wave frequencies. The fundamental, second and third harmonics are considered. The fundamental frequency is increased in steps of 25 GHz from an initial value of 100 GHz.

At fundamental frequencies above 175 GHz, the length and nominal doping concentration of the transit region are adjusted appropriately to maintain the 'n_0L' product above the critical value as given by Equation 2.1.

Figure 5.7 presents the simulated output power at the fundamental, second and third harmonic frequencies. The simulation results are summarised in Table 5.3.

No appreciable output power was evident at a fundamental frequency above 225 GHz. This is ascribed to excessive heating; the cathode contact temperature increases to 530 K due to the deterioration of Gunn domain formation and decreased efficiency.

From Figure 5.7, the fundamental frequency limit of operations extrapolates to 250 GHz – 300 GHz, which is in agreement with the empirical estimation of Chapter 3. As explained there, the operational frequency limit of actual NDR devices will be less than that of the NDR mechanism itself, due to the dynamics of domain formation in the diode. It should be noted that external circuit losses have not been incorporated in the simulations; hence, the simulated output power at the second and third harmonics above 450 GHz could be negligible.

The diode admittances present practical matching impedances to the external circuitry.

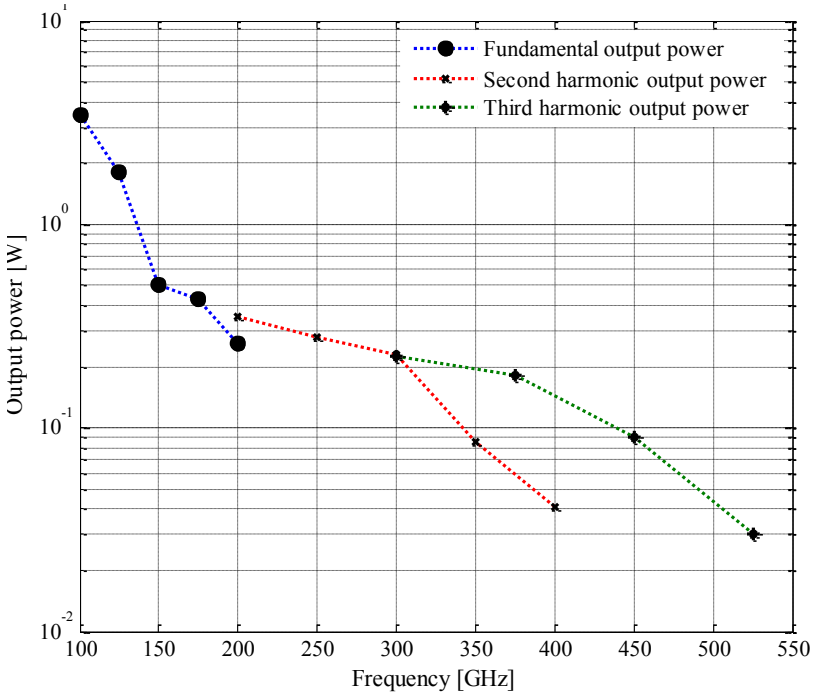

Figure 5.7 Simulated RFoutput power of the optimised single-domain GaN Gunn diode as a function of frequency

Table 5.3 RF performance of the optimised single-domain GaN Gunn diode at higher operational frequencies

Parameter	Unit	#1	#2	#3	#4	#5
Fundamental frequency	GHz	100	125	150	175	200
'n_0L' product	10^{17} m^{-2}	1	1	1	1	0.8
Bias voltage (V_{DC})	V	40	40	40	40	40
Fundamental output power	W	3.43	1.8	0.5	0.43	0.26
Second harmonic output power	W	0.350	0.278	0.230	0.086	0.041
Third harmonic output power	W	0.223	0.180	0.090	0.030	-
RF efficiency at fundamental	%	7	5.6	4	1	0.1
Admittance at fundamental	S	-0.2+j0.6	-0.2+j0.6	-0.2+j0.5	-0.01+j0.3	-0.2+j0.1
Admittance at second harmonic	S	-0.2+j0.6	-0.2+j0.6	-0.2+j0.6	-0.1+j0.5	-0.1+j0.2
Admittance at third harmonic	S	-0.3+j0.8	-0.4+j0.6	-0.7+0.4	-0.7+j0.2	-
Cathode contact temperature	K	500	500	500	502	518

In the next section, the RF performance of the optimised single-domain diode is compared to the reference diode design by Joshi *et al.* (2003:4836-4842) to establish the validity of the Monte Carlo device simulations in this chapter.

5.2.3 RF performance comparison of optimised single-domain benchmark and reference diodes

The RF performance of the optimised diode at fundamental frequencies varying from 150 GHz to 200 GHz is presented in Table 5.4, together with the reported simulation results of the reference diode by Joshi *et al.* (2003:4836-4842). The output power of the reference diode is adjusted to compensate for the smaller device cross-section of the reference diode, compared to the optimised diode.

Table 5.4 RF performance comparison of optimised single-domain benchmark and reference GaN diodes

Frequency	Output power at fundamental frequency		
	Optimised diode	Reference diode	Reference diode adjusted
150 GHz	500 mW	265 mW	629 mW
175 GHz	430 mW	100 mW	238 mW
200 GHz	260 mW	20 mW	48 mW

The expected roll-off in output power with increased frequency is evident in both the reference and optimised diode simulation results. The far more rapid decline in output power of the reference diode can be attributed to the fixed external LCR resonator circuit model employed by Joshi *et al.* (2003), whereas the Monte Carlo simulations assume an optimum matching condition at each simulated frequency through tuning the harmonic voltages. This does not lead to an external circuit-driven roll-off in output power.

The discrepancy in output power at 150 GHz of the optimised and reference diodes can further be attributed to different bias conditions; 50 V for the reference diode compared to 40 V implemented in this research (to prevent excessive heating).

It can be concluded that the simulated RF performance of the optimised diode compares favourably with the reference diode and that the simulation model used, is satisfactory.

To conclude the optimisation of the single-domain diode, the effect of an exponentially graded doping profile of the transit region on the RF performance of the diode is investigated.

The author has not found any published literature on the effect of a graded transit region doping profile on the performance of GaN Gunn diodes.

5.2.4 Effect of exponentially graded transit region doping profile on RF performance of optimised single domain diode

For the further optimisation of the single-domain diode, the effect of an exponentially graded doping profile of the transit region is investigated at a fundamental frequency of 175 GHz and its second and third harmonics. This is the highest fundamental frequency at which appreciable power was simulated at both higher harmonics, according to Table 5.3.

Three instances of an exponentially graded transit region doping profile are investigated; over-doped with g_f = 1.5, flat-doped with g_f = 1, and under-doped with g_f = 0.5. The exponential grading of the doping profile is limited to the 25% of the transit region length adjacent to the anode (G_F = 0.25), as illustrated in Figure 5.8 (Francis *et al.,* 2013:177-182).

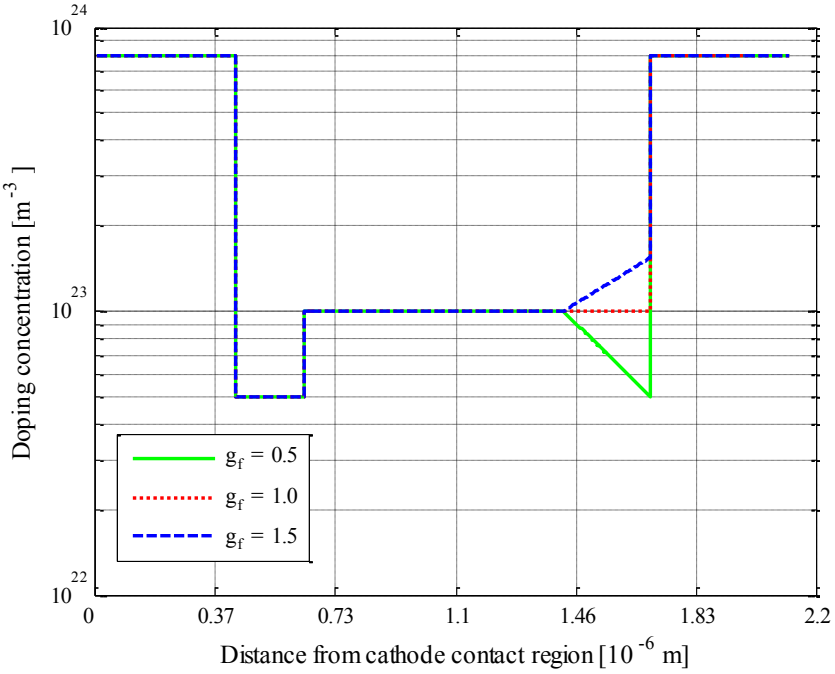

Figure 5.8 Transit region graded doping profile of single-domain GaN Gunn diode

(From Francis *et al.,* 2013:177-182)

Table 5.5 tabulates the simulated RF performance results at 175 GHz for the three instances of graded profiles. It is evident that an exponentially over-doped transit region doping profile yields higher output power, improved efficiency and a reduced cathode contact temperature as compared to diodes with flat and under-doped doping profiles.

Table 5.5 RF performance of single domain GaN diode with different transit region doping profiles

Parameter	Unit	#1	#2	#3
Fundamental frequency	GHz	175	175	175
g_f	-	1.5	1.0	0.5
Bias voltage (V_{DC})	V	40	40	40
RF efficiency at fundamental	%	2	1	0.8
Fundamental output power	mW	728	430	355
Second harmonic output power	mW	110	86	44
Third harmonic output power	mW	36	30	5
Cathode contact temperature	K	495	502	505

To explain the enhanced output power of the diode with an over-doped transit region, the associated time-averaged electric field distributions for the three instances of transit region doping profiles are simulated. The results are presented in Figure 5.9.

It is evident that the doping profile that increases exponentially towards the anode (g_f = 1.5) reduces the electric field in that region. This reduces heat dissipation within the device and translates to a lower operating temperature, as shown in Figure 5.10. This will increase the efficiency and output power of the device.

It is also observed that the curvature of the electric field suggests more mature Gunn domain formation than for the other two cases.

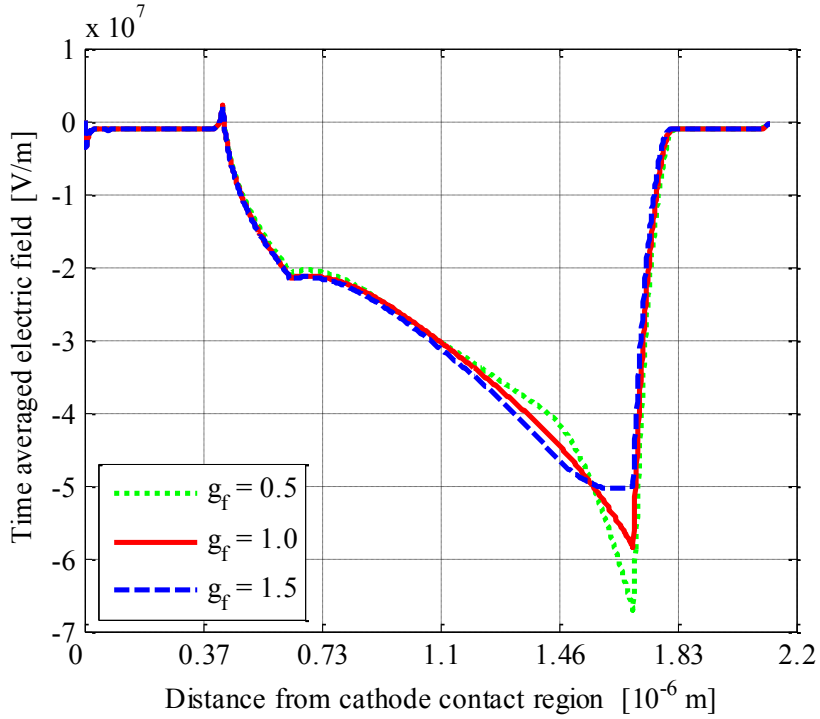

Figure 5.9 Time-averaged electric field distribution of single domain GaN diode with varying transit region doping profiles

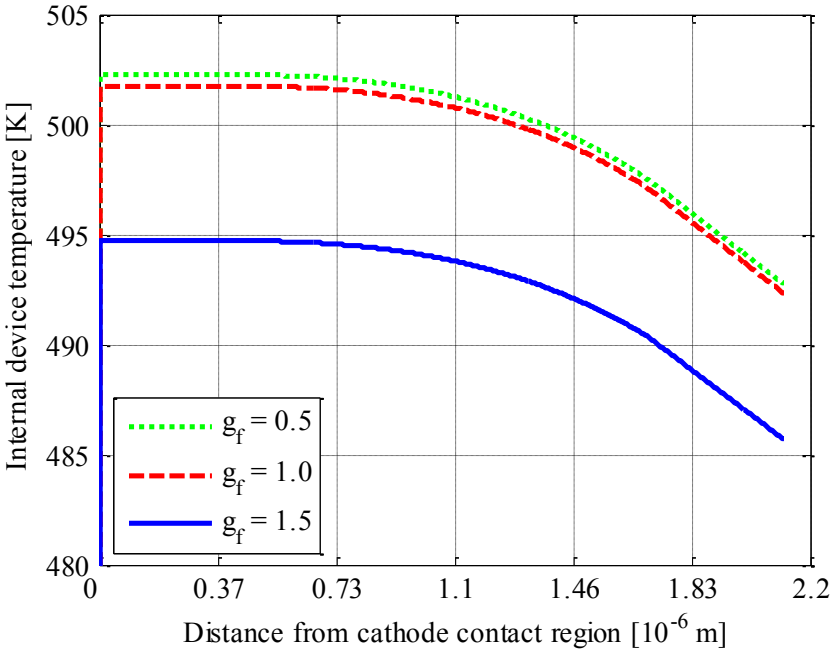

Figure 5.10 Internal temperature distribution of single domain GaN diode with varying transit region doping profiles

5.2.5 RF performance at higher mm-wave frequencies of optimised single-domain diode with exponentially graded transit region doping profile

Having established that the transit region with an exponentially increasing doping profile (g_f = 1.5) improves the RF performance of the single domain diode at 175 GHz, its performance is now studied at higher frequencies and compared to the optimised diode with a uniform doping profile presented in Section 5.2.2. The fundamental, second and third harmonics are considered. The fundamental frequency is increased in steps of 25 GHz from an initial value of 175 GHz.

The length and nominal doping concentration of the transit region are adjusted appropriately to maintain a sufficient 'n_0L' product above the critical value as given by Equation 2.1.

The simulation results are summarised in Table 5.6.

Table 5.6 RF performance at higher mm-wave frequencies of the optimised single-domain diode with exponentially graded transit region doping profile

Parameter	Unit	#1	#2	#3	#4
Fundamental frequency	GHz	175	200	225	250
'n_0L' product	10^{17} m^{-2}	1	1	1	1
Bias voltage (V_{DC})	V	40	40	40	40
Fundamental output power	mW	728	590	482	126
Second harmonic output power	mW	110	67	60	4
Third harmonic output power	mW	36	0	0	0
RF efficiency at fundamental	%	2	1.4	1.1	0.5
Cathode contact temperature	K	495	510	513	515

The output power at higher operational frequencies degrades sharply towards the fundamental frequency of 250 GHz, and its associated harmonics. This is consistent with the simulated upper frequency limit of the transferred electron mechanism presented in Chapter 3. As explained previously, external circuit losses, parasitic inductances and capacitances are not modelled in this work; hence, the output power can be expected to be less than the simulated values.

The RF performance of the single-domain diode with a uniformly doped transit region can now be compared to the diode with a graded transit region doping profile. The harmonic output power of each diode is summarised in Table 5.7.

Table 5.7 Comparison of RF performance of the optimised single-domain diode with uniform and graded transit region doping profiles

Parameter	**Uniformly doped**			**Graded doping profile**		
Fundamental frequency (GHz)	175	200	250	175	200	250
Fundamental output power (mW) [relative increase (%)]	430	260	0	728 [**69%**]	590 [**127%**]	126 [n/a]
Second harmonic output power (mW) [relative increase (%)]	86	41	0	110 [**28%**]	67 [**63%**]	4 [n/a]
Third harmonic output power (mW) [relative increase (%)]	30	0	0	36 [**20%**]	0 [n/a]	0 [n/a]

The following observations can be made:

- an exponentially increasing transit region doping profile increases the fundamental output power by between 69% and 127% over the frequency range of 175 GHz to 200 GHz, compared to that of the diode with a uniformly doped transit region;
- a similar trend is observed at the second and third harmonics, increasing the harmonic output power by between 20% and 63% over the frequency range of 350 GHz to 525 GHz; and
- appropriate engineering of the transit region doping profile (by exponentially increasing the doping concentration towards the anode) extends the operational frequency limit of the diode to 500 GHz in second harmonic mode, compared to 400 GHz of the corresponding diode with a uniformly doped transit region.

5.3 Simulation and optimisation of two-domain diode

In this section, the RF performance of a two-domain diode is simulated at a fundamental frequency of 175 GHz and its second and third harmonics. The performance of the two-domain diode is compared to that of the single-domain diode.

5.3.1 Simulation model of two-domain diode

The two-domain diode is effectively the series connection of two single-domain diodes and is broadly based on the optimised single-domain diode that was established in the previous section. The simulation model of the two-domain diode is discussed in the following sections.

Transit region length and doping concentration

In the previous section, where an optimised single-domain diode design was established for fundamental frequencies upward of 100 GHz, a transit region length of 1 μm was used for simulations up to 175 GHz.

During the optimisation of the two-domain diode at 175 GHz, specifically, it was found that reducing the transit region to 0.8 μm increases the output power at the fundamental and harmonics substantially. The nominal doping concentration is maintained at 1×10^{23} m^{-3}, yielding an nL_0-factor of 0.8×10^{17} m^{-2}, which still meets the condition as set by Equation 2.1. A transit region length of 0.8 μm is therefore defined for all simulations henceforth.

Graded (g_f = 0.5 and 1.5) and uniformly doped (g_f = 1) transit regions are investigated, as has been done for the single-domain diode.

Doping notch width and doping concentration

The width of the doping notches is the same as that of the single-domain diode, namely 0.2 μm. The doping concentration of the notch has been reduced to 0.25×10^{23} m^{-3} but with no noticeable effect on the performance of the two-domain diode.

Buffer region width and doping concentration

A buffer region with a width of 0.25 μm and doping concentration of 1×10^{24} m^{-3} are chosen in agreement with Sevik *et al.* (2004:S188-S190). Preliminary simulations with different buffer region widths have been performed, which further confirmed that the 0.25 μm buffer width is in fact an optimum. These simulations yielded output power at the fundamental frequency of 3.7 W, 3.8 W and 3.1 W for buffer widths of 0.2 μm, 0.25 μm and 0.3 μm, respectively.

Figure 5.11 illustrates the doping profile of the two-domain diode (Francis *et al.,* 2015:25-34) that will serve as the benchmark two-domain design:

- Regions 1 and 7 are heavily doped contact regions;
- Regions 2 and 5 are lightly doped notches;
- Region 4 is the heavily doped buffer region;
- Regions 3 and 6 are the two transit regions (with uniform doping profiles illustrated).

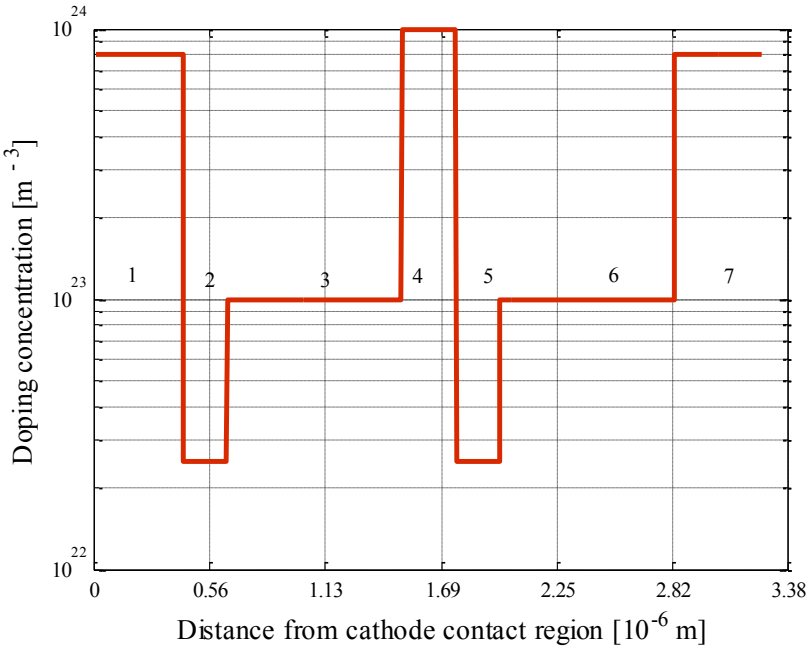

Figure 5.11 Doping profile of the benchmark two-domain GaN Gunn diode

(Francis *et al.,* 2015:25-34)

Bias voltage

To compensate for the increase in the length of the two-domain diode and to maintain its internal electric fields, the applied bias voltage is increased to 80 V, from 40 V for the single-domain diode. Also, to maintain the impedance level of the single-domain diode, the cross-sectional area of the two-domain diode is increased to twice that of the single-domain diode.

This increase in bias voltage and diode diameter is bound to increase the thermal dissipation in the two-domain diode significantly. The increase in the temperature of the two-domain GaN Gunn diode is countered by again incorporating a diamond integral heat sink on the anode side of the diode and by applying a pulsed bias voltage with even shorter duty cycles than what was applied to the single-domain diode.

Preliminary simulations have shown that a reduced duty cycle of 0.8% limits the operating temperature to satisfactory levels.

5.3.2 Simulated RF performance of the optimised two-domain diode at mm-wave frequencies

The RF performance of the two-domain diode established in the previous section is simulated at a fundamental frequency of 175 GHz and its second and third harmonics. The transit region doping profiles considered, are again exponentially graded (g_f = 0.5 and 1.5) and uniformly doped (g_f = 1).

Table 5.8 tabulates the simulated harmonic output power and conductance (real value of diode admittance) of the two-domain diode. The corresponding values for the single-domain diode are also tabulated for comparison.

The simulated cathode contact temperatures of the one and two domain diode were 480K and 500K, respectively.

Before summarising the simulation results presented in Table 5.8, the substantial increase in output power of the single-domain diode compared to the results presented for the optimised single-domain diode in the previous section needs to be explained. The output power at the fundamental has increased from 728 mW to 3.4 W. As mentioned earlier, the shorter transit region of 0.8 μm, instead of 1 μm, can attribute to the increase of the output power. However, the author is of the opinion that the decreased average operational temperature by 20 K (from 500 K to 480 K) through the shorter bias voltage duty cycle has a significant positive impact on the output performance of the diode. There is an obvious trade off between output power and duty cycle of the diode.

Table 5.8 RF performance of single- and two-domain diodes with graded transit region doping profiles g_f = 0.5, 1.0, 1.5

Doping profile	Frequency	Output power / Conductance		Factor increase in output power
		Single-domain diode	Two-domain diode	
g_f = 1.5	175 GHz	3.4 W -0.20 S	5 W -0.10 S	1.5
	350 GHz	259 mW -0.20 S	514 mW -0.20 S	2
	525 GHz	42 mW -0.20 S	87 mW -0.4 S	2.1
g_f = 1.0	175 GHz	3 W -0.17 S	3.8 W -0.15 S	1.3
	350 GHz	229 mW -0.18 S	460 mW -0.20 S	2
	525 GHz	14 mW -0.05 S	60 mW -0.6 S	4.3
g_f = 0.5	175 GHz	2.6 W -0.16 S	3.1 W -0.10 S	1.2
	350 GHz	160 mW -0.13 S	420 mW -0.12 S	2.6
	525 GHz	8 mW -0.03 S	30 mW -0.5 S	3.75

From Table 5.8 it is evident that the conductances of the single- and two-domain diodes are similar (except at the third harmonic). This indicates that the doubling of the cross-sectional area of the two-domain diode has had the desired effect of retaining the conductance of the single-domain diode.

As is the case with the single-domain diode, the exponentially increasing transit region doping profile (g_f = 1.5) enhances the output power consistently over the full frequency range.

However, the expected four-fold (N^2) increase in output power of the two-domain diode compared to the single-domain diode is generally not achieved. This may be attributed to the higher operating temperature of the two-domain diode. A secondary factor is the

observation that the Gunn domains in each of the two transit regions of the two-domain diode are dissimilar. This suggests that further optimisation of the transit region doping profiles is possible.

It is, therefore, instructive to further investigate the behaviour of the two-domain diode based on the internal electric field, temperature and valley occupation distributions.

Electric field distribution

The time-averaged internal electric field distribution is illustrated in Figure 5.12 (Francis *et al.,* 2015: 25-34).

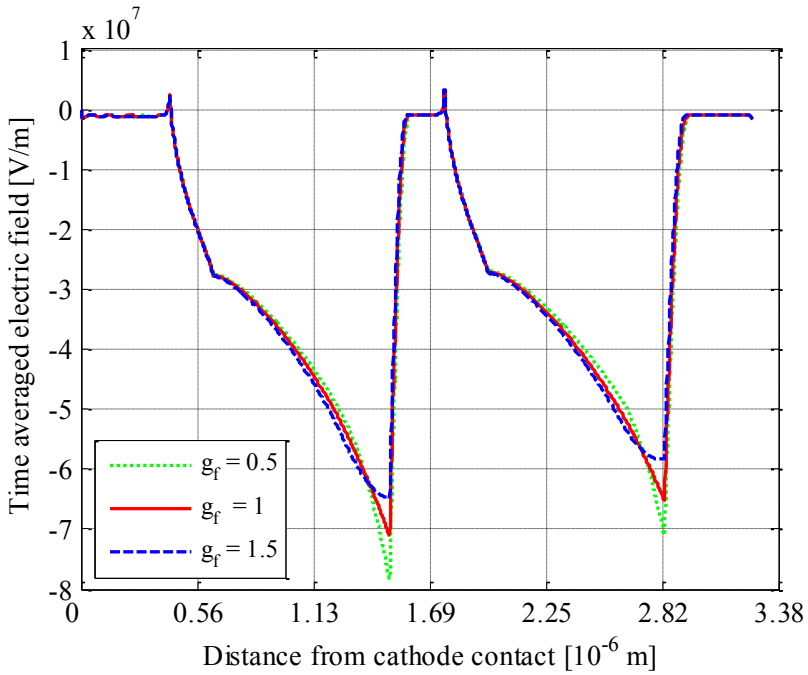

Figure 5.12 Time-averaged electric field distribution of two-domain GaN diode with varying transit region doping profiles

(From Francis *et al.,* 2015: 25-34)

The electric fields exhibit an improved curvature of the Gunn domains for the exponentially increasing transit region doping profile (g_f = 1.5). The higher electric field peaks associated with the under-doped transit region doping profile (g_f = 0.5) implies that Gunn domains are formed further away from the cathode side than for the over-doped case. This degrades the power efficiency. It is observed that the domain formation in the two transit regions is not identical as is ideally assumed. This can be attributed to the difference in nominal temperature of the two regions, as is illustrated

next in Figure 5.13. This impacts the nominal electron mobility in each region (Levinstein *et al.,* 2001). The dissimilar nature of the Gunn domains in the two-domain diode results in a decrease in output power and efficiency of the diode.

It is clear that the buffer region width of 0.25 µm is adequate for quenching the Gunn domains in-between the transit regions.

Temperature distribution

The steady state internal temperature distribution is illustrated in Figure 5.13 (Francis *et al.,* 2015: 25-34). It is noted that the over-doped transit region (g_f = 1.5) exhibits a marginally lower operating temperature. This can be attributed to the improved curvature of the electric fields in the transit regions, which translates into improved efficiency and lower thermal loss.

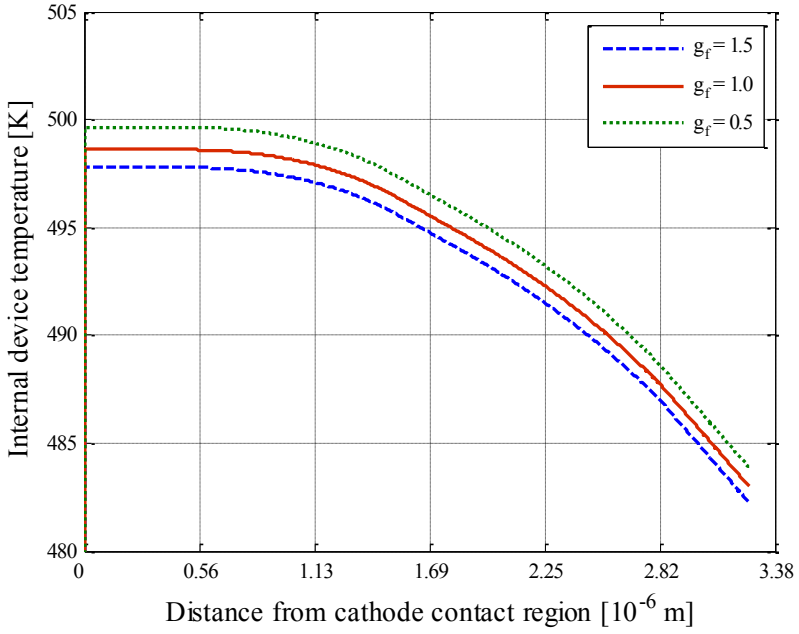

Figure 5.13 Internal temperature distribution of two-domain GaN diode with varying transit region doping profiles

(From Francis *et al.,* 2015: 25-34)

Energy band valley occupation by electrons

The mm-wave behaviour of Gunn diodes is intrinsically linked to the transferred electron effect. Figure 5.14 and Figure 5.15 (Francis *et al.,* 2015: 25-34) illustrate the steady state electron occupation of the central (C) and satellite (L, X) valleys of the energy band throughout the single- and two-domain diodes, respectively. It is evident that the single-domain diode exhibits improved electron transfer from the central to satellite valleys close to the doping notch (40% L-valley occupation for the single-domain diode compared to 35% for the two-domain diode). A further observation is that the transfer of electrons from the central to satellite valleys increases towards the anode, but is incomplete due to the short transit regions. The buffer region serves as a low resistance connector between the two transit regions. The transferred electrons revert to the C-valley upon entry into the buffer region. This is a necessity for two-domain operation. The valley occupation in the first transit region is marginally higher than in the second transit region. This also manifests as the slightly dissimilar Gunn domains evident in Figure 5.12.

Importantly, from a modelling perspective, the negligible occupation of the X-valleys suggests that a two-valley (C, L) energy band model can be implemented to reduce the computational load associated with the simulation.

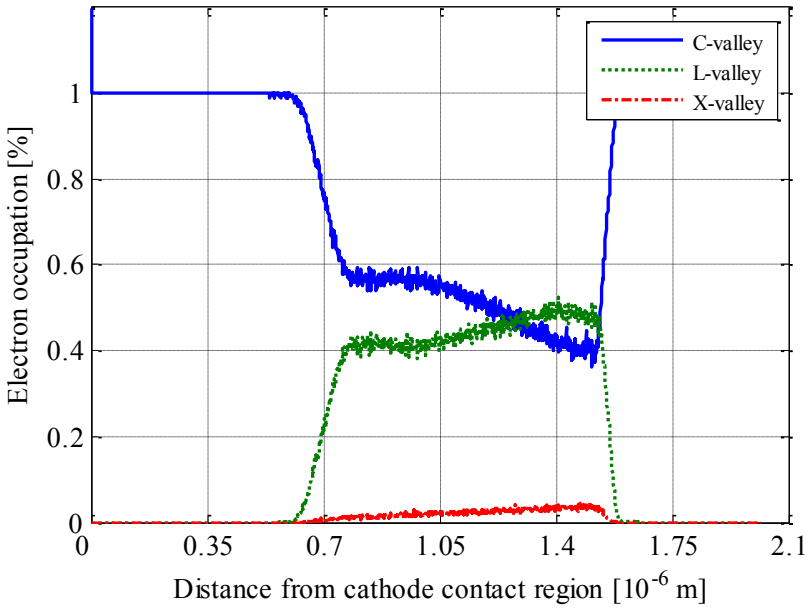

Figure 5.14 Steady state electron occupation of the central (C) and satellite (L and X) valleys for the single-domain diode with g_f = 1.5

(From Francis *et al.,* 2015: 25-34)

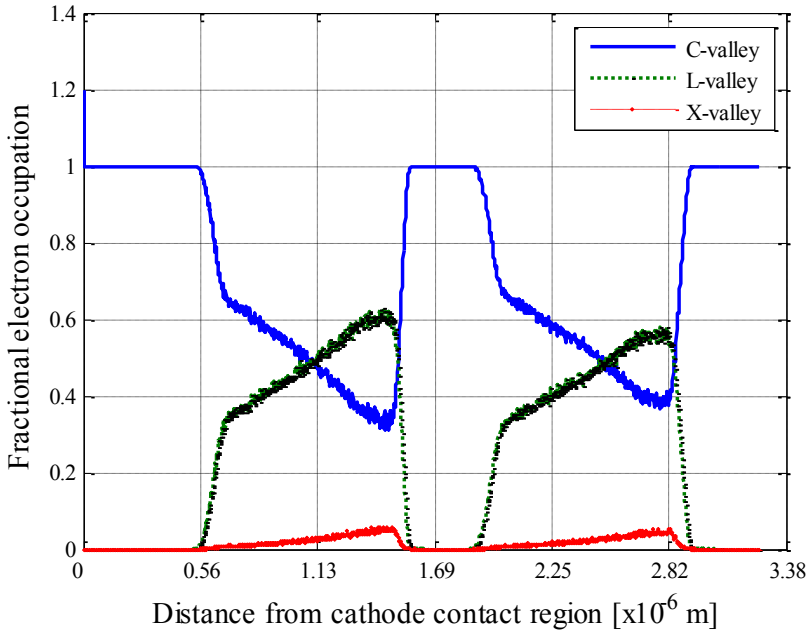

Figure 5.15 Steady state electron occupation of the central (C) and satellite (L and X) valleys for the two-domain diode with g_f = 1.5

(From Francis *et al.,* 2015: 25-34)

5.4 Conclusion

The chapter deals with the optimisation of single- and two-domain GaN Gunn diodes.

Following a similar approach to the optimisation of GaAs diodes, it has been shown that appropriate profiling of the transit region doping concentration improves the output power of the single- and two-domain diodes significantly. A doping notch has been incorporated throughout to improve the efficiency of Gunn domain nucleation.

In the case of the single-domain diode, an exponentially increasing transit region doping profile ('over-doped') increases the fundamental output power by between 69% and 127% over the frequency range of 175 GHz to 200 GHz, compared to that of the diode with a uniformly doped transit region. Similar increases in harmonic output power were also simulated. Furthermore, the over-doped transit region extends the operational frequency limit of the diode to 500 GHz in second harmonic mode, compared to 400 GHz of the corresponding diode with a uniformly doped transit region.

The operational frequency limit of the optimised single-domain diode in the fundamental mode is simulated to be of the order 250 GHz to 300 GHz, which is in agreement with the simulated upper frequency limit of the transferred electron mechanism presented in Chapter 3. This is, however, a more conservative estimate than reported in literature, which can be attributed to the appropriate incorporation of thermal effects in the Monte Carlo simulation model used in this work.

Heating of GaN Gunn diodes is a major concern, which can be overcome by proper heat sinking of the device and by decreasing the average bias current. This is achieved through applying a pulsed bias voltage to the diode. A bias voltage with a 1.5% duty cycle for the single-domain diode limits the highest internal diode temperature to about 500 K.

The simulated output power of the optimised single-domain diode has been shown to be consistent with a state-of-the-art diode reported in literature.

The research further shows that it is indeed feasible to increase the output power of GaN Gunn diodes by incorporating two transit regions, but that proper thermal management of the diode becomes even more important. The internal heating of the diode was limited to acceptable levels by further reducing the duty cycle of the pulsed bias voltage from 1.5% for the single-domain diode, to 0.8%.

The author is of the opinion that increasing the number of domains to more than two will render the performance of the Gunn diode ineffective as the duty cycle will have to be reduced dramatically to counter thermal losses; thus, rendering the microwave output power of the diode impractical.

The simulation of a two-domain diode with an over-doped transit region yields an output power of 5 W, 514 mW and 87 mW at a fundamental frequency of 175 GHz, and its second and third harmonics, respectively. This is significantly higher than for the single-domain diode, with corresponding output power of 3.4 W, 259 mW and 42 mW, respectively.

The expected four-fold increase in output power of the two-domain diode compared to the single-domain diode is generally not achieved. As discussed in this chapter, it may be attributed to the higher operating temperatures of the two-domain diode. It has also

been shown that the Gunn domain formation in each of the two transit regions is dissimilar. This suggests that further optimisation of the transit region doping profiles is possible, with an expected increase in output power and efficiency.

The work reported in this chapter on graded doping profiles of the transit regions has not been found elsewhere in literature.

6 RESULTS AND CONCLUSION

6.1 Introduction

The demand for mm-wave and terahertz devices due to the growing prospective market has sparked research in this field. Gunn diodes can serve as mm-wave sources with appreciable output power, coupled with their superior phase noise characteristics. They currently find application in various emerging fields, such as automotive Autonomous Cruise Control (ACC), imaging systems, missile guidance, smart munitions and mm-wave radar systems.

The research presented here investigates the performance of two-domain GaAs diodes, as well as single- and two-domain GaN diodes. All simulations are based on the ensemble Monte Carlo particle simulation technique. The simulation model incorporates thermal heating consistently with the evolution of electrons through the device, which is generally ignored or modeled overly simplistic in the reported literature. The simulated RF performance of the GaAs and GaN diodes presented here are therefore more conservative than that found in the literature.

The salient achievements of this research that address the objectives stated in Chapter 1 can be summarised as follows:

- A novel empirical method to estimate the operational frequency limit of Gunn devices, based on the dynamic velocity-field characteristic of the bulk material, is developed and verified. This method predicts operational frequency limits of between 80 GHz and 100 GHz for GaAs Gunn diodes, and between 250 GHz and 300 GHz for GaN devices operating in the fundamental mode.
- The research shows that it is feasible to enhance the mm-wave performance of single-domain Gunn diodes by incorporating two transit regions, and also through appropriate engineering and profiling of the transit region doping concentration. It has been argued that incorporating more than two transit regions is counter-productive, mainly due to increased thermal dissipation.
- The two-domain GaAs diode reported by Van Zyl (2006) has been optimised further to increase the output power from 160 mW to 182 mW at the 94 GHz harmonic. The optimised diode has been shown to operate at fundamental frequencies up to 90 GHz, with harmonic output power available up to 186 GHz. These observations are consistent with the simulated upper frequency limit of the transferred electron mechanism presented in Chapter 3.

- A single-domain GaN Gunn diode has been optimised and shown to benefit from the optimisation approach for GaAs devices. The optimised diode yielded 3.4 W at a fundamental frequency of 175 GHz, and third harmonic output power of 42 mW at 525 GHz. The operational frequency limit of the diode was simulated to be of the order 250 GHz, which is again in agreement with the expected upper frequency limit of the transferred electron mechanism presented in Chapter 3.
- The single-domain GaN diode served as a basis for a novel two-domain diode, which was subsequently further optimised. Output power of 5 W, 514 mW and 87 mW at a fundamental frequency of 175 GHz and its second and third harmonics, respectively, have been simulated. This is significantly higher than for the single-domain diode, although the expected four-fold increase in output power of the two-domain diode, compared to the single-domain diode, has not been achieved.

Each of these is described briefly below.

6.2 Overview of results

6.2.1 Empirical determination of upper operational frequency limits of the transferred electron mechanism in bulk GaAs and GaN

A novel approach was presented whereby the hysteresis in the dynamic, high frequency velocity-field characteristics of bulk GaAs and GaN are exploited to determine the upper frequency limit at which these materials still exhibit NDR. These predictions, which inherently consider the non-stationary dynamics of electrons at frequencies approaching the NDR relaxation frequency and at different temperatures and doping conditions, do not suffer from the theoretical time-constant based assumptions.

The empirical method presented in this research can be applied to any material that exhibits NDR and provides a reliable estimation of the frequency limits of operation of NDR-based oscillators, such as Gunn diodes. Furthermore, the predicted operational frequency limit of the NDR mechanism does not depend on the structure of the devices that exploit this mechanism, but is an intrinsic characteristic of the material.

The simulation results predict a fundamental mode frequency limit of between 80 GHz and 100 GHz for GaAs and between 250 GHz and 300 GHz for GaN. These values of

the upper frequency limits are consistent with the simulation of the actual devices presented in Chapters 4 and 5.

Specific findings reported in this work include:

- The average negative slope of the dynamic velocity-field curve increases monotonically from negative values at low frequencies to positive values at higher frequencies, indicating a progressive deterioration of the NDR with increased frequency.
- Higher operational temperatures degrade NDR significantly.
- The nominal doping concentration of bulk GaAs has an insignificant effect on the frequency dependence of NDR. The designer of GaAs Gunn devices can therefore adjust the nominal concentration of the transit regions for practical impedance levels and output power, without having to be concerned about its effect on the frequency behaviour of the device. However, the frequency behaviour of GaN has been shown to be more sensitive to the nominal doping conditions and, accordingly, needs to be considered.
- The upper frequency limit for bulk GaAs to support NDR is between 80 GHz at 450 K and 97 GHz at 300 K.
- The upper frequency limit for bulk GaN to support NDR is between 255 GHz and 300 GHz, depending on the operating conditions.

6.2.2 Gunn diode optimisation

Gunn diode optimisation in this work relates to the RF output power and frequency behaviour of the devices. The relevant design parameters that have been optimised, are the dimensions and doping profile of the transit regions, the width of the doping notches and buffer region (for two-domain devices), and the bias voltage. In the case of GaAs diodes, hot electron injection has also been implemented to improve the efficiency and output power of the device.

Multi-domain operation has been explored for both GaAs and GaN devices and found to be an effective way of increasing the output power. It has also been found that increasing the doping profile of the transit region exponentially over the last 25% towards the anode by a factor of 1.5 above the nominal doping concentration enhances the output power of the diodes.

GaAs Gunn diodes

A two-domain GaAs Gunn diode, based on the benchmark design by Van Zyl (2006), has been optimised. As mentioned earlier, the optimised diode outperforms the benchmark diode with an enhancement of 14% in its output power; 182 mW, compared to 160 mW at 94 GHz.

The simulated output power of the optimised diode is 218 mW at a fundamental frequency of 62 GHz, and 42 mW and 890 µW at the second and third harmonics of 124 GHz and 186 GHz, respectively. Beyond a fundamental frequency of 62 GHz, the performance of the two-domain diode degrades sharply in terms of efficiency to below 0.1 %. However, appreciable output power is still simulated at a fundamental frequency approaching 90 GHz. This is in agreement with the expected frequency limit as estimated empirically for the transferred electron mechanism. It is, however, questionable whether the fundamental mode of operation for frequencies above 62 GHz is practical, due to the low RF efficiency and negligible output power at its associated second and third harmonics (refer to Figure 4.12).

The simulated output power of the optimised diode was shown to be comparable to state-of-the-art diode performance as reported by Priestley *et al*. (2010).

It is the author's opinion that due to the sensitivity of Gunn diodes to thermal heating, three, four and eight domain Gunn diodes as reported by Teoh *et al.* (2002:830-831) will be rendered impractical and unfeasible. As with GaN diodes, the bias voltage will have to be pulsed with *exceedingly* short duty cycles to limit the thermal dissipation associated with such devices. The practicality of generating such short pulses in terms of the high current required and the impedance of the diode itself is also questionable.

In conclusion, a comparison between single-domain and two-domain devices has indeed shown that the incorporation of more domains increase the output power. This is, however, only observed for frequencies well below the operational frequency limit of the devices (see Figure 4.13).

GaN Gunn diodes

Compared to GaAs, relatively little is published on GaN diodes and their optimisation. As discussed in this work, GaN supports Gunn operation at much higher frequencies

than GaAs. The extensive body of simulations presented here on both bulk and device levels, confirm the superior RF performance of GaN devices. Furthermore, the operational feasibility and performance at mm-wave frequencies of single- and two-domain GaN (Wz) Gunn devices have been investigated.

A single-domain diode was first optimised, which also served as the benchmark for the two-domain design. Both the single- and two-domain devices have been simulated for RF performance at frequencies approaching their operational limits. The work concluded with a comparison between the single- and two-domain diodes in terms of output power.

The simulation results for the GaN diodes have already been discussed in Chapter 5, but a summary of the main findings is repeated here for ease of reference.

- Single-domain diode:

    - Exponentially increasing the transit region doping profile ('over-doping') increases the fundamental output power by between 69% and 127% over the frequency range of 175 GHz to 200 GHz, compared to that of the diode with a uniformly doped transit region.
    - A similar trend is observed at the second and third harmonics, increasing the harmonic output power by between 20% and 63% over the frequency range of 350 GHz to 525 GHz.
    - The over-doped transit region extends the operational frequency limit of the diode to 500 GHz in second harmonic mode, compared to 400 GHz of the corresponding diode with a uniformly doped transit region.
    - The operational frequency limit of the optimised diode in the fundamental mode is between 250 GHz and 300 GHz, which agrees with the simulated upper frequency limit of the transferred electron mechanism presented in Chapter 3.
    - Heating of GaN Gunn diodes is a major concern and can be countered effectively by applying a pulsed bias voltage to the diode. A bias voltage with a 1.5% duty cycle limited the highest internal diode temperature to 500 K.
    - The simulated output power of the optimised single-domain diode is consistent with a state-of-the-art diode reported in literature.

- Two-domain diode:

    - The optimised device yields output power of 5 W, 514 mW and 87 mW at a fundamental frequency of 175 GHz and its second and third harmonics, respectively.
    - This is significantly higher than for the single-domain diode, with corresponding output power of 3.4 W, 259 mW and 42 mW, respectively.
    - The theoretically expected four-fold increase in output power of the two-domain diode compared to the single-domain diode is generally not achieved. This can be attributed to the higher operating temperatures of the two-domain diode, as well as dissimilar formation of the Gunn domains in each of the two domains.
    - It should be possible to improve the symmetry of the domain formation in the two transit regions through further optimisation of the doping profiles in each domain.
    - Heating of the devices is much more pronounced than for the single-domain devices, mainly due to the increased biasing levels. Hence, the duty cycle of the pulsed bias voltage has been reduced further to 0.8 %. As stated earlier, the practicality of such short duty cycles could be questioned.
    - The author is of the opinion that increasing the number of domains to more than two will render the performance of the Gunn diode ineffective and impractical as the duty cycle will have to be reduced dramatically to counter thermal losses.

6.2.3 Performance comparison of two-domain GaAs and GaN Gunn devices

It is informative to conclude the discussion by comparing the RF performance of the optimised two-domain GaAs and GaN devices. This is illustrated in Figure 6.1. The GaAs diode is simulated at a fundamental frequency of 62 GHz and its second and third harmonics. The GaN diode is simulated at a fundamental frequency of 175 GHz and its associated second and third harmonics.

GaN Gunn diodes clearly present significant advantages to their GaAs counterparts in terms of output power capability and operational frequency. The significant increase in the operational frequency of GaN diodes is accompanied by two orders of magnitude enhancement of the output power at comparable frequencies. This is in agreement with

the much higher *Johnson's figure of merit,* reported to be about 100 times higher than for GaAs (refer to Table 2.1).

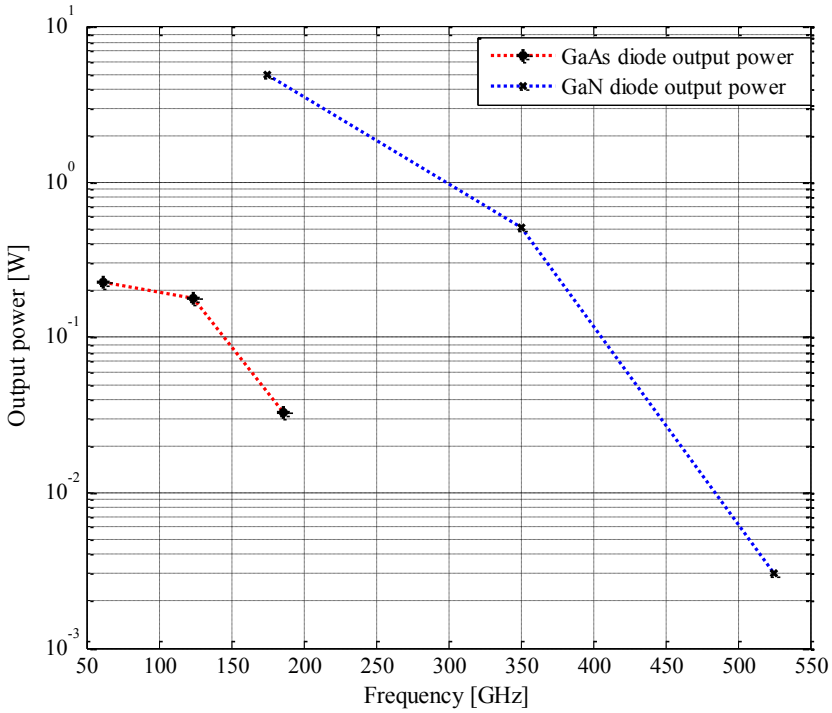

Figure 6.1 Comparison of harmonic output power for two-domain GaAs and GaN Gunn diodes

6.3 Proposed future work

Items for future research include:

- The Gunn domain formation in the two-domain diodes has been found to be slightly dissimilar in each of the transit regions. Further optimisation of the transit region doping profiles should be done to ensure that the domains form identically in each region. This may improve the diode efficiency further.
- Transit regions of unequal lengths should be investigated. This will improve the tuning bandwidth of actual devices (refer to Section 2.3.6).
- Incorporate hot electron launchers in the optimisation of GaN diodes.
- Augment the conduction energy band model of GaN to enable the simulation of GaN (Zb) and the investigation of inflection-based NDR.
- The possible electric field breakdown of the air external to the diode has not been assessed. SF6 gas has been used in the test chamber as an inhibitor of

breakdown in ‘mesa’ diodes, but this may not be feasible or practical using any current packaging technology. A further study of the breakdown of the external air should be conducted[1].

[1] From conversations with Dr Novak Farrington.

REFERENCES

Alekseev, E. and Pavlidis, D. (2000). Large signal microwave performance of GaN based NDR diode oscillators. *Journal of Solid State Electronics,* 44(6), pp. 941- 947.

Alekseev, E. and Pavlidis, D. (2000). GaN based Gunn diodes: their frequency and power performance and experimental considerations. *Solid State Electronics,* 44, pp. 245-252.

Amir, F., Farrington. N., Tauqeer, T. and Missous, M. (2008). Physical modelling of a step-graded AlGaAs/GaAs Gunn diode and investigation of hot electron injector performance. *Advanced Semiconductor Devices and Microsystem Conference Proceedings,* pp. 51-54.

Aloise, G., Vitanov, S. and Palankovski, V. (2011). Performance study of Nitride based Gunn diodes. *NSTI-Nanotech*, 2, pp. 599-602.

Alvi, P.A., Gupta, S., Siddiqui, M.J., Sharma, G. and Dalela, S. (2010). Modeling and simulation of GaN/$Al_{0.3}Ga_{0.7}N$ new multilayer nano-heterostructure. *Physica B: Condensed Matter,* 405 (10), pp. 2431-2435.

Arabshahi, H. (2008). Low-field electron transport properties in zincblende and wurtzite GaN structures using iteration model for solving Boltzmann equation. *Rom. Journal of Physics*, 54(5-6), pp. 547:555.

Batchelor, A.R. (1992). On the design of doping concentration profiles for GaAs transferred- electron device layers. *Solid-State Electronics*, 35(5), pp. 735-741.

Benbakhti, B., Rousseau, M., Soltani, A. and De Jaeger, J. (2009). Electron transport properties of Gallium Nitride for microscopic power device modelling. *Journal of Physics conference series,* 193,012005.

Beton, P.H., Couch, N.R. and Spooner, H. (1988). Use of n^+ spike doping regions as non-equilibrium connectors. *Electronic Letters*, 24(7), pp. 434-435.

Bosch, B.G. and Engelman, R.W.H. (1975). *Gunn effect electronics.* New York: Pitman Publishing.

Bulman, P.J., Hobson, G.S. and Taylor, B.C. (1972). *Transferred electron devices.* London and New York: Academic Press.

Buniatyan, V.V. and Arountionian, V.M. (2007). Wide gap semiconductor microwave devices. *Journal of Physics D: Applied Physics*, 40, pp. 6355-6388.

Caroll, J.E. (1970). *Hot electron microwave generators.* London: Edward Arnold Publishers.

Carslaw, H.S. and Jaeger, J.C. (1950). *Conduction of heat in solids*. Oxford: Oxford University Press.

Chen, J.F. and Hao, Y. 2009. A theoretical study of harmonic generation in a short period AlGaN/GaN superlattice induced by a terahertz field. *Chinese Physics Society,* 18(12), pp. 5451-06.

Chitara, B., Jebakumar, D., Rao, C.N.R. and Krupanidhi, S.B. (2009). Negative differential resistance in GaN nano-crystals above room temperature. *Nanotechnology,* 20, pp. 205-209.

Coeu, S.E. and Sussmann, R.S. (2000). Optical, thermal and mechanical properties of CVD diamond. *Diamond and Related Materials,* 9, pp. 1726-1729.

Couch, N.R., Kelly, M.J., Spooner, H. and Kerr, T.M. (1989). Hot electron injection in mm-wave Gunn diodes. *Solid-State Electronics,* 32(12), pp. 1685-1688.

Dunn, G.M. and Kearney, M.J. (2003). A theoretical study of differing transit region doping profiles for W band (75-110 GHz) InP Gunn diodes. *Semiconductor Science and Technology,* 18(794), pp. 794-802.

Dinesh, P. and Shirvastava, V. (2009). *Fundamentals of Electronic devices*. Meerut, India: Krishna Prakashan Media, Ed. 1.

E2V Technologies (September 2002). *Gunn diode application notes*. Issue 4. Available at: http://e2v.com/applications/diodes.html.

Esaki, L. (1958). New phenomena in narrow Germanium p-n junctions. *Phys. Rev*., 109, p. 603.

Elta, M.E. and Haddad, G.I. (1979). High-frequency limitations of IMPATT, MITATT and TUNNETT mode devices. *IEEE Transactions on Microwave Theory and Techniques*, 7(5), pp. 442-449.

Elta, M.E. and Haddad, G.I. (1979). Large-signal performance of microwave transit-time devices in mixed tunneling and avalanche breakdown. *IEEE Transactions on Electron Devices,* 26(6), pp. 941-948.

Farrington N., Norton P., Carr M., Sly J., and Missous M. (2008). 'A ruggedly packaged D-Band GaAs Gunn diode with hot electron injection suitable for volume manufacture'. *IEEE Int. Microwave Symposium Dig.*, pp. 281-284.

Forester, A., Stock, J., Montanani, S., Lepsa, M.I. and Luth, H. (2006). Fabrication and characterisation of GaAs diode chips for application at 77 GHz in automotive industry. *Sensors,* 6(3), pp. 350-360.

Foutz, B.E., Eastman, L.F., Bhapkar, U.V. and Shur, M.S. (1997). Comparison of high field electron transport in GaN and GaAs. *Applied Physics of the Journal American Institute of Physics*, 70 (20), pp. 2849 -2852.

Francis, S.A. and Van Zyl, R.R. (2013). Evaluating graded doping profiles of single-domain GaN Gunn diodes for THz applications. *Terahertz Science and Technology*, 6 (3), pp. 177-182.

Francis, S.A., Van Zyl, R.R. and Perold W.J. (2015). An empirical determination of upper operational frequency limits of transferred electron mechanism in bulk GaAs and GaN through ensemble Monte Carlo particle simulations. *Indian Journal of Physics*, 89(8), pp. 825-828.

Francis, S.A. and Van Zyl R.R. (2015). Evaluating the microwave performance of a two-domain GaN Gunn diode for THz applications. *Terahertz Science and Technology,* 8(1), pp. 25-34.

García S., Íñiguez-de-la-Torre, I., Pérez, S., Mateos, J. and González, T. (2013). Numerical study of sub-millimeter Gunn oscillations in InP and GaN vertical diodes: dependence on DC bias, doping and length. *Journal of Applied Physics*, 114(7).

Gelmont, B., Kim, K. and Shur, M. (1993). Monte Carlo simulation of electron transport in gallium nitride. *Journal of Applied Physics*, 74(3), pp. 1818-1821.

Graebner, J.E. and Jin, S. (1998). Chemical Vapour Deposited diamond for thermal management. *Journal of Minerals*, 6, pp. 52-55.

Greenwald, Z., Woodard, D.W., Calawa, A.R. and Eastman l.F. (1988). The effect of a high energy injection on the performance of mm wave Gunn oscillators. *Solid State Electronics*, 31(7), pp. 1211-1214.

Gunn, J.B. (1963). Microwave oscillations of current in group III-V semiconductors. *Solid State Communications,* 1(4), pp. 88-91.

Gurbuz, Y., Esame, O., Tekin, I., Kang, W.P. and Davidson, J.L. (2005). Diamond semiconductor technology for RF device applications. *Solid State Electronics*, 49, pp. 1055-1070.

Hao, Y., Yang, L-A. and Zhang, J-C. (2008). GaN-based semiconductor devices for terahertz technology. *Terahertz Science and Technology*, 1(2), pp. 51-64.

Hasegawa, F. and Suga, M. (1972). Effects of doping profile on the conversion efficiency of a Gunn diode. *IEEE Transactions,* 19, pp. 26-27.

Hockney, R.W. and Eastwood, J.W. (1992). *Computer simulation using particles*, Philadelphia: Institute of Physics Publishing.

Haydl, W.H. (1983). Fundamental and harmonic operation of mm-wave Gunn diodes. *IEEE Transactions on Microwave Theory and Techniques*, 31(11), pp. 879-889.

Hughes, L.J., Castro, C. and Johnston, M.B. (2005). Simulation and optimisation of terahertz emission from InGaAs and InP photoconductive switches. *Solid State Communications*, 136(11-12), pp. 595-600.

Jacoboni, C. and Lugli, P. (1989). *The Monte Carlo method for semiconductor device simulation.* New York: Springer Verlag.

Jethanandani, R. (1997). The development and application of diamond like carbon films. *Journal of Electronic Materials*, 2, pp. 63-65.

Joshi, R.P., Viswanadha, S., Shah, P. and del Rosario, R.D. (2003). Monte Carlo analysis of GaN-based Gunn oscillators for microwave power generation. *Journal of Applied Physics,* 93, pp. 4836-4842.

Kelly, M.J. (1993). A second decade of semiconductor heterojunction devices. *Microelectronics Journal*, 24(8), pp. 723-739.

Khalid, A., Li, C., Papageorgiou, V., Pilgrim, N.J., Dunn, G.M. and Cumming, D.R.S. (2013). Multi-channel GaAs-based planar Gunn diodes. *40th International Symposium on Compound Semiconductors*, Kobe, Japan.

Kohn, E., Ebert, W. and Vescan, A. (1998). Devices at high temperatures - status and prospects. *Israel Journal of Chemistry*, 38(1-2), pp. 105-112.

Kolni`ck, J., Oğuzman. I.H., Brennan. K.F., Wang. R. and Ruden. P. (1995). Electronic transport studies of bulk Zincblende and Wurtzite phases of GaN based on an ensemble Monte Carlo calculation including a full zone band structure. *Journal of Applied Physics,* 78(2), pp. 1033-1038.

Krishanmurthy, S., Schilfgarrde, M., Sher A. and Chen A. (1997). Band structure effect on high field transport in GaN and GaAlN. *Applied Physics Letters,* 71(14), pp. 1999-2001.

Kroemer, H. (1966). *IEEE Proceedings*, 54, pp. 1980-1981.

Lau, K.S., Tozer, R.C., David, J.P.R, Hopkinson, M., Rees, G.J., Carr, M., Priestley, N., Teoh, Y.P. and Dunn, G.M. (2007). Double transit region Gunn diodes. *Semiconductor Science Technology, 22*, pp. 245–248.

Levinshtein, M.E., Rumyantsev, S.L. and Shur, M.S. (2001). *Properties of Advanced Semiconductor Materials.* John Wiley and Sons.

Lee, C. and Ravaioli, U. (1990). Monte Carlo comparison of heterojunction cathode Gunn oscillators. *Electronics Letters*, *26*, pp.425-427.

Li, C., Khalid, A., Pilgrim, N., Holland, M., Dunn, G. and Cumming, D.S.R. (2009). Novel planar Gunn diode operating in fundamental mode up to 158 GHz. *Journal of Physics Conference Services,* 193:012029.

Littlejohn, M.A., Hauser, J.R. and Glisson, T.H. (1975), *Applied Physics Letters,* 26, p. 625.

MacPherson, R.F., Dunn, G.M. and Pilgrim N.J. (2008). Simulation of GaN Gunn diode at various doping levels and temperature for frequency up to 300 GHz by Monte Carlo simulation and incorporation of thermal effects. *Semiconductor Science Technology*, 23:055005-055012.

MacPherson, R.F. and Dunn, G.M. (2008). The use of doping spikes in GaN diodes. *Applied Physics Letters,* 93:062, pp. 103-105.

Maricar, M.I., Glover, J., Khalid, A., Li, C., Evans, G, Cumming, D.S.R. and Oxley, C.H. (2014). An AlGaAs/GaAs based planar Gunn diode oscillator with a fundamental frequency operation of 120 GHz. *Microwave and Optical Technology Letters,* 56(10), pp. 2449–2451.

Min, J.B., Chan, C.T. and Ho, K.H. (1992). First principles total energy calculation of gallium nitride. *Physics Rev.,* 45, pp. 159-1162.

Moglestue, C. (1993). *Monte Carlo simulation of semiconductor devices*. London: Chapman and Hill.

Mohamed, M., Faisal, A. and Colin, M. (2009). Advanced step graded Gunn diode and millimetre-wave imaging applications. *The International Society for Optics and Photonics.*

Müncheberg, S., Krischke, M. and Lemke, N. (1996). Nanosatellites and micro systems technology - capabilities, limitations and applications. *Acta Astronautica,* 39(9-12), pp. 799-808.

Neylon, S., Dale, J., Spooner, H., Worley, D., Couch, N., Knight, D. and Ondria, J. (1989). State-of-the-art performance mm-wave Gallium Arsenide Gunn diodes using ballistically hot electron injectors. *IEEE MTT-S Digest,* 47, pp. 519-522.

Pavlidis, D. (2004), GaN GHz Electronics. *12th GaAs Symposium,* pp. 551-554.

Pavlidis, D. (2005). GaN Gunn diodes for GHz signal generation. *IEEE MTT-S International Microwave Symposium Digest*, 3, pp. 1905-1908.

Panda, A.K. (2009). A comparative study of two terminal GaN based Gunn and IMPATT devices as high frequency signal generators. *International Journal of recent trends in engineering,* 2(6), pp. 4-6.

Parida, R.K., Agrawala, N.C., Dash, G.N. and Panda, A.K. (2012). Characteristics of GaN based Gunn diode for THz signal generation. *Journal of Semiconductors,* 33(8), pp. 001-007.

Pearton, S.J., Ren, F., Zlang, A.P. and Lee K.P. (2000). Fabrication and performance of GaN electronic devices. *Journal of Material Science and Engineering,* 30, pp. 55-212.

Pilgrim, N.J., Khalid, A., Dunn, G.M. and Cumming, D.R.S. (2008). Gunn oscillations in planar heterostructure diodes. *Semiconductor Science Technology,* 23:075013.

Priestley, N. and Farrington, N. (2010). Millimetre-wave Gunn diode technology and applications. *UK Automated RF & Microwave Measurement Society Conf*erence.

Seelmann-Eggebert, M., Meisen, P., Schaudel, F., Koidl, P., Vescan, A. and Leier, H. (2001). Heat-spreading diamond films for GaN-based high-power transistor devices. *Diamond and Related Materials,* 10, pp. 744-749.

Sevik, C. and Bulutay, C.C. (2004). Simulation of millimetre-wave Gunn oscillations in Gallium Nitride. *Turkish Journal of Physics,* 28, pp. 369-377.

Sevik, C. and Bulutay, C.C. (2004). Efficiency and harmonic enhancement trends in GaN-based Gunn diodes: Ensemble Monte Carlo analysis. *Applied Physics Letters*, 85, pp. 3908-3910.

Sevik, C. and Bulutay, C.C. (2004). Gunn oscillations in GaN channels. *Semiconductor Science Technology, pp.* 188-190.

Sharma, S.K. and Kim, D.Y. (2015). Design, simulation, fabrication, packaging and testing of an AlGaAs/GaAs Gunn diode at 94 GHz. *Journal of the Korean Physical Society*, 67(4), pp; 619-624.

Shur, M. (1990). *Physics of Semiconductor devices*. Prentice Hall.

Spooner, H. and Couch, N.R. (1989). Advances in hot electron injector Gunn diodes. *GEC Jn1. Research,* 7(1), pp. 34-45.

Slater, M. and Harrison, R.I. (1976). An investigation of multiple domain Gunn effect oscillators. *IEEE Transaction of Electron Devices*, 23(06), pp. 560-567.

Starikov, E., Shiktorov, P., Grunžinskis, V., Raggiani, L., Varani, L., Vaissière, J.C. and Zhao, J.H. (2001). Monte Carlo simulation of terahertz generation in nitrides. *Journal of Physics Condensed Matter,* 13, pp. 7159-7168.

Sze, S.M. and Ng, K.K. (2007). *Modern Semiconductor Device Physics*, John Wiley and Sons.

Talwar, A. (1979). A dual-diode 73 GHz Gunn oscillator. *IEEE Transactions MTT,* 27(5), pp. 510-519.

Teoh, Y.P., Dunn, G.M., Priestley, N. and Carr, M. (2005). Monte Carlo simulations of asymmetry multiple transit region Gunn diodes. *Semiconductor Science Technology,* 20, pp. 418-422.

Teoh, Y.P. and Dunn, G.M. (2002). Monte Carlo modeling of multiple transit regions Gunn diodes. *Electronic Letters,* 38(15).

Thim, H.W. (1968). Series-connected bulk GaAs amplifiers and oscillators. *Proceedings of the IEEE*, 56.

Tomizawa, K. (1993). *Numerical simulation of submicron semiconductor devices.* Boston: Artech House.

Tsay, J., Schwarz, S.E., Raman, S. and Smith, J.S. (1990). Multi domain Gunn diodes. *Microwave and Optical Technology Letters*, 3(2), pp. 54-60.

Turin, V.O. (2005). A modified transferred-electron high-field mobility model for GaN devices Simulation. *Solid State Electronics,* 49, pp.1678-1682.

Tyagi, M.S. (1991). *Introduction to Semiconductor Materials and Devices*. John Wiley and Sons.

Van Zyl, R.R., Perold, W.J. and Botha, R. (1999). Multi-domain Gunn diodes with multiple hot electron launchers: a new approach to mm-wave GaAs Gunn oscillator design. *IEEE Africon Conference Proceedings*, pp. 1193-1196.

Van Zyl, R.R., Perold, W.J. and Grobler, H. (2000). An efficient parallel implementation of the Monte Carlo particle simulation algorithm on a network of personal computers. *International Journal of Numerical Modelling: Electronic Networks, Devices and Fields,* 13(4), pp. 369-380.

Van Zyl, R.R. (2006). *The optimisation of mm-wave GaAs Gunn diodes using a parallel implementation of the Monte Carlo particle simulation technique*. PhD thesis*,* University of Stellenbosch, Stellenbosch*.*

Van Zyl, R.R. and Francis S.A. (2011). State of the art Gunn diodes: current and future trends in design and optimisation. *South African Conference on Sensors, MEMS and Electro-optical Systems Conference,* South Africa.

Vaidyanathan, R. and Joshi, R.P. (1991). Simulations for improved heterostructure Gunn oscillator based on transit region doping variations. *Electronic Letters*, 27(17), pp. 1555-1557.

Wu, G.M., Tsai, C.W., Chen, N.C. and Chang, P.H. (2007). Investigation of GaN crystal quality on silicon substrates using GaN/AlN super lattice structures Crystal. *Research Technology,* 42 (12), pp. 1276-280.

Yilmazoglu, O., Mutamba, K., Pavlidis, D. and Karaduman T. (2007). Measured negative differential resistivity for GaN Gunn diodes on GaN substrate. *Electronic Letters,* 43(8), pp. 1-2.

Zhao, J.H., Gružinskis, V., Weiner, M., Pan, M., Shiktorov, P., Starikov, E. (2000). Monte Carlo simulation of Gunn effect and microwave power generation at 240 GHz in n^+-n^--n-n^+ GaN structures. *Materials Science Forum*, 338-342, pp. 1635-1638.

Zybura, M.F., Jones, S.H., Tait, G. and Duva, J.M. (1995). Efficient computer aided design of GaAs and InP mm-wave transferred electron devices including detailed thermal analysis. *Solid-State Electronics,* 38(4), pp. 873-880.

ANNEXURE A: BULK MATERIAL PARAMETERS FOR GAAS AND GAN AT 300 K

Table 1: Valley dependent material parameters for bulk GaAs and GaN

Parameter		GaAs	GaN
Effective mass	m_C	0.067 m_0	0.2 m_0
	m_L	0.290 m_0	0.7 m_0
	m_X	0.450 m_0	0.471 m_0
Band non-parabolicity (eV^{-1})	α_c	0.67	0.187
	α_L	0.4	0.065
	α_X	0.55	0.029
Valley separation (eV)	Δ_L	0.284	5.5
	Δ_X	0.447	5.6
Number of equivalent valleys	Z_c	1	1
	Z_L	4	4
	Z_X	3	3
Polar optic phonon frequency (r/s)	ω_{op}	5.37×10^{13}	1.54×10^{14}
Inter-valley phonon frequency (r/s)	ω_{CL}	4.60×10^{13}	9.88×10^{13}
	ω_{CX}	4.60×10^{13}	9.88×10^{13}
	ω_{LX}	4.60×10^{13}	9.88×10^{13}
	ω_{LL}	4.41×10^{13}	7.6×10^{16}
	ω_{XX}	4.60×10^{13}	7.6×10^{16}
Inter-valley deformation potential (eV/m)	Ξ_{CL}	1.0×10^{11}	1.1×10^{11}
	Ξ_{CX}	1.1×10^{11}	1×10^{11}
	Ξ_{LX}	1.1×10^{11}	1×10^{11}
	Ξ_{LL}	1.0×10^{11}	0.5×10^{11}
	Ξ_{XX}	1.1×10^{11}	0.5×10^{11}
Acoustic deformation potential (eV)	Ξ_{ac}	7	8.3

Table 2: Material parameters for GaAs

Sound velocity (m/s)	v_s	5240
Density (kg/m^3)	ρ	5360
Low-frequency dielectric constant	ε_s	12.53
High frequency dielectric constant	ε_∞	10.82
Breakdown field (MVm^{-1})	E_b	n.a.
Thermal conductivity (Wcm^{-1}K^{-1})	C	55

Table 3: Selected material parameters for GaN (Wz) and GaN (Zb)

Parameter		**GaN (Wz)**	**GaN (Zb)**
Sound velocity (m/s)	v_s	4750	4330
Density (kg/m^3)	ρ	6100	6087-6150
Low–frequency dielectric constant	ε_s	9.5	9.5 - 9.7
High frequency dielectric constant	ε_∞	5.35	5.28 - 5.35
Thermal conductivity (Wcm^{-1}K^{-1})	C	1.3	1.3
Bandgap (meV)	E_g	3.2 - 3.3	3.39 - 3.5
Non-parabolicity (eV^{-1})	α	0.213	0.189